Mechanical design of a humanoid robot's lower body

Improved walking and posture dynamics

M.H.P. Dekker

D&C 2010.063

Mechanical design of a humanoid robot's lower body

Improved walking and posture dynamics

M.H.P. Dekker

Masters' thesis

Committee: prof. dr. H. Nijmeijer[1] (chairman)
prof. dr. ir. P.P. Jonker[2]
dr. ir. P.C.J.N. Rosielle[1] (coach)
dr. D. Kostic[1]
ir. E. Dekkers[3]

[1]Eindhoven University of Technology
Department of Mechanical Engineering
Dynamics and Control Group

[2]Delft University of Technology
Faculty of Mechanical, Maritime and Materials Engineering (3ME)
Biomechanical Engineering Department

[3]Eindhoven University of Technology
Gemeenschappelijke Technische Dienst

Eindhoven, December 2010

Summary

In general, a robot is a machine that is able to perform tasks autonomously. These tasks can be very diverse and are generally intended to take over human tasks. A humanoid robot can be the design of a specific body part to even an imitation of the total human beings (bio-) mechanics.

To gain experience in humanoid walking and posture control, Dutch Robotics designed TUlip; an anthropomorphic humanoid robot. Studies and practice with TUlip demonstrated some major mechanical issues.

A new robot's lower body is designed to completely overcome these issues. The more human like lower body consists of a waist, upper legs, lower legs and feet in a redundant and human like kinematic configuration of 16 DOFs. Each leg consists of five DOFs and the waist section consists of six DOFs.

The actuations are designed to be stiff, backdrivable with no backlash (either backlash free or imperceptible backlash) and are capable to provide ample torque for the joints. Actuation consists of brushed DC motors combined with a planetary gearbox and a final gear set, or a ball screw transmission (direct or with a push pull arm).

The result is a humanoid robot's lower body with a human like configuration, human like link dimensions, human like link masses and a human like Range of Motion. The robot is able to perform movements that are more human like because the robot is more agile than TUlip. Intersecting axes of rotation ensure that the computation of (inverse) kinematics is relatively simple.

Preface

This report is the outcome of a master's thesis in the Dynamics and Control group, carried out in the Constructions and Mechanisms subgroup at the department of Mechanical Engineering of the Eindhoven University of Technology, the Netherlands.

The project is about the mechanical design of a humanoid robot. It was extremely educational: I learned a lot about constructions and mechanisms, how to approach a design assignment and how to operate in a design-team. During this thesis, I also learned more and more about the human body and human movements. The way we are 'built' and move is pretty refined!

First of all, I would like to thank my coach, dr. ir. P.C.J.N. Rosielle. Nick: Your devoted coaching and your efforts to let me think on solutions, not about problems really motivated me to get to more creative ideas, not only in mechanical engineering but also in sideline work.

Furthermore I would like to thank my student-colleagues who assessed and encouraged me, especially on monday-meetings, enabling me to get more out of the project.
I would also like to give thanks to prof. dr. Henk Nijmeijer, also for supervising the project and for the trust in the humanoid-team; I really had a good time and learned a lot while having fun.

Finally, I would like to thank my family: Thank you all for your endless and unlimited trust, patience, assistance and care!

Nomenclature

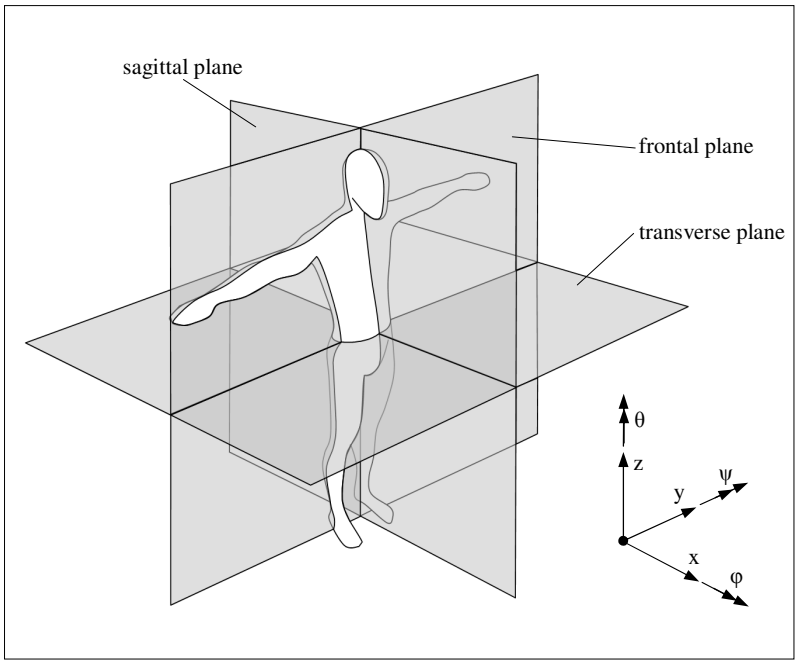

Figure 0.1: Definition of global coordinate system, relative to a human being in anatomical position, from (Whittle, 1996). Forward walking is the positive x-direction. Positive direction of rotation by means of the right hand rule.

Notation

A	(cross sectional) Area	m^2
c	Linear stiffness	N/m
D	Diameter	m
E	Young's modulus	N/mm^2, MPa
F	Force	N
h	Height	m
i	Ratio	-
j	Index	-
k	Rotational stiffness	Nm/rad
L	Length	m
p	Lead	m
r	Radius	m
t	(plate) Thickness	m

T	Torque	Nm
η	Efficiency	-
σ	Stress	N/mm^2
τ	Shear stress	N/mm^2
$\dot{\square}$	Velocity	m/s
$\ddot{\square}$	Acceleration	m/s^2
Ø	Diameter	m

Abbreviation

CAD	Computer Aided Design
CAN	Controller Area Network
COM	Center Of Mass
COP	Center Of Pressure
DOF, DOFs	Degree Of freedom, degrees of freedom
DS	Double Support
EDM	Electrical Discharge Machining
e.g.	Exempli Gratia, for example
GTD	Gemeenschappelijke Technische Dienst
HD	Harmonic Drive
i.e.	Id est, that is
N.B.	Nota Bene, note well
ROM	Range Of Motion
SAM	Synthesis and Analysis of Mechanisms
SEA	Series Elastic Actuation
SP	Support Polygon
SS	Single Support
TUD	Delft University of Technology
TU/e	Eindhoven University of Technology
UT	University of Twente
ZMP	Zero-Moment Point

Contents

Chapter 1
1 Introduction

1.1 Humanoid robots

In general, a robot[A] is a machine that is able to perform tasks autonomously. These tasks can be very diverse and are generally intended to take over human tasks. Robots can be divided into three types: *industrial robots*, *service robots* and *humanoid robots.* Industrial and service robots are intended to perform one specific task like in an industrial environment e.g. welding (common in industrial automotive plants) and respectively in domestic situations like vacuum cleaning (currently a popular commercial service robot).

Humanoid robots are different. A humanoid robot can be the design of a specific body part to even an imitation of the total human beings (bio-) mechanics. Arguments for developing humanoids are to learn more about the human body and its movements so we can acquire better understanding of the human body to build e.g. better prostheses for injured people or to design a *multi-purpose* humanoid operating in a human environment so it can assist in, or even completely take over human everyday jobs.
An imitation of the total human being mechanics is regularly entitled with *anthropomorphic robot.* Such a robot resembles a human being the most, implying that it consists of a torso, head with neck, arms with hands and legs with feet. Moreover, these robots typically consist of similar Degrees of Freedom (DOFs) to a human being. Currently, there are several of these robots, but they all have less dexterity than real human beings. However, the two humanoids currently showing the most resemblance to human beings are most likely Asimo (Sakagami et al., 2002) and Wabian-2 (Takanishi et al., 2005), depicted in Figure 1.1.

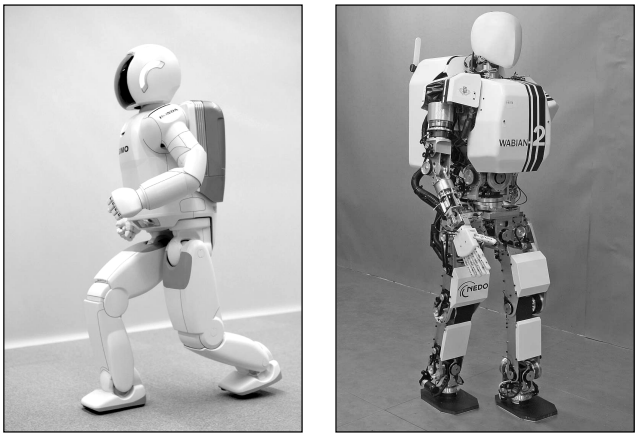

Figure 1.1: Currently, most likely, the most advanced anthropomorphic humanoids: Asimo of Honda (left) and Wabian-2 of Waseda University (right).

[A] In 1920, the Czech Karel Čapek introduced the term robot in a play called Rossums Universal Robots. Robot is subtracted from the Czech term robota which means 'forced labour'. (Menzel & D'Aluisio, 2002)

1.2 Walking of humanoid robots

The main reason why humanoids are still not part of our society is because of their mobility in a human environment. Our environment is based on moving around on two legs, often called *biped locomotion*, like walking, climbing stairs and even climbing on stepladders. In addition, our ways to move faster are based on two legs: riding a bicycle, a motorcycle or an automobile. Although walking seams effortlessness for humans, it is one of the most complex movements to imitate.

Human walking could be defined as follows: *Movement by putting forward each foot in turn, not having both feet off the ground at once* (Vukobratović et al., 2007). The development of humanoid walking is still at its early stages because we simply do not know exactly how humans walk and how every muscle is used. Human walking is a periodic orbit of a stable phase (standing on two legs) that alternates with an unstable phase (standing on one leg and swinging the other). This is a complex process, though highly energy efficient way of biped locomotion, since 'falling' due to gravity (unstable phase), ensures the forward movement.

Every human has a certain *gait*[B], so there is no unambiguous definition of human walking. Elderly people walk differently from a teenager or a baby, nevertheless, they all walk. Through gait analysis, via *motion capture*, trajectories for joints could be derived. Such a gait has not yet been realized with a humanoid robot because: if the monitored trajectories from this motion capture are used, a robot will fall over due to different dimensions, masses, inertias, ground impact dynamics and movement of other DOFs from the upper body that differ from the people who have been observed. Therefore, humanoid walking can be seen as an imitation more than a replication of human walking.

In the early seventies, Miomir Vukobratović introduced his theorem of the *Zero-Moment Point*, in short ZMP (Vukobratović & Borovac, 2004), to moderate biped locomotion. His theorem mathematically explains how robots can walk while maintaining dynamic stability at all time.
Simultaneously, in Japan, the first known robot to walk was Wabot-1, demonstrated in 1973 by the late Prof. Kato at Waseda University. Wabot-1, shown in Figure 1.2, achieved some statically stable steps, implying that the robot's *Center of Mass*, denoted with the acronym COM, is above the support area, usually named *Support Polygon*, or SP. This achievement was the starting point of a prolific generation of humanoid robots in Japan. The ZMP criterion also takes the dynamical effects during walking into consideration; it is a dynamic stability criterion and consequently, an extension to the static stability criterion used by Kato. Currently; the majority of humanoid robots still use the ZMP theorem to maintain their stability. Asimo and Wabian-2 (see Figure 1.1) are ZMP based as well.

Another approach of humanoid walking was initiated in the eighties, called *Passive dynamic walking* (McGeer, 1988). This way of walking is based on the unstable phase of walking. Like the Museon Walker, designed by Delft University of Technology and displayed in Figure 1.2, there are several of these passive dynamic walkers: typically these robots have fewer joints that are actuated than ZMP-based robots and they can only walk down on slopes. The energy from the gravity (the unstable phase) completely balances the loss of energy due to friction as a result of ground contact (Van Zutven, 2009). Currently there are few actuated dynamic walkers which are able to walk on flat ground: one example is Flame, possibly the most advanced actuated dynamic walker so far and designed by Delft University of Technology, see Figure 1.2.

[B] Every human has a specific unique walk, hence gait means: "Manner of walking or running" (Vukobratović et al., 2007).

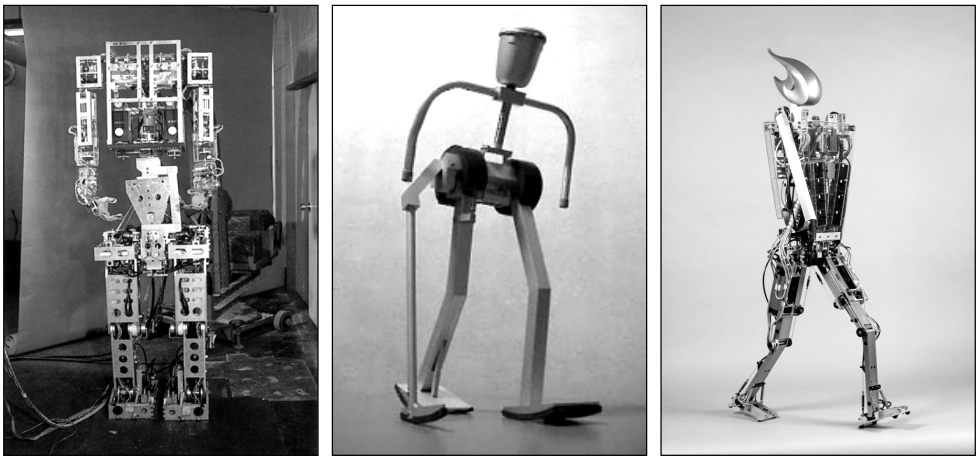

Figure 1.2: Wabot-1, first known walking robot (left), Museon walker, typical passive dynamic walker (middle), Flame, most advanced actuated dynamic walker (right).

1.3 Humanoid robot TUlip

Three universities of the Netherlands (University of Twente UT, Delft University of Technology TUD and Eindhoven University of Technology TU/e), combined efforts in humanoid robot design and development. This initiative, called Dutch Robotics, designed TUlip (Hobbelen et al., 2008), an anthropomorphic humanoid robot, intended as a platform to gain experience in humanoid walking. From now on, this robot will be denoted with *initial TUlip*.

The initial design was based on the dynamic walker Flame from TUD. Consequently, TUlips' actuations were designed to be compliant in order to be sustainable to contact instability and to measure joint torques to control the robot on torque level. These kinds of actuations are called *Series Elastic Actuation* (Pratt & Williamson, 1995), in short SEA: an elastic element with known (and relatively low) stiffness, such as a spring, is added to the actuation. By measuring the elongation of the spring the force (and subsequently the torque) can be computed.

In practice SEA is found out to be too progressive for now: it is intended for force control of joint actuations, while gait generation at the TU/e is done on position level. SEA is very difficult for position-control and bandwidths of such actuations are low due to the aforementioned compliances.
Furthermore, an internship on ZMP walking (Dekker, 2009) demonstrated that the configuration and actuations were not optimal for dynamically stable walking according to the ZMP criterion. Practice with the robot did show that the actuations were unable to deliver enough torque to the joints in order to withstand its own weight, let alone enough torque for more challenging tasks like walking, stair climbing or lifting up (heavy) objects.

Team Eindroid, the Dutch Robotics division from Eindhoven together with the Gemeenschappelijke Technische Dienst (GTD), performed some mechanical modifications on the robot, suggested by P. C. J. N. Rosielle, to alleviate these symptoms as a short time measure. This 'improved' TUlip is displayed in Figure 1.3. From now on, this 'improved' TUlip will be denoted with *modified TUlip*. On Robocup 2010 (Robocup, 2010), the modified TUlip actually achieved walking several steps statically stable.

Figure 1.3: After some mechanical modifications: modified TUlip of Team Eindroid.

1.4 A new humanoid robot

The development of (anthropomorphic) humanoid robots is still in its infancy. Compared to human beings, all existing humanoid robots:

- show a too simplified kinematic structure,
- are too heavy,
- have inefficient actuations,
- can move around for a short amount of time due to poor energy sources (batteries),
- use simple control schemes for walking and posture stability,
- use less sensors to examine their surroundings,
- have less computational power.

To investigate and improve all these aspects, a lot of time (and thus money) should be invested. Meanwhile, modified TUlip should be the platform to test and show that it is able to walk and perform other tasks that appeal to the sentiment of people and demonstrate that steps towards success are taken. Success can be measured as follows: a more human like robot that is capable of performing more human tasks.

Although modified TUlip achieved some stable steps, there are still configurational and mechanical issues, which will obstruct this robot from more human like walking and posture control. Accordingly, a new platform to investigate humanoid robot walking is needed. The goal is to design a new humanoid robot which can be this platform for the coming years. This platform should be human like. Because humanoid walking is the first priority of Team Eindroid, the focus of this thesis is on the lower body of the robot. Therefore, the goal of this thesis is: *To design a human like robot's lower body suitable for humanoid walking.*

Initial and modified TUlip lack on configuration, walking/posture aspects and have some mechanical issues, elaborated in chapter 2. These issues intensify the need for a new humanoid robot, from now on denoted with *new robot*. In this thesis, a new *mechanical design* for a lower body is proposed in chapters 3 and 4 to be able to improve humanoid walking and posture control to perform versatile tasks on two legs. After this, the new robot's lower body design is evaluated in chapter 5.

Chapter 2
Considerations for the new robot

2.1 A human like robot

The human *musculoskeletal system* basically consists of bones, cartilage, muscles, tendons and skin. It contains more than 206 bones and more than 600 muscles. Via biomechanics, the musculoskeletal system can be considered as a mechanical system: the bones can be considered as rigid links, the cartilage connects these links, muscles and tendons actuate the links and the skin can be regarded as a protection cover with sensors.

The lower body consists of a waist, upper legs, lower legs and feet in a redundant and human like kinematic configuration, similar (or scaled) link dimensions, similar *Range of Motion* (ROM) and similar joint velocities and accelerations, all to have a human like robot.

Redundant kinematic configuration
At the start of this thesis, initial TUlip consisted of 6 DOFs per leg: 3 at the hip joint, 1 at the knee joint and 2 at the ankle joint. This makes a total of 12 DOFs for the lower body, as can be seen in Figure 2.1 (left). The ankle joint had some major issues: ankle φ was passively actuated by springs and ankle ψ unidirectional actuated (retraction was done with a spring).

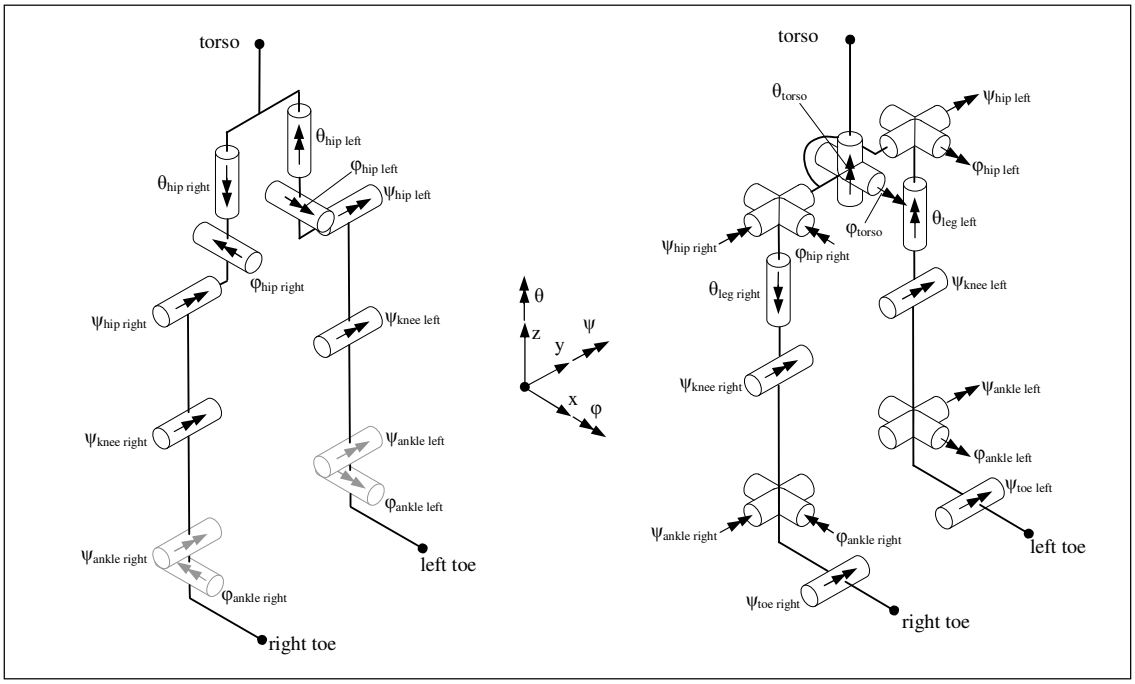

Figure 2.1: Kinematic structure of TUlip (left), kinematic structure of the new robot (right). At the start of this thesis, initial TUlip's ankle DOFs (in gray) were not actively actuated bidirectionally, modified TUlip's ankles are.

The aforementioned mechanical modifications on initial TUlip ensured that both the ankle φ and ψ are both bidirectional and actively actuated. However, modified TUlip's current kinematic chain from torso to toe is still not redundant. The kinematic structure of the new robot, consists of a total of 16 DOFs: 7 per leg and the waist has a 2 DOFs joint to the torso. So, the new robot, has 9 DOFs from torso to toes, and therefore, it is redundant. Thus it is able to step over objects, walk on slopes and stairs, etc. These redundancies also can contribute to reducing joint loads: algorithms can be used for redundancy resolution, while an objective function can be used to reduce joint velocities and accelerations (Dekker, 2009) and to take other criteria, such as singularity avoidance and joint limits, into account.

Independent movement of upper body

Modified TUlip's upper body (consisting of a torso, two arms and a head with a neck) can not be moved independently of the legs. When in *double support* (both feet are in contact with the ground), in short DS, the upper body can be regarded as a link in a closed kinematic chain and thus, has to take over a position and orientation as computed by e.g. inverse kinematics. A body that could be moved separately improves the control of the robot's COM, see Figure 2.2, because the upper body contains the majority of the total mass (average of human beings: 53% (Dirken, 1999)). If the COM can be controlled with more freedom, walking can become more human like and joint torques can be reduced. The pelvis can be regarded as a universal joint: φ and θ (Takanishi et al., 2005). So, these DOFs are incorporated in the new robot. Extra functionality of the θ rotation is explained in section 2.2. The ψ rotation of a human's upper body is made by the spinal column, so this rotation is actually in the upper body itself and not taken into account in this design.

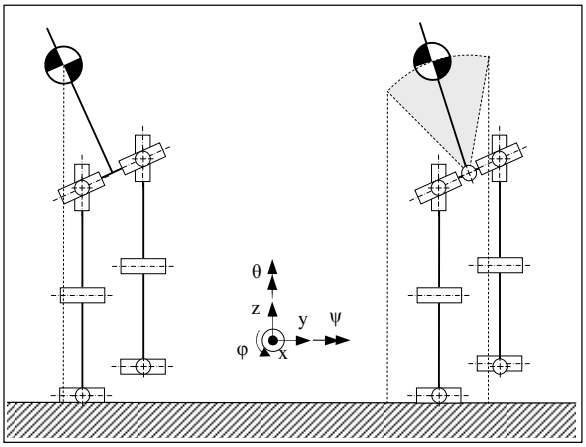

Figure 2.2: Schematic view of Frontal plane: torso without DOF (left), torso with DOF φ (right). Gray area is ROM of torso.

Hip θ

As can be seen in Figure 2.1 (and Figure 1.3), modified TUlip's hip θ rotation is not in line with the knee and ankle joints: the distance between the θ-axis and the leg itself is 52.5 mm. This implies that if the orientation of the foot (and knee) is changed an additional displacement of the foot (and knee) is unavoidable, see Figure 2.3a. This is highly problematic, especially in DS: due to friction between the soles of the feet and the ground, the feet cannot slide over the ground and other DOFs have to compensate for this additional displacement which restricts the robot's total freedom of movement. The hip θ rotation of a human being and the new robot is in line with the leg itself. It appears differently: the femur (upper leg bone) is not in line but the knee and ankle joint are (see Appendix A). This 'misalignment' is to offer moment-arms for muscles.

In the new robot, hip θ is placed in the upper leg, therefore it is renamed to leg θ, from now on. This has the advantage that the θ rotation of leg is done with leg θ, while hip ψ can be in any position. Modified TUlip has the hip θ axis 'on top' of the hip joint, and thus to rotate the leg in θ, a combination of hip angles has to be used. If hip ψ is rotated 90°, this problem becomes very clear, see Figure 2.3b. The leg θ axis still intersects with hip φ and hip ψ, thus; it can still be regarded as a ball joint.

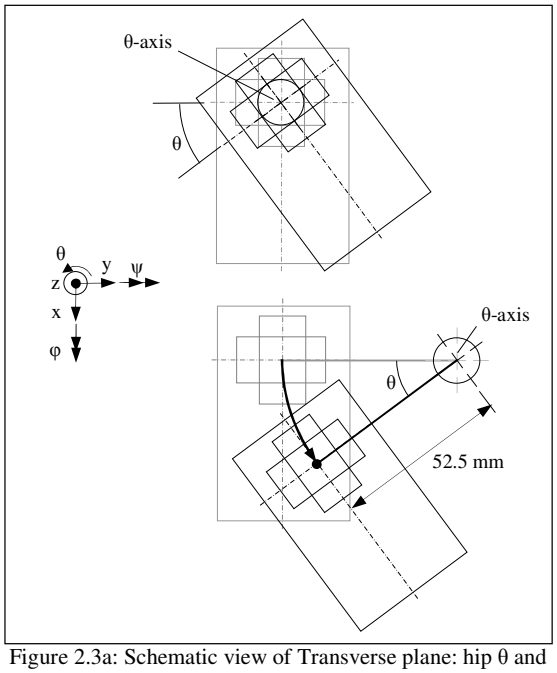

Figure 2.3a: Schematic view of Transverse plane: hip θ and foot. Hip in line with leg (above): no ankle translation. Hip θ not in line with leg (below): additional ankle displacement (curved arrow),

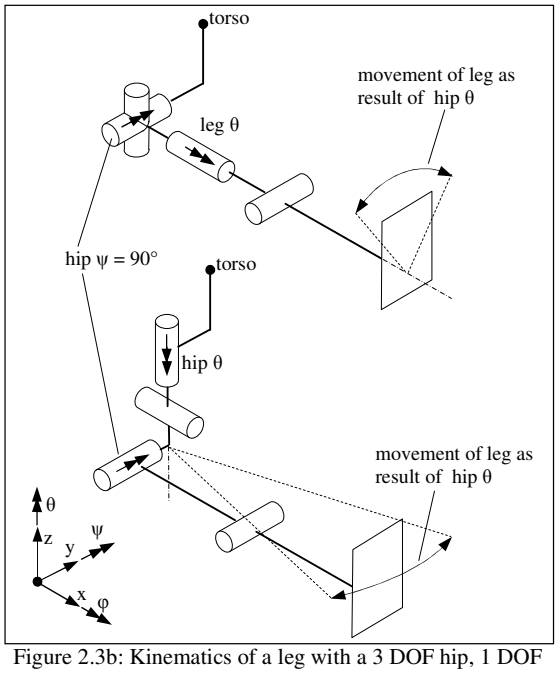

Figure 2.3b: Kinematics of a leg with a 3 DOF hip, 1 DOF knee and a foot, with hip ψ rotated 90°. Correct movement of leg: leg θ in upper leg (above). 'Incorrect' movement of leg: hip θ above hip joint, like in TUlip (below).

Hip φ

Because modified TUlip's hip φ is not in line with the leg (just as its hip θ), another problem occurs. When the hip φ axis is not in line with the leg; hip φ and ankle φ form a trapezium, see Figure 2.4 a. To get the COM above one foot, it is not sufficient to rotate hip φ and ankle φ alone (Figure 2.4 b); the knee ψ must be rotated, implying that hip ψ and ankle ψ need to be rotated as well (Figure 2.4 c). In the new robot, hip φ is in line with the leg, so, hip φ and ankle φ form a parallelogram. To move the COM above one foot it is sufficient to rotate hip φ and ankle φ, see Figure 2.4 d and e, which improves dexterity and computation of (inverse) kinematics.

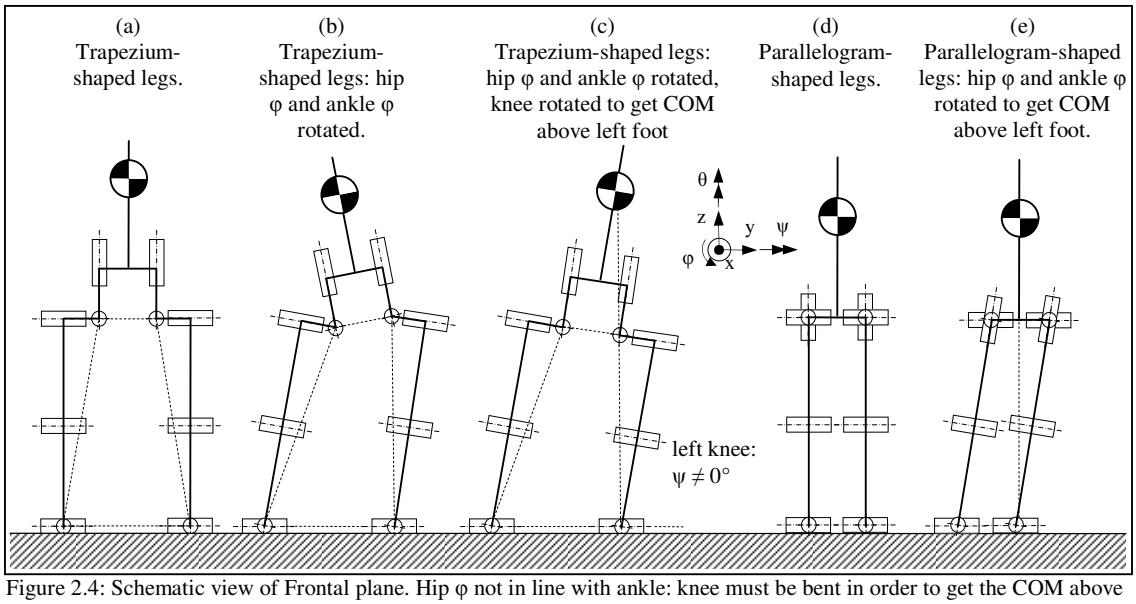

Figure 2.4: Schematic view of Frontal plane. Hip φ not in line with ankle: knee must be bent in order to get the COM above one foot (a, b and c). Hip φ in line with ankle: by parallelogram-mechanism, the COM can get above one foot; no other rotations are necessary (d and e).

Intersecting hip and ankle axes
Modified TUlip's hip φ- and hip ψ-axis do not intersect and the same holds for ankle φ- and ankle ψ-axis. This introduces additional joint torques and expands the computation of (inverse) kinematics. This kinematic computation is a major issue: Suppose the robots (modified TUlip and the new robot without waist DOFs) are standing with flat feet on the ground. If the legs are considered separately, they can be regarded as a 6 DOF kinematic chain with the foot sole fixed and the hip as robot-tip, see Figure 2.5. The tip of each chain can now be positioned in 6 DOF: x, y, z, φ, ψ and θ. Now, suppose that the ankle joints and knee joint are kept in arbitrarily chosen positions in such way that the distance between the hip joints is exactly the hip width. To connect the two kinematic chains, modified TUlip can not orientate the tips, with hip φ, hip ψ and hip θ without additional displacement of tips, so the knee and ankle joints should also move to connect the tips. The new robot, however, can orientate the tips without any additional displacement, so the tips can be connected while the knee and ankle joints positions can be kept. This decreases the complexity of computing the (inverse) kinematics a lot.

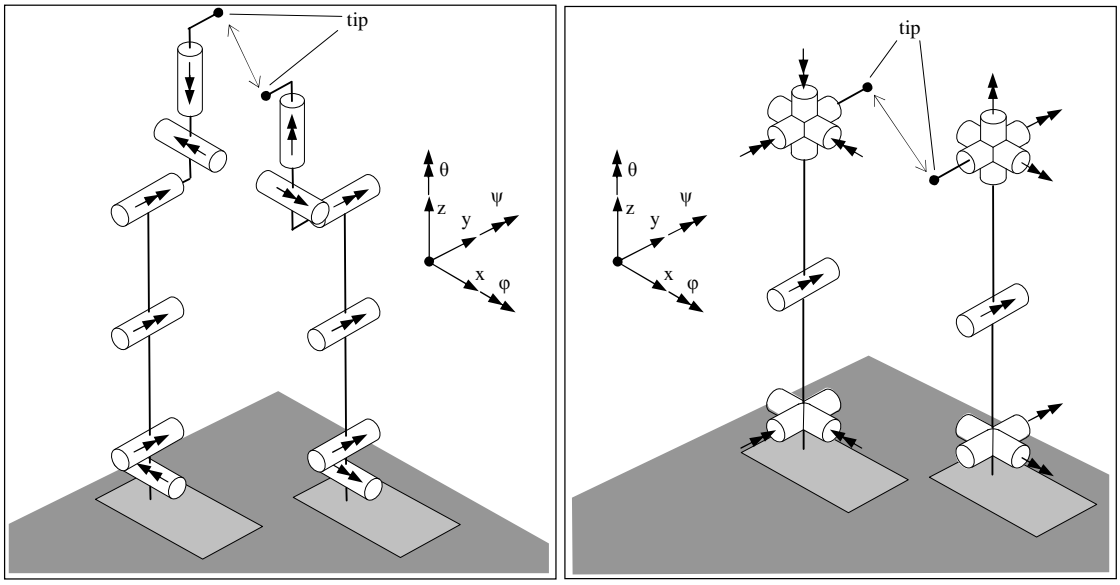

Figure 2.5: Each leg regarded as an individual kinematic chain with the hip as tip and foot fixed to the floor. Modified TUlip's (left) kinematic computation comprises additional displacement to the tips in order to connect the tips, the new robot (right) can connect the tips without additional displacement.

Toe joint
The new robot incorporates a toe joint for the following three arguments.

First of all, the robot is more redundant to position the COM, which is an improvement to the robot's dexterity.

Figure 2.6 shows a robot with a toe joint (new robot) and a robot without a toe joint (initial and modified TUlip). Both robots are letting down their hips, while remaining statically stable. In both cases a particular joint is limited by another joint. As can be seen, the robot with a toe joint is limited by the knee joint, whereas the robot without a toe joint is limited by the ankle joint. Because the ROM of the ankle is inferior to the ROM of the knee, the robot with a toe joint is able to let down the hip further. This improves the robot's posture range.

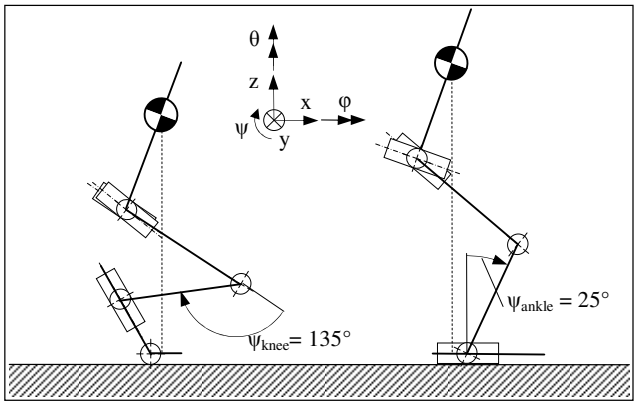

Figure 2.6: Schematic view of Sagittal plane: robot with toe joint (left), robot without toe joint (right).

Another advantage of a joint is the ability to make larger sidesteps. With a toe joint it is no longer necessary to place the whole foot flat on the ground, it is possible to place only the toe on the ground. With this, the foot can be used as an extension of the leg which extends the reach. This also contributes to improve the dexterity of the robot. Finally, the joint can also be operated in the positive ψ direction. This can be helpful to restore the stability if the robot is tipping over its toe joint (heel lift).

Link dimensions and ankle joint width
A dexterous robot has link dimensions matching with the human skeleton. Therefore, in appendix A, the dimensions of the human skeleton are given as a fraction of the total height.

A major issue is the distance between the ankles of modified TUlip. If the total height of the (robot's) leg is specified with H_{leg}, modified TUlip's distance between the ankles is $0.430H_{leg}$. Humans have a hip joint width of $0.236H_{leg}$, and because of the alignment of the hip joint with the ankle; the distance between the ankles is also $0.236H_{leg}$.
To balance on one foot, like in the swing phase of walking, the COM has to be positioned above the so called stand foot. Thus, modified TUlip needs to move further in the frontal plane, see Figure 2.7. As a result of this, walking becomes more of a swaying motion which is not very human like. Modified TUlip's performed gait at Robocup 2010 demonstrated this swaying motion. In addition to a smaller distance between the ankles, the independent movement of the upper body, as described above, can also be helpful to reduce this swaying motion.
Another advantage of a human like distance between the ankles is to reduce joint torques. Moment arms of the gravity force of each link reduce and consequently, the torque reduces as well.

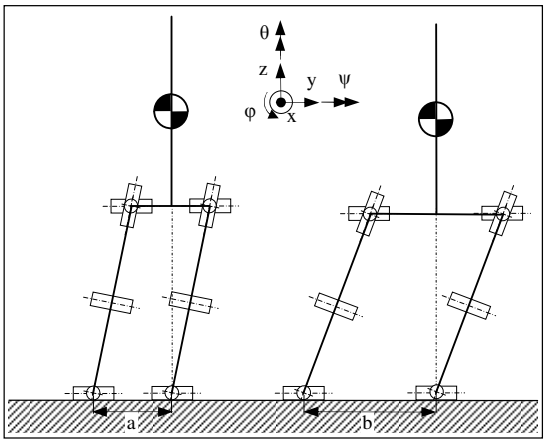

Figure 2.7: Schematic view of Frontal plane: A more human like distance between the ankles a, improves the resemblance of human walking (left). A wide distance between the ankles b, results in a more swaying motion (right).

Range of Motion
When walking, human beings do not use their full ROM; this over capacity is used for other tasks like sitting, crouching, etc. In Table 2.1, it can be seen that the ROM of the new robot resembles human beings, which improves its agility. To compare with Modified TUlip, its ROM is also given in Table 2.1.

Table 2.1: Range of Motion of Human (Kaneko et al., 2002), Modified TUlip (Measurements) and the new robot (sign convention according Figure 2.1).

		Human			**Modified TUlip**			**New robot**		
joint		min [°]	max [°]	range [°]	min [°]	max [°]	range [°]	min [°]	max [°]	range [°]
waist	φ	-5*	5*	10	-	-	-	-15	15	30
	θ	-4*	4*	8	-	-	-	-15	15	30
hip	φ	-20	45	65	-35	70	105	-20	45	65
	ψ	-125	15	140	-135	45	180	-90	45	135
leg	θ	-45	45	90	-25	40	65	-45	45	90
knee	ψ	0	135	135	0	135	135	0	135	135
ankle	φ	-30	20	50	20	20	40	-25	25	50
	ψ	-20	45	65	-30	40	70	-25	45	70
toe	ψ	-45	20	65	-	-	-	-70	20	90

* From (Takanishi et al., 2005)

Joint velocities and accelerations
Joint velocities and accelerations similar to human beings can be obtained by light weight design of robot links (body segments) and powerful actuations. Desired power in the actuations is discussed per joint in the concerning sections (chapter 3 and 4). Masses of human body segments are incorporated in Appendix A.

2.2 Walking aspects

Due to the division in walking strategies there is no explicit stability criterion for humanoid walking. A stable humanoid gait can only be defined with: *A humanoid gait is stable if the only contact between the biped and the ground is realized with the soles of the foot or feet, i.e. no other extremity of the biped is in contact with the ground* (Dekker, 2009).

Although the ZMP way of walking is not very 'human-like' and very energy inefficient due to the constant stability criterion, it can definitely ensure the above stated walking stability (therefore it is robust) and it can also be used for *posture control* (the stability control of tasks while standing on two legs). (Passive) Dynamic walking of humanoid walking is more human like and energy efficient than ZMP based walking. However, there is one major disadvantage. Currently, there is no mathematical theorem which can facilitate the generation of joint trajectories so they are generated by means of trial and error. Furthermore, this implies no robustness, hence, such a walk is marginally stable and a perturbation can cause the humanoid to fall over. Following this, Team Eindroid decided to get the robot to walk according to the ZMP criterion.

Appendix B describes the ZMP criterion in more detail. From this, computing and to controlling the location of the ZMP utilizes joint positions, velocities and accelerations. The current control of modified TUlip is also based on positions, velocities and accelerations. Therefore, it can be concluded that actuations have to be stiff, in order to have accurate measurement and control of these three parameters.

Human like walking
To improve the ZMP gait to a more human like gait, the following aspects increase the ROM of some joints.

Humans extend their steps during walking by rotating the pelvis to make use of the hip width, see Figure 2.8. This θ rotation can be from 0° to ±15°, dependent on the gait (Winter, 1991). So, the step length can be extended with a maximum of $0.061H_{leg}$. Simultaneously, this rotation also reduces the projected hip width in the frontal plane, which facilitates the control of the COM, described above (Figure 2.2). While walking like this, humans tend to make use of the pelvis θ rotation (±4°, see Table 2.1) and spinal column (the remaining 11°) to keep the shoulders parallel to the frontal plane. To compensate for the spinal column, in this design the pelvis can rotate ±15°. Note that the pelvis θ rotation becomes even larger while running, but then the shoulders are not kept parallel to the frontal plane anymore.

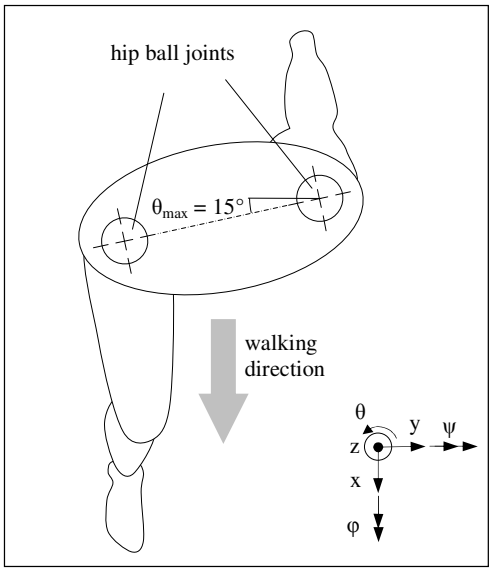

Figure 2.8: Transverse plane section view: pelvis rotation to extend step length.

As can be seen in Table 2.1, human toe joints (ψ_{toe}) have a ROM of 65° see Table 2.1. However, this is the active movement of the toes. If moved passively, the toe joint has a ROM of 90°. Dependent on different gait this passive movement is used when a human pushes off during walking, see Figure 2.9. Humans are capable of retraction to ψ = 0°, thus, from -45° to -70° this joint is driven unidirectionally. To simplify this, the new robot incorporates a bidirectional driven toe joint, with a ROM of 90°.

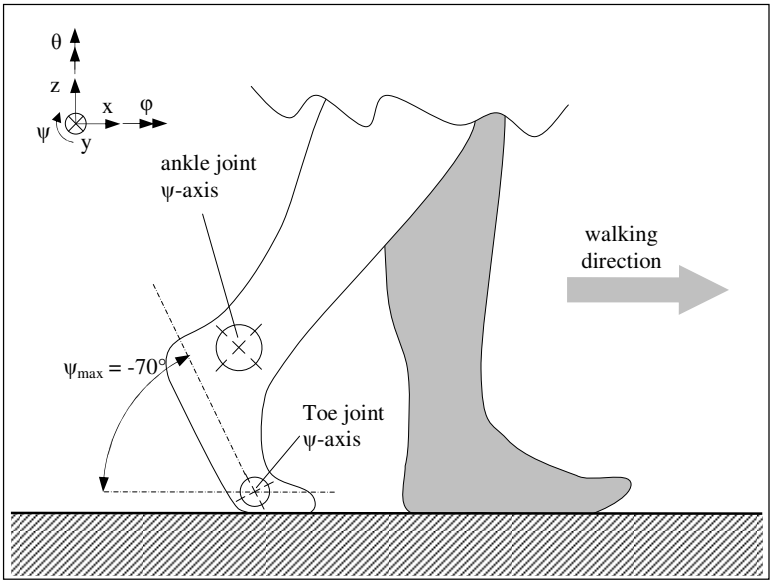

Figure 2.9: Sagittal plane view: toe push off during walking.

2.3 Practice with modified TUlip

Modified TUlip's total height is about 1.3 m. Official regulation of Robocup will gradually enlarge the minimum height; thus the new robot will encompass a total robot height of 1.5 m. The new robot is scaled from a human being with a total height of 1.8 m and a mass of 80 kg. Therefore, the scaling factor for the height is 0.83 and for the mass this is $0.83^3 = 0.57$, which results in a total robot mass of around 45 kg.

In efforts to let modified TUlip walk some mechanical aspects became apparent.

Modified TUlip's actuations
All modified TUlip's actuations consist of a motor and a planetary gearbox from Maxon motor company (Maxon, 2010). In hip ψ, knee ψ and ankle ψ a steel wire rope in combination with two pulleys (ratio $i < 1$, due to different pulley radii) is added. These kinds of transmissions increase torque and reduce backlash. Because the stiffness of this steel wire rope and two pulleys combination is lower than the stiffness of a gear set and it is in series with the planetary gearbox, the total actuation stiffness decreases.

Backlash
Planetary gearboxes include relatively high backlash, modified TUlip's gearboxes have a backlash of about 1° (Maxon, 2010). For hip φ, hip θ and ankle φ, the final backlash is up to 1°, because the gearboxes are the final transmission. For hip ψ, knee ψ and ankle ψ, the final backlash is about 0.2°, because of the extra transmission of the steel wire rope in combination with two pulleys.
Backlash must to be kept to a minimum, in order to accurately control joint positions and to minimize collision forces, which induce vibrations and wear (of gearboxes).

Actuation stiffness
If the stiffness of a planetary gearbox c_{gear} is compared to the stiffness of the steel wire rope $c_{steel\ wire\ rope}$, then: $c_{gear} >> c_{steel\ wire\ rope}$. Because the stiffnesses are in series, the stiffness of the steel wire rope can be regarded as the actuation stiffness. The steel wire rope transmissions of hip ψ and knee ψ have a steel wire rope (E = 210 GPa) with a cross section diameter of Ø 2 mm and a length of ≈ 350 mm. Stiffness of this steel wire rope is 1.9 kN/mm, and an end pulley with r = 50 mm implies a rotational stiffness of 4.7 kNm/rad. Ankle ψ has an end pulley with r = 33 mm, so a rotational stiffness of 2.0 kNm/rad. In practice, the stiffness drops even more because other components, such as pulleys that ensure the steel wire rope to make angles, all contribute to the loss of stiffness, are not incorporated in the calculation.
ψ Rotations are critical in walking because, for the greater part, they ensure the forward movement. In the new robot the rotational stiffnesses of all joints was aimed to be significantly higher.

Assembly related hysteresis
Modified TUlip's parts are mounted to each other without lead-in edges, dowel pins or other facilities to line up parts. In accordance, hysteresis occurs via micro slip between contact areas and deviation of axes is unavoidable which result in deviation of generated trajectories, which ultimately can cause instability. So for the new robot: parts should be assembled with minimum hysteresis.

Backdrivability
The joints of modified TUlip are all *backdrivable*[c]. Major advantages of this are:
- While in operation, impacts can be (partly) dissipated in the actuations. Protection of the robot as well as its environment (contact with human beings) can be ensured.
- Encoders can quantify trajectories which are induced manually. The actuations can 'play-back' these trajectories to verify e.g. stability.
- If the robot is powered off, joints are still movable for e.g. maintenance.

[c] A drive line is 'back-drivable' if an applied force/torque on the load side can enforce the actuator to move.

Impact forces
Modified TUlip's achieved gait is very slow and the foot lift during swing is minimal, so impact forces are low. If the new robot is going to walk more human like, impact forces will increase, thus, impact absorbing capabilities must be incorporated in the new robot's feet.

Motor choice
Because the aim of the design is on the mechanics, the choice of motors is unchanged, i.e. again brushed DC motors are used. Brushed DC motors have a smaller power to weight ratio compared to brushless DC motors (Chevallereau, et al., 2009). However, brushed DC motors have a higher stall torque which is beneficial for intermittent peak torques, they comprise simple drive electronics (only 2 conductors) and they are relatively cheap. Another advantage is the analogy with modified TUlip; the same (kind of) amplifiers and other electronics can be (re-) used.
Replacement of brushes only has to take place when motors are extensively used. Because the new robot will be a platform to test humanoid walking, this replacement will not occur frequently.

Encoders
Rotary encoders are (usually) used to determine the position and velocity of the rotary joints and motor rotors. Absolute encoders are essential to be able to position-control the joints efficiently. Incremental encoders at the joint side are less required (currently not even used) but can e.g. prevent the motors from over-heating.
In the new robot, incremental encoders are placed at the back of the motor. They can be purchased and assembled but if they are not used yet, they can also be left out. Absolute encoders are not incorporated in the design, because currently, they are designed and the way they have to be installed is not yet clear. It is expected that the implementation of these encoders is with relatively simple components that do not alter the design significantly.

2.4 Transmissions

Planetary gearboxes
Modified TUlip's actuations all incorporate multistage planetary gearboxes. Each gear contact has an estimated efficiency of 97%. Per stage a planetary set has six gear-contacts, so the efficiency of a planetary gearbox η can be estimated with:

$$\eta = (0.97)^{6n} \tag{2.1}$$

With n the number of stages. Modified TUlip's gearboxes are all three staged planetary gearboxes, so efficiencies are about 60 %. Disadvantage of these efficiencies is the low output torque. To obtain the required torque, high reduction ratios are needed and velocity reduces. So, planetary gearboxes are useful if there is another final transmission which increases the torque with more efficiency, so a minimal number of stages is needed and the reduction of the gearbox can be kept small.

Harmonic Drives
The majority of humanoid robots utilize *Harmonic Drives* (HD) (HarmonicDrive, 2010) as a transmission. HDs work as follows. According to Figure 2.10, the HD basically consists of 3 components. The *wave generator* (1), an elliptic disc with a ball bearing (2) which adapts to the elliptic shape elastically. Around this wave generator the *flexible spline* (3) is mounted, an elastic toothed ring with an elastic cup (3a) which adapts to the shape of the wave generator. The *circular spline* (4), a stiff outer ring with internal teeth, meshes with the teeth of the flexible spline at 2 contact 'areas' due to the elliptical shape. Typically, the wave generator is connected to an input shaft (1a), whereas the flexible spline is mounted to an output shaft (3b) and the circular spline is fixed.

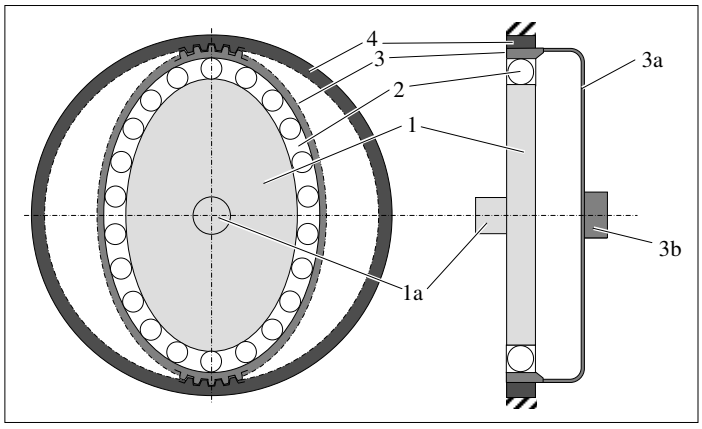

Figure 2.10: Schematic view of the working principle of a Harmonic Drive.

Simultaneously, 15% of all teeth are in contact (De Haas, 1991) which results in high torque transmission despite of small teeth. In the setup of Figure 2.10, the (transmission) ratio can be determined with:

$$i = 1 - \frac{z_{\text{circular spline}}}{z_{\text{flexible spline}}} \tag{2.2}$$

As can be seen from this equation, high ratios of around 1:100 are possible (e.g. if $z_{\text{flexible spline}} = 202$ and $z_{\text{circular spline}} = 200$), and the flexible spline rotates in the opposite direction of the wave generator.

Ball screw drives
A ball screw, see Figure 2.11 (left), is efficient in converting a rotary motion into a linear motion. The balls roll in a helical groove between the screw spindle and the nut. Usually, the spindle rotates and the nut (kept from rotating) translates because the spindle has a smaller inertia. If the stroke of the nut is small, the balls do not have to recirculate in the nut, otherwise the balls have to recirculate and the nut must provide a ball return guide way.

Ball screws are used contrary to power screws on the following arguments: ball screws have lower friction and higher efficiency (90% to 95% is typical). Advantages of this low friction are the backdrivability of the ball screw and there is little wear and little thermal effects.
Roller screws, which incorporate planetary rollers, are more efficient than ball screws because the planetary rollers have a similar helical to the spindle and they roll, whereas the ball in a ball screw are stowed forward. However, the efficiency of a roller screw is not significantly higher but the prices are.

Generally, ball screws are not backlash free, because they are form-closed without any pre-tensioning. To eliminate backlash in ball screws there are primarily two ways: one is to use two nuts which are pre-tensioned to each other (e.g. by a spring) and another way is to alter the shape of the helical grooves in such way that the balls have two contact points (actually small, but finite, areas), see Figure 2.11 (right).
In both cases, the friction increases and the efficiency drops a little. The concept with altered helical grooves is light weight and is the standard option of almost every supplier to eliminate backlash.

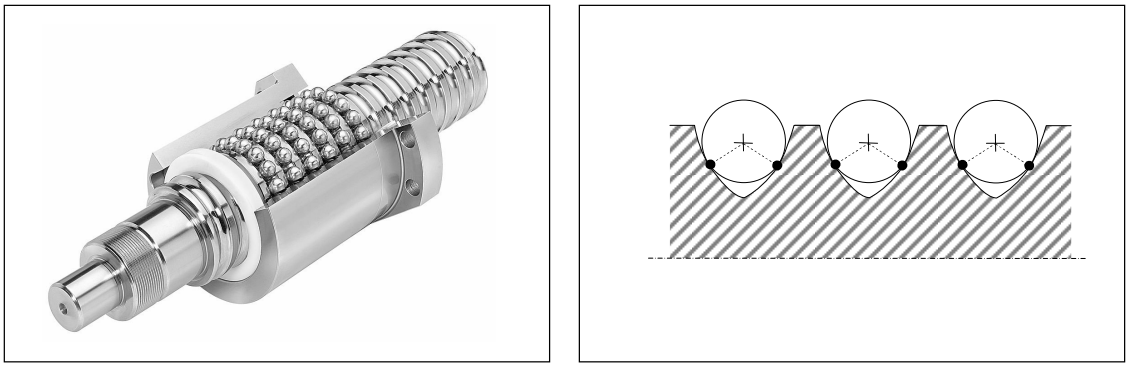

Figure 2.11: Ball screw open view (left) and a section view of a spindle with altered helical grooves to eliminate backlash (right).

The axial force of the nut can be calculated with (SKF, 2010):

$$F_{axial} = \frac{2\pi\eta T_{motor}}{p} \tag{2.3}$$

With T_{motor} the torque provided to the spindle by a (rotary) motor, the efficiency η of the ball screw and p the lead of the ball screw. With respect to operating life of the ball screw, it is important that a ball screw is loaded only with axial forces. With these parameters, also the ratio i can be calculated:

$$i = \frac{p}{2\pi} \tag{2.4}$$

Because this is a rotation to translation transmission, the ratio is not dimensionless but in [m/rad]. Because the lead of a ball screw actuation generally is in mm-range, the ratios are low and therefore, large reductions are possible, while the efficiency remains relatively high.

2.5 Design outline

The robot is designed to be human like. Accordingly, the COM of the robot should be located in the vicinity of its 'belly button'. The fact that joint actuators account for approximately one third of the weight (Buschmann et al., 2009), the actuations of a joint are in the 'parent' link: e.g. the knee actuation is in the upper leg and the ankle actuation in the lower leg.
Since the robot's mass and mass distribution have a strong influence on the dynamics, lightweight construction is of great importance. However, lightness of construction must be balanced with stiffness and the performance of the actuations in order to achieve the desired torques and velocities. High torque is of more importance than high velocity; since walking is expected to remain relatively slow for the coming years.

In the next chapters (3 and 4) the mechanical design is explained in more detail. Chapter 3 will elaborate on the design of the legs, consisting of an upper leg, a lower leg and a foot. Chapter 4 will clarify the design of the hip, waist and upper body.

On the next page an overview of the design is shown.

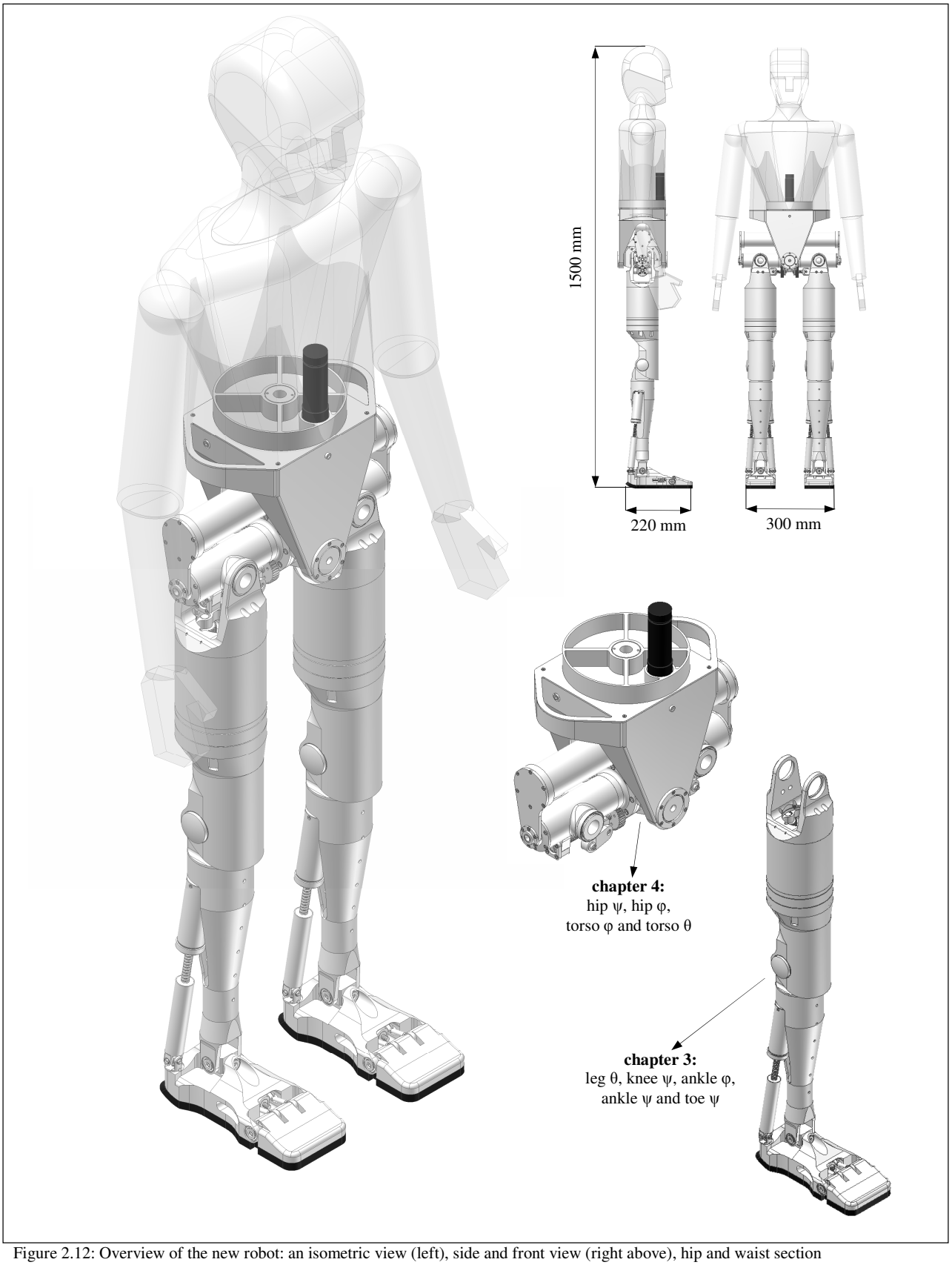

Figure 2.12: Overview of the new robot: an isometric view (left), side and front view (right above), hip and waist section (right middle) and a leg (right below).

Chapter 3
Joints and joint actuations of the legs

3.1 Design overview

This chapter explains in detail the mechanical design of the joints and the joint actuations of the leg. Each leg, from the hip down, consists of an upper leg (1), a lower leg (2) and a foot with a toe (3). It incorporates the following joints: leg θ, knee ψ, ankle φ, ankle ψ and toe ψ. This, and general dimensions of the leg, can be observed in Figure 3.1.

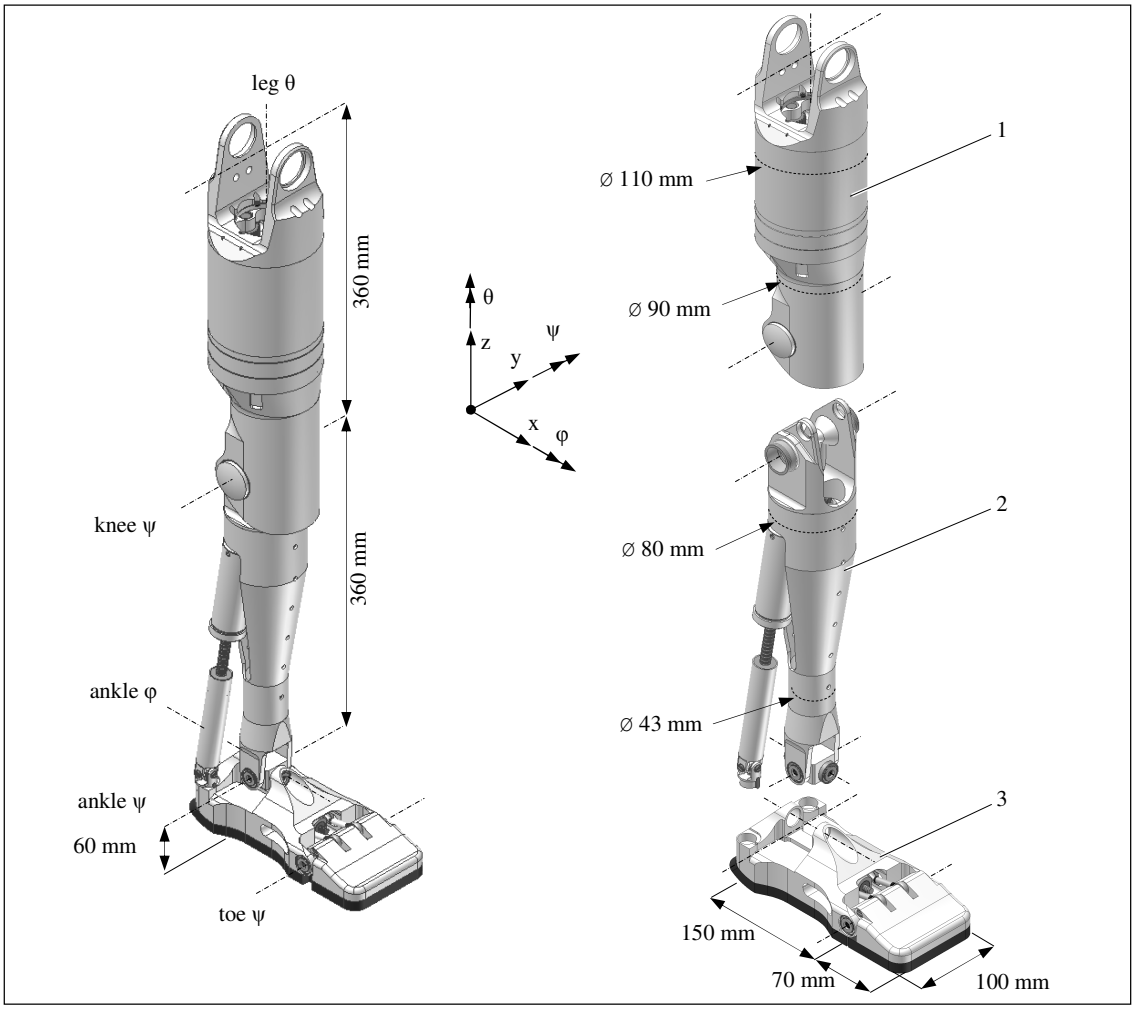

Figure 3.1: The leg (left) and the upper leg (1), the lower leg (2) and the foot with toe (3) exploded.

Joints and joint actuations
The joints: leg θ, knee ψ, ankle φ, ankle ψ and toe ψ, are each fully actuated over its entire ROM and actuated bi-directionally. Of every DOF, first the joint construction is explained, followed by a description of the actuation of this joint. After this detailed explanation of the design, the design is analyzed with respect to transmission ratio, transmission efficiency, joint torque, actuation stiffness and backlash.

Chapter outline
The upper leg is connected to the hip section through the hip φ joint, explained in chapter 4. The upper leg can be regarded as two separate links; the thigh section and the knee section which can rotate with respect to each other through leg θ. The connection of these links and its actuation is explained in section 3.2.
The upper leg is connected to the lower leg through the knee ψ joint, explained in section 3.3. The design of the actuation of this joint, which is mainly located in the upper leg, is also explained in this section.
In section 3.4, the construction of the lower leg and the design of the ankle joint are explained. The actuation of the ankle joint is a parallel actuation of two DOFs, being ankle φ, ankle ψ. Section 3.5 explains the reasoning behind this parallel actuation prior to the explanation of the physical design of this actuation.
The design of the foot, the toe joint and its actuation is explained in section 3.6.
The foot and toe also incorporate a sole. The sole will be the contact area with the ground and therefore this is an significant part of the robot. Ideas with respect to the sole(s) are given in section 3.7.
Some general concluding remarks about the leg, such the use of purchase components and the fabrication of parts as well as the total masses of the links are given in section 3.8.

3.2 Leg θ

Joint construction
As can be seen in Figure 3.2, the upper leg can be divided into two sections; the *thigh section* (1) and the *knee section* (2). The top part of the thigh section is the *upper leg hip connector* (3), which is connected to the hip section, explained in chapter 4.
The knee section is placed into the thigh section by means of a *crossed roller bearing* (INA FAG SX011814) (4) and a *single row needle roller bearing* (INA FAG K95X103X30) (5). These bearings share the same centerline (θ axis) so they fix x, y of the knee section with respect to the thigh section. Fixation of φ and ψ is done by placing the two bearings 99 mm from each other.
The outer ring of the crossed roller bearing is axially fixed to the thigh section by a *retaining ring* (6) with M3 bolts. The inner ring of the crossed roller bearing is axially fixed to the knee section by a *retaining ring* (7) with M3 bolts as well. The X-arrangement of the cylindrical rollers of the crossed roller bearing allows it to support axial forces (dynamically a maximum of 18 kN) in both directions. Therefore, this bearing is used to fix the z of the knee section. As a result, the only knee section's DOF with respect to the thigh section, is θ.

The crossed roller bearing can also withstand tilting moment loads; whereas the single row needle roller bearing over-constrains the design. However, it increases the tilting stiffness, and if the fitting tolerances are met, the assembly of the knee section into the thigh section is improved (thus friction is reduced). Instead of the crossed roller bearing a combination of two axial needle roller bearings could be used. Although this would be more light weight than a crossed roller bearing and the combination with a single row needle roller bearing would not be over constrained, this reduces the internal space in the upper leg due to the relatively small inner diameter. This is a major advantage of the crossed roller bearing because: this internal space is used for conductors that have to pass through the upper leg and the actuation of the knee also utilizes this space.

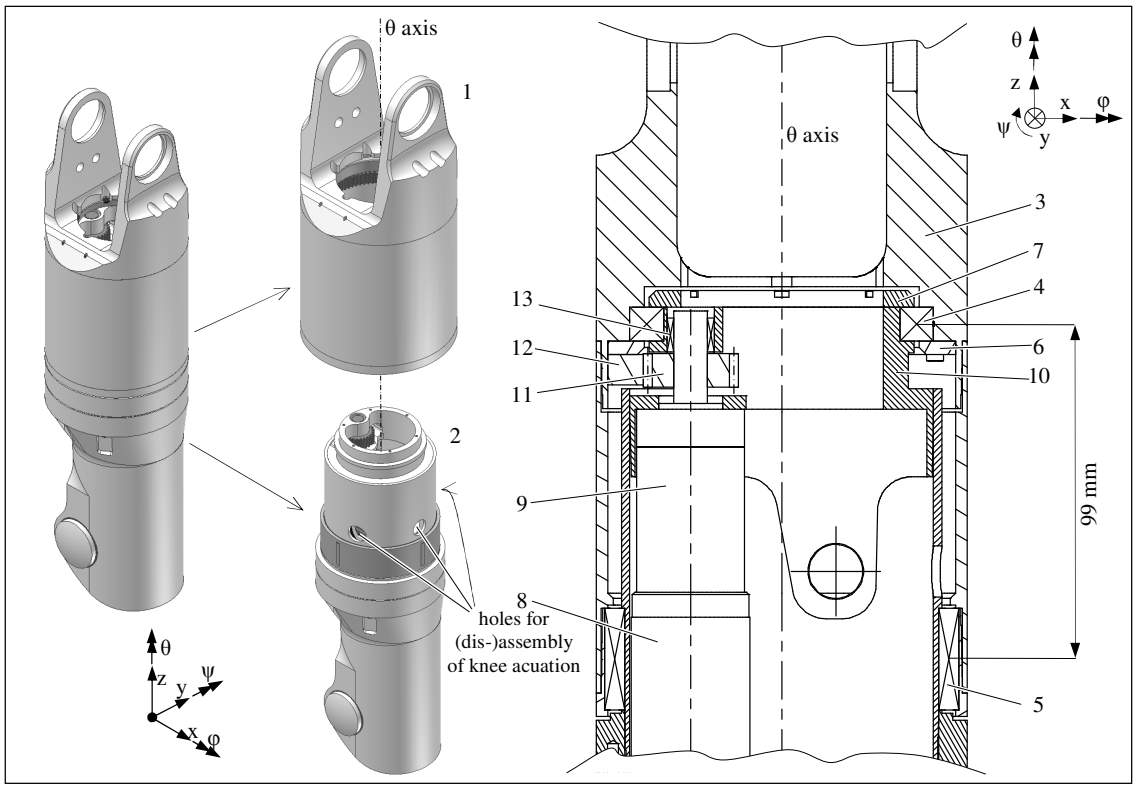

Figure 3.2: Assembled and exploded view of the upper leg with the thigh section (1) and the knee section (2) (left). A xz-plane section view (right) of the assembly of knee section into the thigh section; Thigh section (rough hatching), knee section (fine hatching), upper leg knee connector (3), crossed roller bearing (4), single row needle roller bearing (5) retaining rings (6,7), DC motor (8), planetary gearbox (9), motor bracket (10), pinion gear (11), ring gear segment (12), single row needle roller bearing (13).

Joint actuation

A *90 W motor* (8), from Maxon (RE35), is placed (by Maxon) at the input side of a *gearbox* (9). This gearbox is eccentrically placed with respect to the θ axis of the upper leg via a lead-in edge onto the *motor bracket* (10). This fixes x, y, φ and ψ of the gearbox. The z and θ of the gearbox are fixed by four M3 bolts. Now the gearbox output shaft can rotate freely (in θ) and parallel to the θ axis of the upper leg. On the gearbox output shaft, a *pinion gear*[p] (11) of m = 1 and with z = 26 is placed. The rotation of the shaft is transmitted to the pinion gear by a parallel key and the axial position of the pinion gear on the axle is fixed with e.g. glue. The pinion gear meshes with a 110° *segment of a ring gear* (12) of m = 1 and with z = 84 with internal teeth. This ring gear segment is placed into the thigh segment with a fitting edge, which fixes x, y, φ and ψ of the ring gear segment, and four M3 bolts fix z and θ of the ring gear segment. With this segment the knee section has a θ ROM of ± 45°, as stated in Table 2.1.

To reduce the radial force on the shaft of the gearbox, a *single row needle roller bearing* (INA FAG HK1010) (13) is placed at he shaft of the gearbox. The radial load capacity of needle roller bearings is compared to ball bearings. Needle roller bearings are more compact in radial direction than ball bearings and because of this, a needle roller bearing has been used here.

Due to the eccentric placement of the pinion gear, no intermediate or 'idler' gear is necessary; accordingly backlash will not increase and efficiency remains high. The final transmission ratio is i =

[p] Generally, gears can be characterized with a modulus m and the number of teeth z. The modulus is: $m = t/\pi$, with t the pitch width of the teeth. The pitch diameter d is related to the modulus and number of teeth with: $d = z \cdot m$.

26/84 (≈ 0.31). Another advantage of this eccentric placement is that the motor and gearbox are also eccentric, which provide space for conductors and e.g. knee ψ actuation.

Transmission ratio, transmission efficiency and joint torque
The gearbox (Maxon: GP 32 HP) is a three staged planetary gearbox with a transmission ratio of i = 1/51 (≈ 0.02), an efficiency of 70% and the nominal torque is 8 Nm (the intermittently permissible output torque is 12 Nm). Although the total actuation has an efficiency of about 68 %, the joint torque is increased significantly with respect to modified TUlip. The absolute, total transmission ratio is i = 13/2142 ($\approx 6.1 \cdot 10^{-3}$), which leads to a nominal joint torque of about 26 Nm and an intermittently permissible joint torque of about 39 Nm.

Actuation stiffness
The stiffness of the actuation is very high because the stiffness of the teeth, from the gearbox as well as from the final transmission is usually much higher than other transmissions e.g. belt and steel wire rope transmissions, (ball) screw transmissions and lever or rocker transmissions.

Backlash
Due to the final transmission, the backlash is reduced from 1° of the gearbox to 0.3° at the joint. Because leg θ is in line with the leg, the backlash, on the tip of the toe when the knee is stretched, is 0.9 mm.

3.3 Knee ψ

Joint construction
The knee ψ joint is one of the major weight bearing joints, it must cope with walking, running, bending, jumping and lifting objects. It also works in conjunction with the hip ψ joint and ankle ψ joint, assisting in static postures (like standing). This is why the knee is one of the most complex human joints: it must be capable of providing a lot of torque, while it must have a large ROM (135°) and its actuation must be compact to fit in the upper leg (surrounded by other joint actuations).

The robot's knee joint is depicted in Figure 3.3. The *upper leg knee connector* (1) has an U-shaped cross section area with the open end at the back of the leg (posterior). Each of the two sides (each side can be seen in Figure 3.3 right) has a hole in it; both are drilled in the same fixture and, consequently, the holes share the same centerline which is the knee axis. The *lower leg knee connector* (2), has two 'ears' with holes that are aligned in the same way as the holes in the upper leg knee connector (each ear can be seen in Figure 3.3 right). The holes are connected with the knee axle, consisting of an *axle* (3) and two *insert stops* (4). The insert stops have M20x1 thread and are screwed into the axle, lead-in edges in the ears and fitting edges on the insert stops ensure the distance between the ears and double the bending stiffness of the ears because the ears are now connected.

A set of *single row deep groove ball bearings* (INA FAG 61806-2RSR) (5), which are placed into the holes of the upper leg knee connector, fix x, z, φ and θ of the lower leg, because the insert stops fit in these bearings. In y-direction, the lower leg is fixed by *distance rings* (6) and *knee caps* (7), which form-close the inner rings of the bearings and the ears of the lower leg knee connector, because the knee caps have M30x1 thread, so, they can be screwed on the insert stops (which have corresponding thread). Because the knee axle is form-closed, the knee caps can be screwed on with high tension. This high tension ensures the axle, and thus the bearing inner rings, to rotate with the lower leg, so no sliding movement of bearing parts can take place.

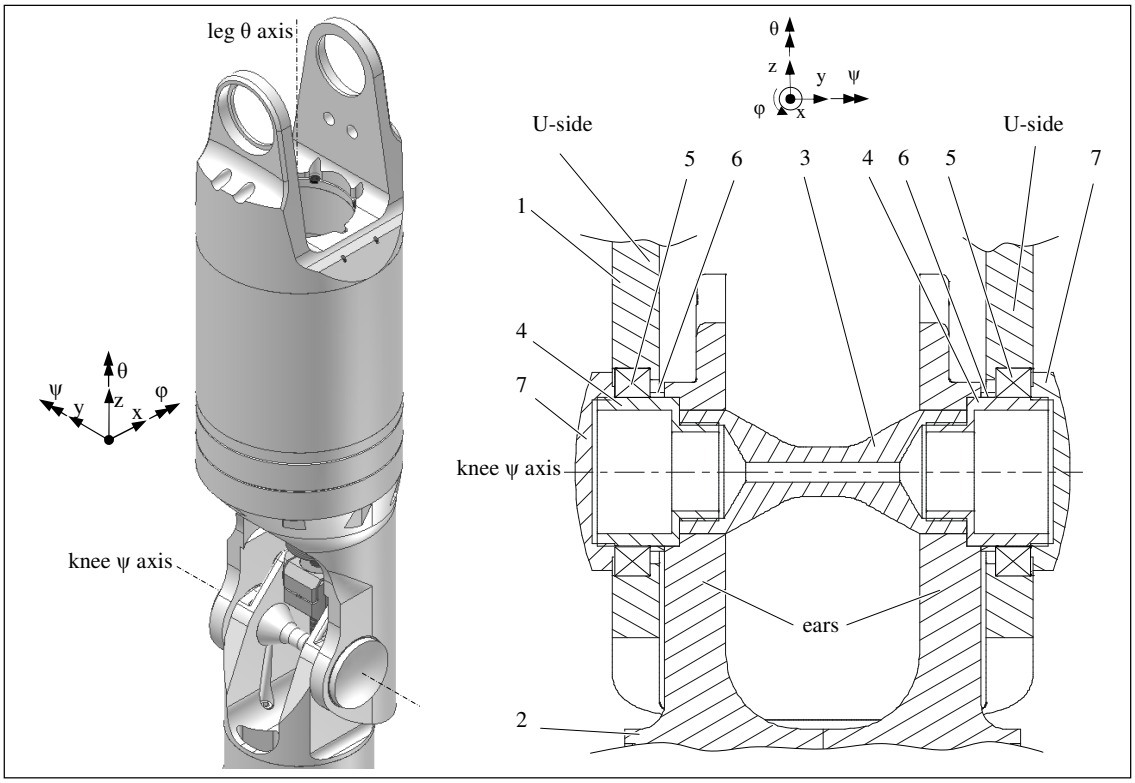

Figure 3.3: Posterior view of knee joint (left). Section view of knee joint, actuation made invisible (right); U-shaped cross section upper leg knee connector (1) with, lower leg knee connector with 'ears' (2), axle (3), insert stops (4), single row deep groove ball bearings (5), distance rings (6) and knee caps (7).

Joint actuation

Several design concepts for the actuation of the knee have been investigated. An overview of these concepts (and a short discussion that evaluates these concepts) is given in Appendix D.

The chosen concept can be described as a direct ball screw actuation, consisting of a motor that drives a ball screw spindle and a ball screw nut that can translate over this spindle. To prevent the motor from rotating, it needs to be fixed with a universal joint. To prevent the ball screw nut from rotating, it needs to be fixed with a universal joint as well. The motor is fixed to the upper leg and the ball screw nut to the lower leg: due to the eccentric fixation of the ball screw nut, with respect to the knee ψ axis, the translation of the nut forces the lower leg to rotate around the knee ψ axis.

The knee joint actuation is shown in Figure 3.4. The *motor bracket* (1) (see also Figure 3.2) has two ears (pointing downwards), each with one hole, of which the axes are coinciding and in which a *single row deep groove ball bearing* (INA FAG 61800-2RSR) (2) is inserted. These bearings share the same centerline and so they fix an *intermediate body* (3) in x, z, φ and θ via two *fitting bolts* (4). The holes where these bolts fit in, are drilled in the same fixture, to ensure alignment of the centerlines of the fitting bolts.
Between the inner rings of the bearing, the intermediate body is fixed in x through two *distance rings* (5). The intermediate body is now free; only in ψ. The intermediate body fixes x, y, z, ψ and θ of the *cup end* (6), via a *fitting bolt* (7) and two *plain bearings* (8). From the motor bracket to the cup end, this functions as a universal joint; the cup end is free in φ and ψ.

Through six *M3 bolts* (9) and a dowel pin (not depicted), the cup end is screwed on the *motor cup* (10) via a lead-in edge. This motor cup has a flange on which the head of a *150 W motor* (11), from Maxon (RE40), is placed with a lead-in edge and six *M3 bolts* (12). This lead-in edge determines that the centerline of the motor intersects with the center of the aforementioned universal joint.

A *flange* (13) is screwed on to the *ball screw spindle* (14), with a nominal diameter of Ø 10 mm, which is fitted on the motor axle. As a result, the spindle and the motor share the same centerline and the ball screw spindle has the same θ orientation as the rotor of the motor because it is secured with e.g. a set screw.
Due to a fitting hole in this flange, that fits on the ball screw spindle, the bearing-faces of this flange are perpendicular to the spindle axis. Two *axial needle roller bearings* (INA FAG AXK1528) (15) fix the spindle to the motor cup in z, φ and ψ. The axial needle roller bearings are held into place by a *cover* (16) and an *axial bearing washer* (INA FAG AS1528) (17). The cover is screwed onto the motor cup and the cover and the axial bearing washer have lead-in edges, so alignment is ensured. Because the flange, the cover and the bearing washer all have bearing-faces, on which the needle rollers are intended to roll, they are made from hardened steel to prevent the needles wearing out the bearing-faces due to the Hertzian contact.
To prevent the tension on the needle rollers to decay, the cover needs to be locked. This can be done with e.g. a retaining ring with internal thread that can be screwed on the thread of the motor cup, prior to the cover. If the cover is screwed on properly, the retaining ring can be screwed back against it. (In this case; the thread of the motor cup needs to be elongated.)

The radial bearing inside the motor (Maxon, 2010) is used to fix the spindle in x and y because the motor is placed in the motor cup by a lead-in edge. The other end of the spindle is free, so, θ of the spindle is the only ‘free’ DOF and thus, it is statically constrained.

The *ball screw nut* (18), on the spindle, is screwed into the *universal joint* (19), prior to locking it with a set screw (but gluing is also an option), so z and θ of the nut are fixed. The universal joint is fixed on the *lower leg knee connector* (20), eccentrically to the knee axis, through two *fitting bolts* (21). The holes in the universal joint have lead-in edges to ensure coinciding axes of these fitting bolts. These fitting bolts also fit into the inner ring of two *single row deep groove ball bearings* (INA FAG AXK1528) (2), and thus, fix x, z, φ and θ of the universal joint. Two *distance rings* (22) fix the universal joint in y. The universal joint has an internal DOF; the φ axis, which intersects with the ψ axis, is created with an elastic hinge. So, the nut has two DOFs: φ and ψ, and it functions as a universal joint.

The *upper leg knee connector* (23), in which the knee joint itself is located, is screwed onto the *knee section* (see section 3.1) by 7 *M4 bolts* (24). This is assembled in this way, to be able to disassemble the upper leg quickly and to provide good access to parts for e.g. maintenance. The upper part of the knee section, an aluminum tube (Ø95mm × 2mm), has three holes in it, see Figure 3.2 left, so the fitting bolts (4, 7) can be (dis-) assembled easily, and then, the whole actuation can be taken loose from the knee section (while it is still attached to the lower leg).

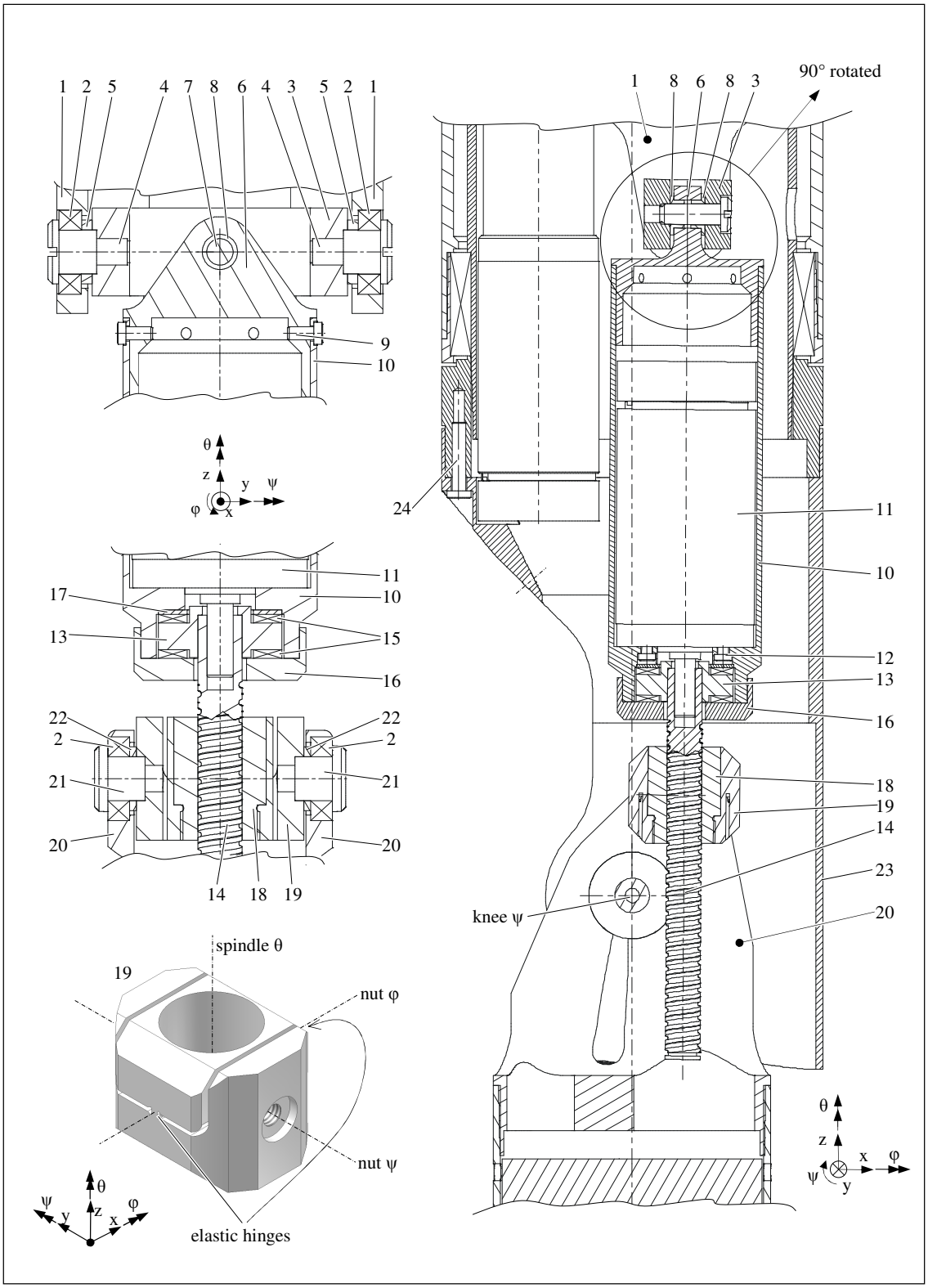

Figure 3.4: Section view (xz-plane) of the upper leg (right) and two section view details of the ball screw actuation (above left and middle left); motor bracket (1), single row deep groove ball bearings (2), intermediate body (3), fitting bolts (4), distance rings (5), cup end (6), fitting bolts(7), plain bearings (8), M3 bolts (9), motor cup (10), Brushed DC motor (11), M3 bolts (12), flange (13), ball screw spindle (14), axial needle roller bearings (15), cover (16), axial bearing washer (17), ball screw nut (18), universal joint (19), lower leg knee connector (20), fitting bolts (21), distance rings (22), upper leg knee connector (23), M4 bolts (24). The universal joint (19) is shown below left.

The extreme positions of the lower leg with respect to the upper leg are shown in Figure 3.5.

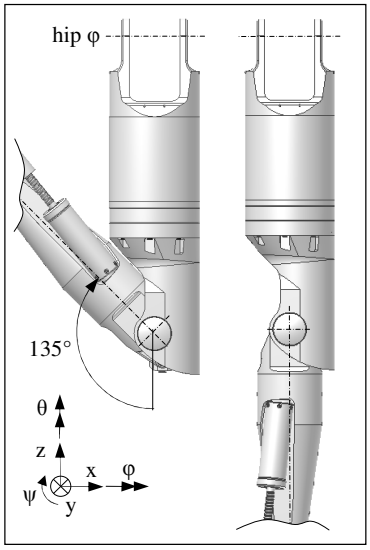

Figure 3.5: Sagittal view of the extreme positions of the knee joint: fully bent (left) and fully stretched (right).

As can be seen in Figure 3.5 (right), the upper leg knee connector is cut out at the back (posterior) so that it does not obstruct the lower leg when the knee is fully bent; knee $\psi = 135°$, see Figure 3.5 (left). The lower leg knee connector also ends below (see Figure 3.4) the knee axis to protect the ball screw from anterior impacts on the knee.
An anterior ball screw actuation has major advantages:

- it does not obstruct the lower leg while bending,
- when the robot has to stand up, which is considered to the heaviest load: the ball screw is under tension,
- the current 150 W motor can easily be replaced by a larger motor, implying that the actuation obtains more power.

Transmission ratio, transmission efficiency and joint torque
With this ball screw actuation, a ratio dependent on knee ψ, which is defined with $i = \psi_{knee}/\theta_{motor}$, is realized, see Figure 3.6.

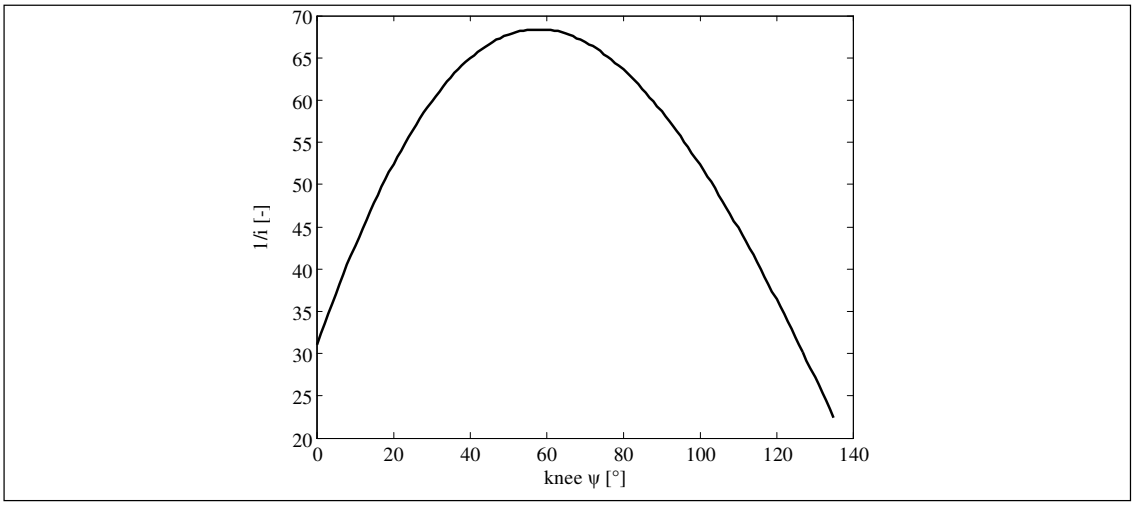

Figure 3.6: Reduction of the actuation in 1/i, dependent on knee ψ.

The efficiency of the actuation is about 90 %, because the transmission is a ball screw. The ball screw has a nominal diameter of Ø 10 mm and a lead of 3 mm. From this and the kinematics, the knee joint torque is computed, nominal torque as well as a stall torque. This is shown in Figure 3.7.

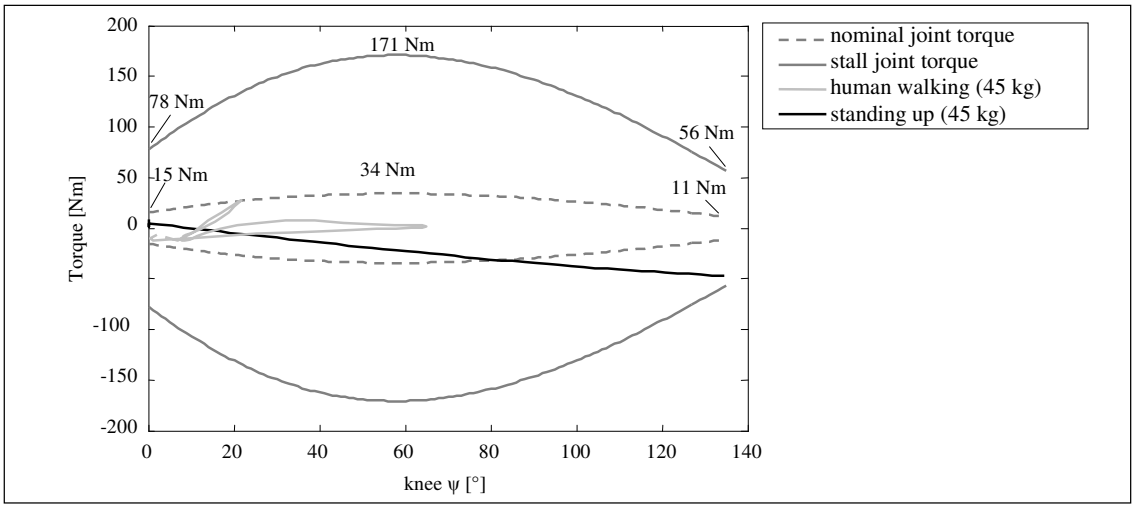

Figure 3.7: Nominal and stall joint torque v.s. human walking and standing up torque if the total body mass is 45 kg. Note that nominal and stall joint torque can be provided in both positive and negative directions.

As can be seen in Figure 3.7, the knee joint has ample torque for walking; almost the whole stride can be realized with nominal joint torque. Even a 'very heavy duty' task like standing up from a squatting position can be performed.

Actuation stiffness

The stiffness from the upper universal joint to the lower universal joint can be regarded as three springs in series. The axial stiffness of the motor cup is $c_1 = 13 \cdot 10^7$ N/m, and the varying axial stiffness $c_2(\psi)$ of the spindle (effective length depends on knee ψ) and the contact stiffness of the nut (via the balls) on the spindle is estimated on $c_3 = 10 \cdot 10^7$ N/m. The replacement stiffness c can be determined with:

$$\frac{1}{c} = \sum_{j=1}^{n} \frac{1}{c_j} \tag{3.1}$$

With j the index of the stiffness and n the total number of stiffnesses. Together with the effective radius r of the spindle axis, c can be converted to a rotational stiffness: $k = cr^2$, see Figure 3.8.

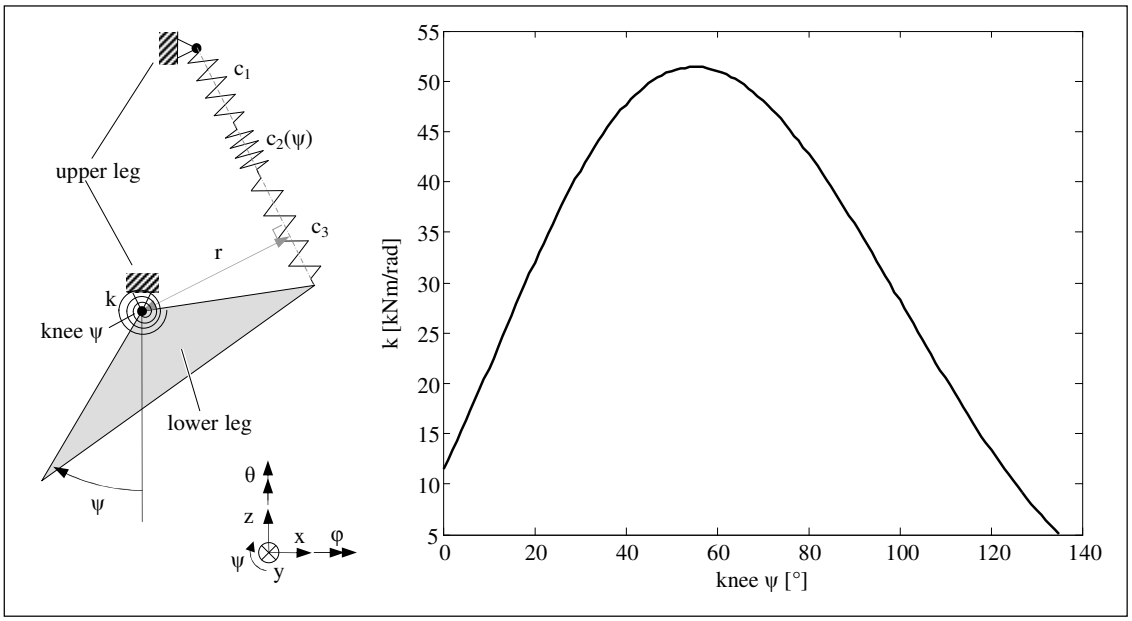

Figure 3.8: Rotational stiffness k (estimation) of the knee actuation, dependent on knee ψ (right) and a schematic view of the kinematics (left).

The axial stiffness of the axial needle roller bearings is assumed to be significantly higher, so the spindle is assumed to be rigidly attached to the motor cup. Figure 3.8 shows that the stiffness at the extreme positions of the lower leg is larger compared to modified TUlip's knee actuation stiffness (5 kNm/rad), and in between this stiffness is increased significantly.

Backlash
As mentioned in section 2.4, the backlash can be eliminated with a ball screw spindle that has altered helical grooves. With this option there will be zero-backlash in the actuation of the knee.

Buckling of the actuation
Because the knee can be actuated into two directions, there are cases, when the actuation is under a compression load and therefore, the actuation must withstand buckling. If buckling occurs, it will be somewhere between the two universal joints. The motor cup has a bending stiffness of around 30 kNm/rad. With the number of needle rollers n and the radial stiffness of the needle rollers c_{roller} of the axial needle roller bearings, the tilting stiffness of the two axial needle roller bearings can be determined with:

$$k_{tilt} = 2 \cdot k_{tilt,bearing} = 2 \cdot \frac{n}{2} c_{roller} r^2 = n \cdot c_{roller} r^2, \tag{3.2}$$

With r the average radius of the needle rollers. Due to the (relatively) high stiffness of the rollers the tilting stiffness of the axial needle roller bearing is also (relatively) high, so, the 'weakest part' of the actuation is the ball screw spindle. Because both ends of the actuation are universal joints, the buckling force can be calculated with:

$$F_{buckling} = \frac{\pi^2 EI}{L^2} \tag{3.3}$$

In this equation, E is the Young's modulus, I the moment of inertia, and L the effective length of the spindle (from the center of the nut to the first axial needle roller bearing). From this, the buckling force can be computed, see Figure 3.9.

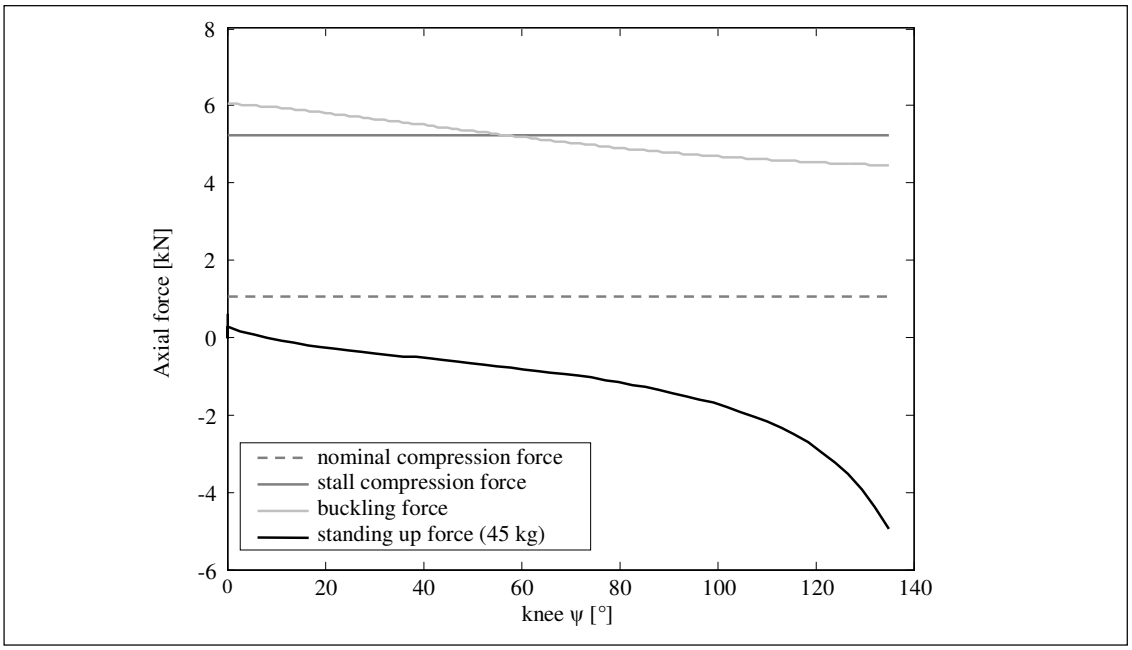

Figure 3.9: Axial forces in the ball screw spindle.

From Figure 3.9, a major advantage of this design can be observed. A direct ball screw actuation on the front of the upper leg implies that the ball screw is under tension, contrary to compression, if trajectories with high torque must be performed, so buckling does not occur.

Universal joints and elastic hinge design
The universal joints incorporate fitting bolts (4,7 and 21 of Figure 3.4) which function as the axles of the joint. Each axle is constructed with the 'double shear' principle. This implies that the fitting bolts experience a shear stress on two cross sections, so bending does not occur. The maximum allowable shear stress τ_{max} can be derived from the material property; yield stress σ_{yield}. Through $\tau_{max} \approx \sigma_{yield}/\sqrt{3}$, this yield stress can be derived with:

$$\sigma_{yield} = \frac{F_{radial}\sqrt{3}}{2A} \tag{3.4}$$

In which, F_{radial} is the radial force on the fitting bolt, in this case the axial load of the actuation, and 2A is the double cross section of the fitting bolt. All fitting bolts have a diameter of Ø 6 mm and the maximum axial force of the actuation is around 6 kN, so a material with a minimum yield strength of 184 MPa has to be chosen for these fitting bolts. Fitting bolts normally have yield strength of > 500 MPa.
These pins could be used as 'shear pins', which implies that they are allowed to break if a certain force is applied. However, this is not advised; if such a pin would break, the actuation mechanism will be able to move freely in the leg, and it is very likely that damage to other components of the upper leg, e.g. the leg θ actuation, would occur.

The ψ axes of both universal joints have a relatively large ROM. In accordance, these axles are supported with single row deep groove ball bearings. A φ motion of these universal joints only occurs when misalignments in the construction, due to tolerances, are present. Therefore, these axes have a small ROM, and thus, the upper universal joint has plain bearings and the lower universal joint has elastic hinges. Each elastic hinge is dimensioned as depicted in Figure 3.10.

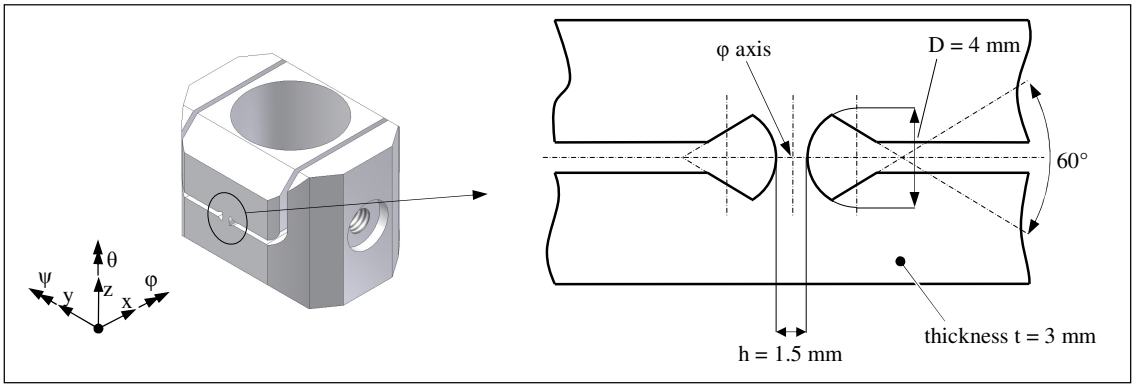

Figure 3.10: Elastic hinge dimensions of the universal joint. Note that the universal joint is symmetrical in the yz-plane, so at the back an identical elastic hinge is present.

These elastic hinges are designed to have a large ratio between the dam's axial stiffness and the dam's bending stiffness. The axial stiffness needs to be higher than the aforementioned nut stiffness of $10 \cdot 10^7$ N/m, and the bending stiffness needs to be low in order to let the elastic hinge act like a pivot. From (Rosielle, 2007), the axial stiffness could be computed with:

$$c_{axial} = 0.48Et\sqrt{\frac{h}{D}}, \tag{3.5}$$

and the bending stiffness with:

$$k_{bend} = 0.093 E t h^2 \sqrt{\frac{h}{D}}. \quad (3.6)$$

In both equations, E is the Young's modulus and h, D and t are the dimensions like depicted in Figure 3.10. With E = 210 GPa, the axial stiffness is around $19 \cdot 10^7$ N/m and the bending stiffness is around 80 Nm/rad. Because the universal joint has two elastic hinges that work in parallel, the axial stiffness and the bending stiffness can be doubled, $38 \cdot 10^7$ N/m and 160 Nm/rad (≈ 3 Nm/°) because the hinges work in parallel.

3.4 Lower leg and ankle joint

Lower leg construction

The lower leg functions are: to connect the ankle to the knee with high stiffness and to fix the actuation of the ankle axes, while remaining light weight. For the greater part, the lower leg is thin walled (thickness 2 mm) to reduce the mass significantly whereas the stiffness approximately remains, because the forces pass through at the 'ultimate fibers'. Therefore, the outer diameter is as large as possible within the acceptable space of the lower leg.

The lower leg, depicted in Figure 3.11, basically consists of three components. The *lower leg knee bracket* (1) is glued into the *lower leg base* (2). At the other end of this base, the *lower leg ankle bracket* (3) is glued. Both brackets are glued into the base by an increasing glue-gap, in three stages of 0.1 mm. Because of the increasing glue-gap, the stress concentration in the glue is reduced. Consequently, less shear stress will occur in the glue-gap if the base is subjected to torsion due to applied torque. With a maximum allowable shear stress of the glue of e.g. 5 MPa, the maximum torque can be 300 Nm (the maximum axial force can be 15 kN) before the glue fails.
Through a fitting edge, the centerline of the base is coinciding with the centerline of the brackets. The knee ψ axis and ankle ψ axis are orientated parallel and in the Frontal plane by dowel pins in the base and the two brackets. After this alignment they are glued. Symmetric gluing determines that no internal stresses are introduced into the construction which can cause misalignment of the axes.

The base consists of a *cone* (2a) and a *septum* (2b). The cone has two cut gaps, see Figure 3.11 left above. These gaps are to let the ball screw actuations of the ankle φ and ankle ψ axis move freely (see section 3.4). On the xz plane of the cone, the septum is plug welded into the cone; hereto holes are machined into the cone (anterior and posterior). The septum increases the bending stiffness in the xz-plane, which is proportional to the septum's x-width^3. This increased stiffness is advantageous, since walking is mainly done in the x-direction.
Due to the gaps and the septum, the base has an I-shaped cross section for length 159 mm, shown in Figure 3.11 right. Between the cone and the septum there are two 'folding lines'; at the intersections of the septum with the cone, and the torsion stiffness is significantly increased by fixing the cross sections at the top and bottom of the cone and septum by the two brackets (2 and 3). Due to the plug welding, only limited internal stresses are introduced. So, after this welding, the upper and lower ends of the cone are finish machined to ensure that the fitting edges are of proper roundness and that the centerlines are coinciding to let the lower leg knee and ankle bracket fit properly.
Because the base is thin walled, it provides much space inside for conductors and possibly other electrical systems like e.g. printed circuit boards (PCBs). Therefore both brackets provide passage for conductors. The cone could have some drilled holes to fasten some electrical components; if there are few and with a small diameter (like e.g. Ø 4 mm), the stiffness is not affected.

Ankle joint construction

The ankle joint is designed as a universal joint see Figure 3.11 left. The lower leg ankle bracket has two 'ears' which together fix x, y, z, φ, and θ of an *intermediate block* (4), through two *single row*

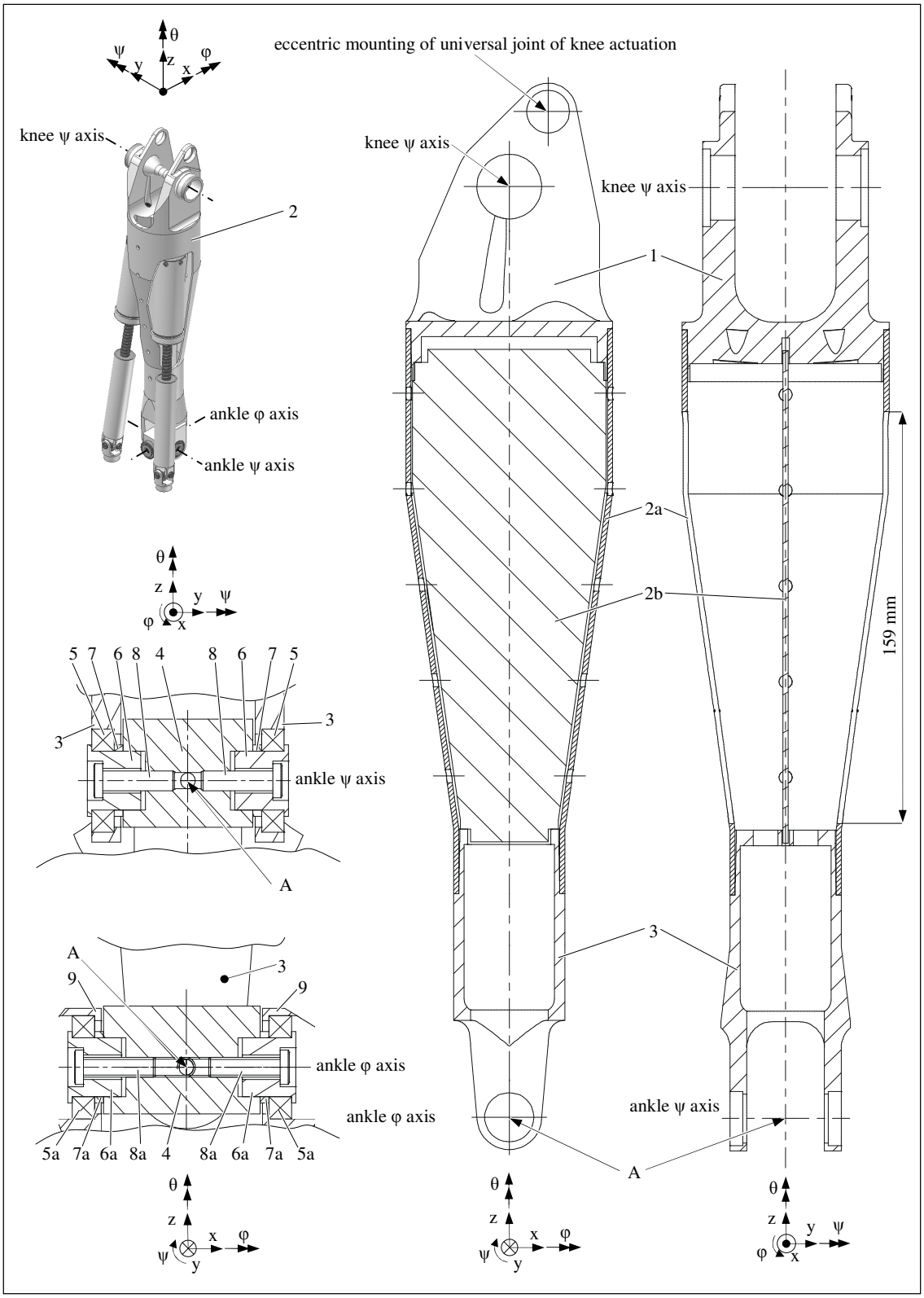

Figure 3.11: Isometric posterior view of the lower leg (left above), two section views of the lower leg construction; xz plane (middle) and yz plane (right) and two section views of the ankle joint; xz plane (left below), yz plane (left middle): lower leg knee bracket (1), lower leg base (2) with a cone (2a) and a septum (2b), lower leg ankle bracket (3), intermediate block (4), single row deep groove ball bearings (5,5a), bushes (6,6a), distance rings (7,7a), M4 bolts (8,8a), foot (9).

deep groove ball bearings (INA FAG 61800-2RSR) (5), two *bushes* (6), two *distance rings* (7) and two *M4 bolts* (8). The intermediate block is form-closed between the ears, so the bolts can be screwed on with high tension. This intermediate block subsequently fixes x, y, z, ψ, and θ of the *foot* (9) with the same components (5a, 6a, 7a and 8a). Each of the ears of the lower ankle bracket has its own bending stiffness, so, by connecting the two ears (via the intermediate block bearing units) the total bending stiffness increases significantly because the bending stiffness of each ear now works in parallel with the other.
At this point, the foot has two DOFs: φ and ψ. The φ and ψ axes intersect in one point, through which the centerline of the lower leg also passes (point A, see Figure 3.11). This centerline, which is also the hip θ axis when the knee is stretched, intersects with the knee axis, so the kinematic configuration, as stated in Figure 2.1, is ensured.

3.5 Ankle φ and ankle ψ

It is favorable for a high location of the robot's total COM, to have both actuations of ankle φ and ankle ψ in the lower leg. Therefore, the DC motors, which have a (relatively) large mass, need to be as high in the lower leg as possible. Another advantage of the high placement of the motors is the ROM of ankle φ and ankle ψ. Motors and transmissions need space, thus; the closer to the actual axis these are, the more they affect the ROM and probably even obstruct parts of the ROM. Placing the motors 'away' from the joint itself means that the ROM is not obstructed anymore.
Ball screw actuations can facilitate this high placement in the lower leg. If the ball screw actuation is fixed on both ends with a universal joint, the ball screw is only loaded with axial forces (if the centers of the universal joints intersect with the axis of the ball screw). Considering the ball screw actuations as linear actuators, is integral.

Kinematics of the actuation
To actuate in two DOFs, i.e. ankle φ and ankle ψ; the (most obvious) solution involves two actuators. For example, each actuator is fixed on one end to the lower leg and at the other end to the foot, like depicted in Figure 3.12.

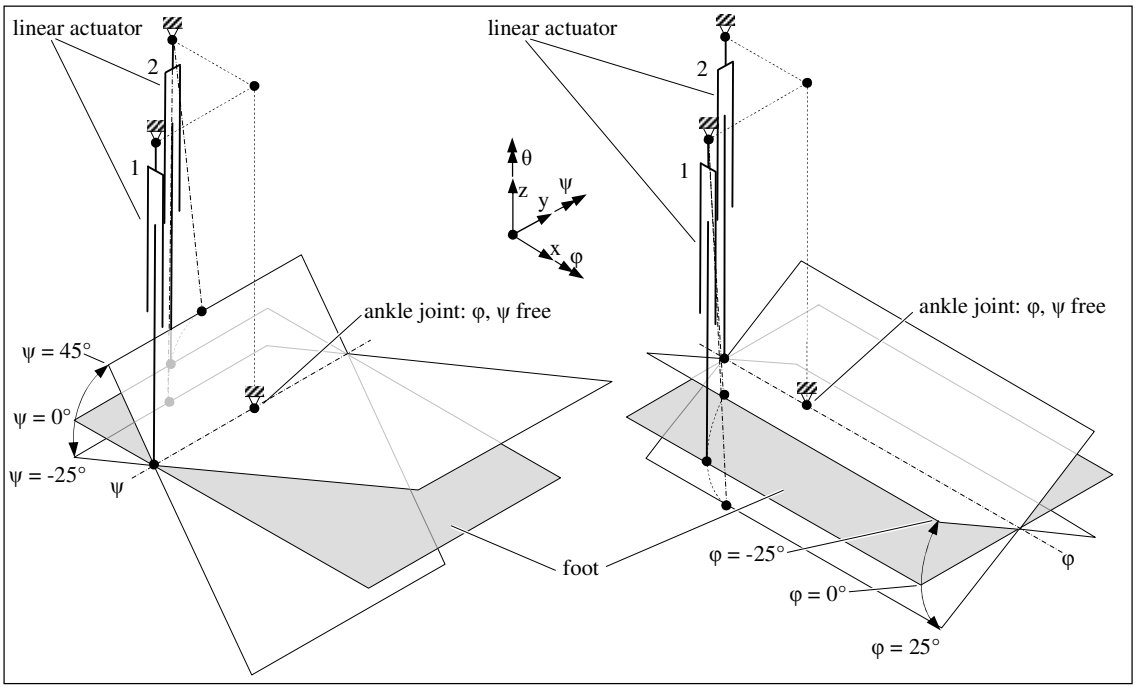

Figure 3.12: Kinematic representation of the ROM of ankle φ and ψ. Linear actuators are placed on the ankle φ and ψ axes. If actuator 1 has nominal length (thus φ = 0°), the ψ ROM can be fully passed through, by elongation or shortening actuator 2, without elongation of actuator 1 (left). The same holds for actuator 2 if the φ ROM is passed through with ψ = 0° (right). If both angles are non-zero, this does not hold anymore and both actuators have to have elongations (not depicted).

In this figure, the ankle joint is not a ball joint; it is a universal joint, implying that θ of the foot is fixed. If one angle (ankle φ or ankle ψ) is zero, then the actuation end of one linear actuator is exactly on the axis of rotation and the actuation does not have to perform work (see Figure 3.12). However if both angles are non-zero, a change of one angle effects the elongation of the other actuator. So, if a ψ rotation has to be performed, and φ is non-zero, the configuration of Figure 3.12, comprises a 'parasitic' elongation of actuator A.

If a gait is performed, the movement of the ankle is merely in ψ, and if the robot is 'side stepping' the movement of the ankle is merely in φ. Moreover; for the majority of possible movements of the robot; the ankle is used either often in ψ or either only in φ. As a result, no combinations of φ and ψ, in a ratio that is close to $\varphi / \psi \approx 1$ will occur often.

A way to use each linear actuator such that it provides the most torque for the aforementioned movements is to place the actuators in a 45° angle between the ankle φ and ankle ψ axes, like depicted in Figure 3.13.

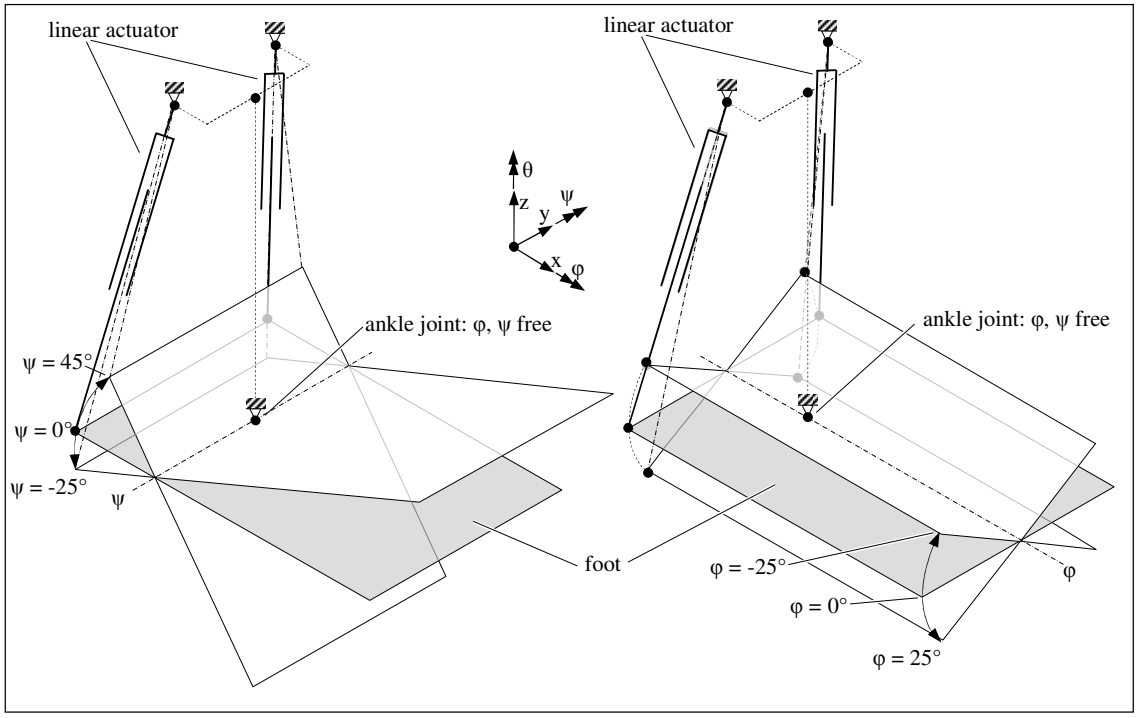

Figure 3.13: Linear actuators on the corner points at the back of the foot. Both actuators have to elongate or shorten together to move about ψ (left). If one actuator is elongated while the other actuator shortens, a φ rotation is performed (right).

Now if a rotation about ψ has to be performed, both linear actuators have to elongate or shorten a significant part. The movement is not 'parasitic' anymore; moreover, the linear actuators provide forces that are in the same order of magnitude. If φ = 0°, the elongation or shortening is exactly the same.
This also holds for a rotation about φ: both linear actuators have to elongate or shorten a significant part, only the direction of the force is opposite. If φ = 0°, the elongation of one actuator is equal to the shortening of the other.

Another advantage of placing the actuators in a 45° angle between the ankle φ and ankle ψ axes, is that the absolute distance from ankle joint to end point of an actuator on the foot is √2 times larger than if the actuator ends are placed on the ankle φ and ankle ψ axes. So, if a rotation is performed about a rotation axis that is in a 45° angle between the ankle φ and ankle ψ axes, the moment arm of this actuator is at its maximum, although it is expected that this will not occur frequently. This is

advantageous because in this particular case, the other actuator performs no work: its end is exactly on the rotation axis so no elongation or shortening of the actuator is performed.

If the actuators ends are fixed to the front of the foot, the moment arms could be increased, but the ball screws are under compression if the robot has to perform a movement like standing up from a squatting position (see Appendix C). It is better to have a ball screw under tension, to avoid buckling and backlash. Another advantage is the esthetics of it: humans have a 'calf muscle' (the Latin name for this muscle is *Gastrocnemius*) at the back of the lower leg (posterior) as well.

Construction of ball screw actuation
The construction of a ball screw actuator is depicted in Figure 3.14. Basically, each ball screw actuator contains a motor that is prevented from rotating about its centerline by the upper universal joint. The rotor (of the motor) actuates a ball screw spindle. A ball screw nut, in a 'sleeve', is prevented from rotating around its centerline by the lower universal joint at the end of the sleeve. Now, the nut can translate over the spindle axis to actuate the foot.

The *lower leg knee bracket* (1), has two fitting holes drilled in it, each with a parallel key way. These holes are oriented towards the center of the universal joint of the actuation on the foot. The *universal joint bracket 1* (2) is placed into the hole. Through a *M5 bolt* (3), this universal joint bracket is fixed in x, y, z, φ and ψ. The universal joint bracket has a parallel key way as well and the universal joint bracket is fixed in θ by a *parallel key* (4×4×10 mm) (4).
In the 'ears' of the universal joint bracket there are two holes drilled; in the same fixture, the centerlines are coinciding. In these holes, *plain bearings* (5) (from e.g. sintered bronze) are placed.
An *intermediate block* (6) has four potholes with a lead-in edge and M4 thread. Two opposite holes share the same centerline. This intermediate block is placed between the raised edges of the plain bearings and then, two *universal joint axles* (7), with a screw slot, are screwed in. These axles have a fitting edge, which fit into the lead-in edges of the intermediate block and also function as a bearing surface for the plain bearings. The axles are made of hardened steel to have a bearing surface that wears minimally and to have a high yield strength to be able to withstand more radial force.
The intermediate block is now fixed in x, y, z, ψ and θ. The *cup flange* (8) has the same ears as the universal joint bracket. So, through two plain bearings and two universal joint axles this cup flange is fixed in x, y, z, φ and θ with respect to the intermediate block. Therefore, the cup flange is now fixed in x, y, z and θ.

The cup flange fits in the lead-in edge of the *motor cup* (9) and is screwed onto it, using six M3 bolts. This lead-in edge ensures that the centerline of the motor cup intersects with the center of the universal joint.
The motor cup has a flange, on which the head of a *60 W motor* (10), from Maxon (RE30), is screwed on with six *M3 bolts* (11). Through a lead-in edge, the centerline of the motor is coinciding with the centerline of the motor cup.

A *flange* (12) is screwed onto the *ball screw spindle* (13), which has a nominal diameter of Ø 10 mm, and is fitted onto the motor axle. So, the spindle and the motor share the same centerline and the spindle takes over the θ orientation of the rotor of the motor, through e.g. a set screw.
Due to a fitting hole in the flange, the bearing-faces of this flange are perpendicular to the spindle axis. Two *axial needle roller bearings* (INA FAG AXK1528) (14) fix the spindle to the motor cup in z, φ and ψ. The axial needle roller bearings are held into place by a *cover* (15) and two *axial bearing washers* (INA FAG AS1528) (16). The cover is screwed onto the motor cup and the axial bearing washers have lead-in edges, so alignment is ensured. Because the flange needs to have bearing-faces, on which the needle rollers are intended to roll, like in the knee actuation, they are made from hardened steel to prevent the needle rollers wearing these bearing-faces.
Like in the knee actuation, the cover needs to be locked with e.g. a retaining ring to maintain the tension on the needle rollers.

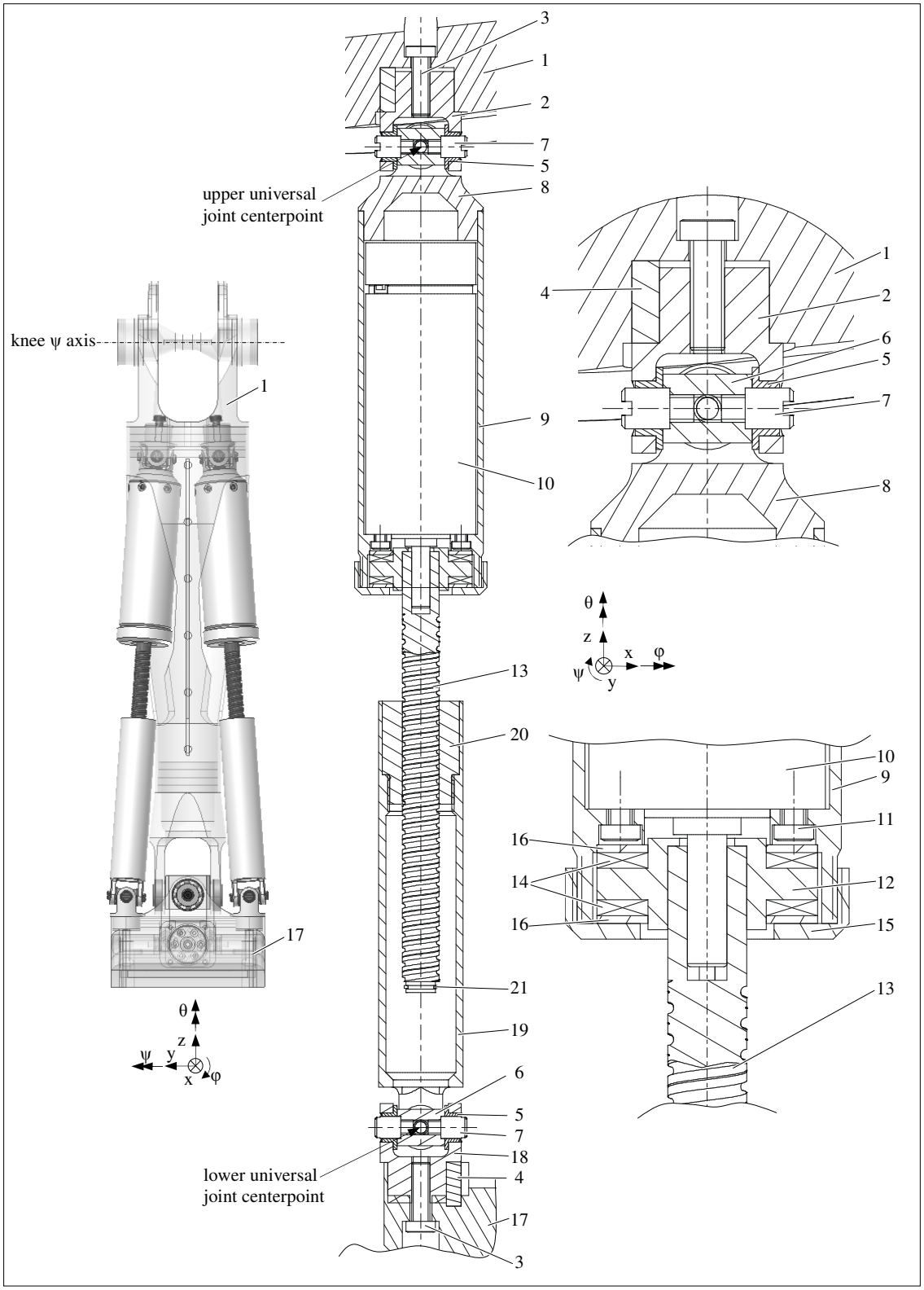

Figure 3.14: Construction of a ball screw actuator. Posterior view with all components, except the ball screw actuators, made transparent (left). A ball screw actuator section view (middle) and two details: the upper universal joint (right above) and the motor to spindle assembly (right below): lower leg knee bracket (1), universal joint bracket 1 (2), M5 bolts (3), parallel keys (4), plain bearings (5), intermediate blocks (6), universal joint axles (7), cup flange (8), motor cup (9), DC motor (10), M3 Bolts (11), flange (12), ball screw spindle (13), axial needle roller bearings (14), cover (15), axial bearing washers (16), foot (17), universal joint bracket 2 (18), sleeve (19), ball screw nut (20), retaining ring (21).

The *foot* (17), has two fitting holes drilled in it (at the back corners of the foot). The *universal joint bracket 2* (18) is placed in the hole, in the same way as the universal joint bracket 1 is mounted to the lower leg knee bracket. This universal joint bracket 2 is not directed towards the center of the upper universal joint because it would not be able to pass through its full ROM. In addition, to have a larger ROM, the universal joint bracket has slightly slimmer ears than the upper universal joint bracket.
In the same way, and with the same components as the upper universal joint, a *sleeve* (19) is fixed in x, y, z and θ to with respect to the foot. This sleeve is hollow in order to let the spindle penetrate. At the top end of the sleeve, a *balls screw nut* (20) is screwed in. This nut is fixed to the sleeve in x, y, z, φ and ψ by a fitting edge and the screwing thread, fixation of θ is done with a set screw. Alternatively, the nut can be glued into the sleeve.
At the end of the spindle, a *retaining ring* (21) is placed to ensure that the nut remains on the spindle. Now, the nut can translate over the spindle and the effective length from universal joint to universal joint can be adjusted, in order to orientate the foot in φ and ψ with respect to the lower leg.

The extreme positions of the ankle are depicted in Figure 3.15.

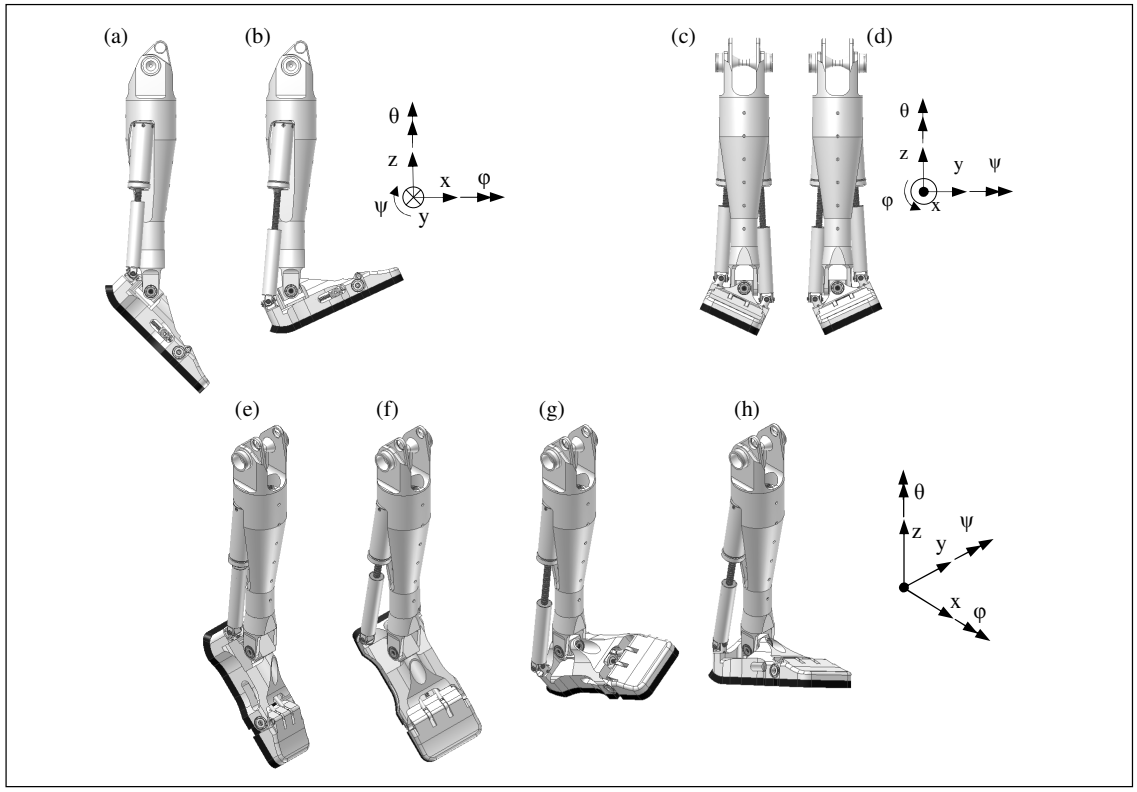

Figure 3.15: Extreme positions of the (left) ankle: (a) φ = 0°, ψ = 45°, (b) φ = 0°, ψ = -25°, (c) φ = -25°, ψ = 0°, (d) φ = 25°, ψ = 0°, (e) φ = -25°, ψ = 45°, (7) φ = 25°, ψ = 45°, (g) φ = 25°, ψ = -25°, (h) φ = -25°, ψ = -25°.

The centers of the universal joint are placed apart as far as possible for the following arguments. First of all, the motors (238 gr. each) can be placed as high as possible in the lower leg which is favorable with respect to the robots total COM.
Another argument is to have an effective length between the universal joints that is as long as possible. In this way, the roll movement of the ball screw actuator is minimal and thus; the universal joints are not obstructed to pass through their full ROM. In addition, this length provides a larger stroke for the balls screw, so, the lead of the ball screw can remain large, which is favorable for speed.

The centerlines of the ball screw actuators are pointing towards the knee axis (in the Sagittal plane) to pass through their axial forces to the upper leg. In addition, actuation of the ankle (especially in ψ)

will induce forces to the lower leg which will try to bend the lower leg base. These bending moments are in the plane of the septum of the lower leg base (see section 3.4), which will withstand these moment loads.

The universal joints are constructed instead of purchased because standard universal couplings are intended with a different objective. Usually, universal couplings are designed for torsion stiffness, whereas now axial stiffness is important too. Therefore, the universal joints in this design have axles with a larger diameter and consequently, a larger cross section, to withstand larger axial forces, because the ball screw is intended to generate axial forces from a torque. To reduce friction, these axles are supported with plain bearings. Plain bearings are chosen because they can withstand high radial loads and because the axles rotate small angles back and forth.

Transmission ratio, transmission efficiency and joint torque
Because the movement of ankle φ and the ankle ψ is coupled, the computation of the exact ratio is complex; if both angles are non-zero, the φ axis is not in the xz plane anymore and the ψ axis is not in the yz plane anymore. In Figure 3.16, an estimate for the ratio of ankle φ as well as ankle ψ is shown, assuming that the φ axis remains in the xz plane and the ψ axis remains in the yz plane. Therefore, this is not the exact ratio between output (joint) and the input (motor), the figures are to give an idea about the ratio.

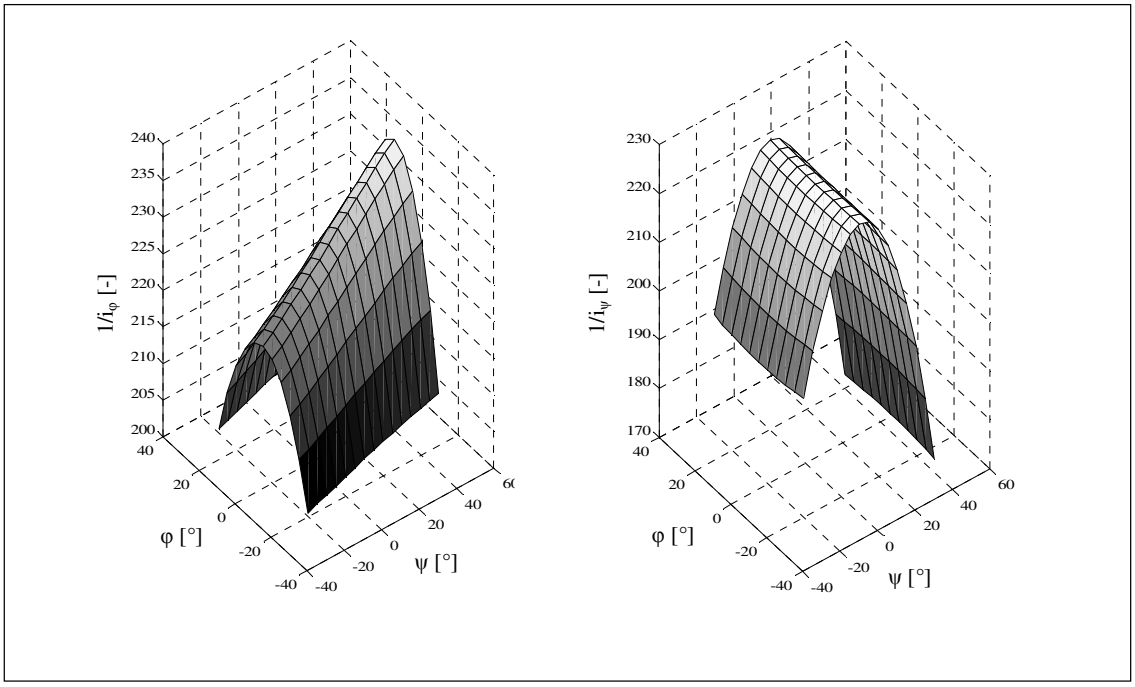

Figure 3.16: An estimate for the reduction in 1/i for the ankle φ (left) and the ankle ψ (right), dependent on the angles φ and ψ. Assumption: The φ axis remains in the xz plane and the ψ axis remains in the yz plane.

These ball screw actuators have an approximate efficiency of 90 % (the ball screw nut contact). Together with the transmission ratio, estimated on 85 %, an estimate for the joint torque is computed, with the aforementioned assumption, see Figure 3.17.

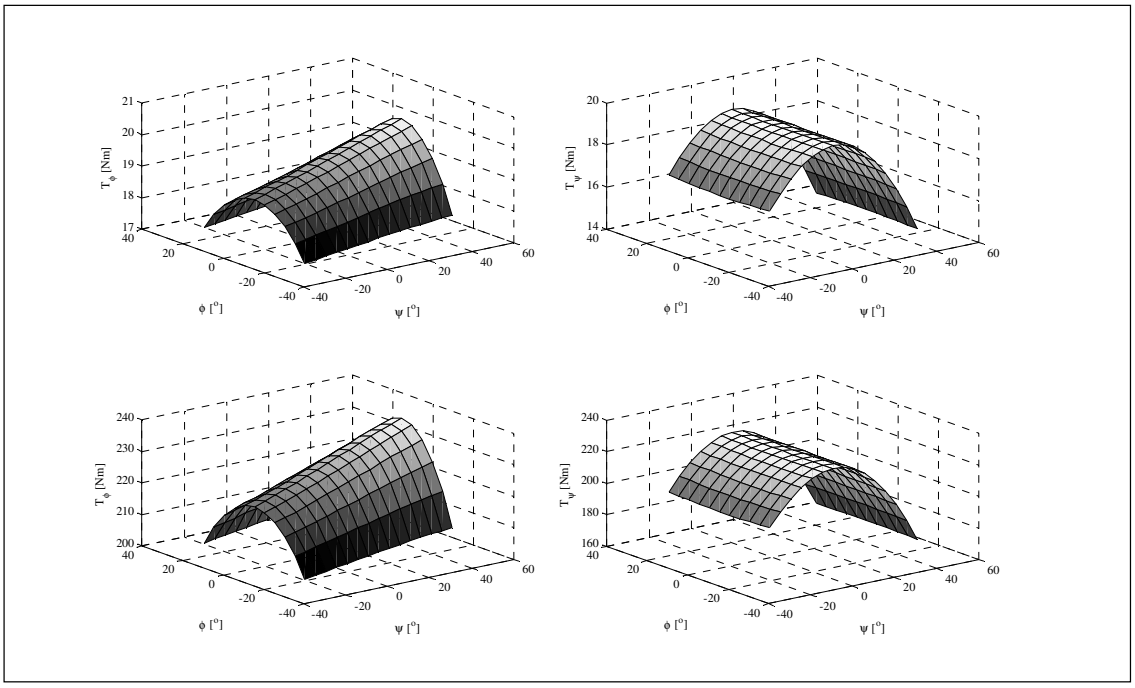

Figure 3.17: An estimate for the nominal (above) and stall (below) joint torque in Nm for the ankle φ (left) and the ankle ψ (right), dependent on the angles φ and ψ. Assumption: The φ axis remains in the xz plane and the ψ axis remains in the yz plane.

Actuation stiffness

Both ball screw actuators have their own axial stiffness, dependent on the effective length. It roughly consists of the axial stiffness of the motor cup, estimated on $c_1 = 13 \cdot 10^7$ N/m, the axial varying stiffness c_2 of the spindle (dependent on effective length) and the contact stiffness of the nut (via the balls) on the spindle; estimated on $c_3 = 10 \cdot 10^7$ N/m. Together with the effective radius r of the spindle axis, c_1, c_2 and c_3 can be converted to a rotational stiffness k_ψ and k_φ, see Figure 3.18. Again, the displayed stiffness graphs are estimates due to the aforementioned assumption.

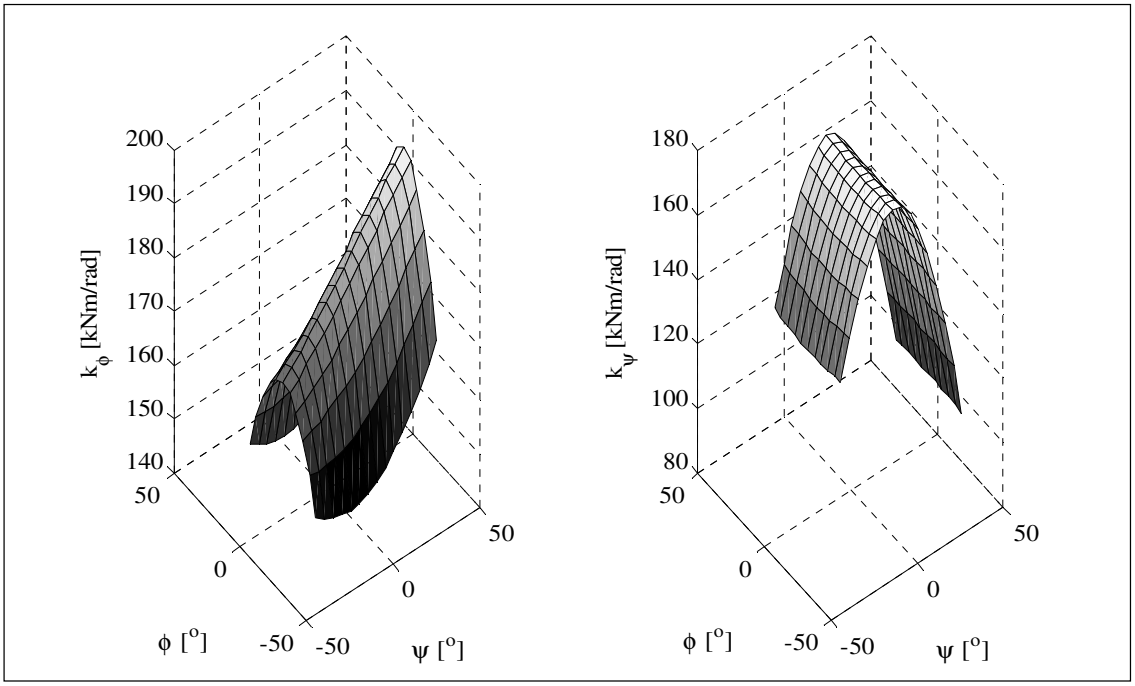

Figure 3.18: An estimate for the rotational stiffness for the ankle φ (left) and the ankle ψ (right), dependent on the angles φ and ψ. Assumption: The φ axis remains in the xz plane and the ψ axis remains in the yz plane.

Backlash
Like in the knee actuation, the backlash can be eliminated with a ball screw spindle that has altered helical grooves. With this option there will be zero-backlash in the actuation of ankle φ and ankle ψ.

3.6 Foot and toe ψ

Basically, the foot and the toe each consist of one part: the *base-foot* (1) and a *toe* (2), depicted in Figure 3.19 (left). Both links are machined pieces of aluminum, which are connected to each other on the toe ψ axis.

Joint construction
Figure 3.19 (right) shows how these parts are assembled. The base-foot has two ears, with two drilled holes of which the centerlines coincide. In these holes, *single row deep groove ball bearings* (INA FAG 61800-2RSR) (3) are placed. Into each bearing a *bush* (4) is inserted. This bush has a fitting edge that fits into the lead-in edge of the toe, so, alignment is ensured. Now, x, z, φ and θ of the toe are fixed, with respect to the foot. Through two *distance rings* (5), the toe is also fixed in y: The inner ring of the bearing is form-closed by a raised edge of the bush and the distance ring, so, a *M4 bolt* (6) can be screwed on with high tension.

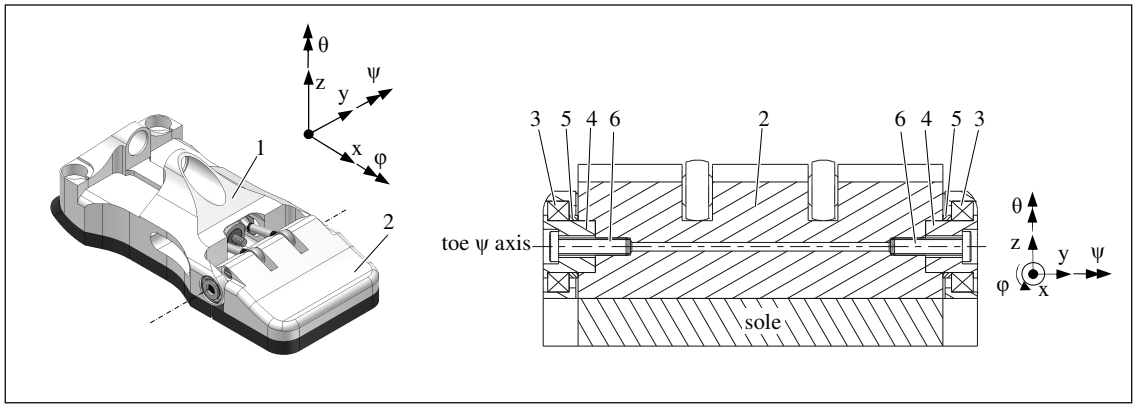

Figure 3.19: Isometric front view (above left) of foot and toe. Section view in yz-plane of the toe ψ joint; base foot (1), toe (2), single row deep groove ball bearings (3), bushes (4), distance rings (5), M4 bolts (6).

Joint actuation
The concept is as follows; a motor rotates a ball screw spindle. The ball screw nut, which is prevented from rotating, transforms the rotary motion of the spindle into a linear motion of the nut. Two push pull rods, on one end mounted to the ball screw nut and on the other end mounted on the toe, (eccentric to the toe joint axis,) transform this linear motion into a rotation of the toe around the toe ψ axis.

To be able to stand statically stable on both toes, with the projection of the COM on 50 mm from the toe ψ axis, the required joint torque (of each toe) must be around 11 Nm. Therefore, a 20 W motor is chosen to perform this; with an efficient transmission of about 85 %, the toe is still able to rotate with a rotational speed of approximate 1.5 rad/s.

In Figure 3.20, the toe actuation is shown. The head of a *20 W motor* (1), from Maxon (RE25), is fixed to the *base-foot* (2) with six M2 bolts. A hardened steel *flange* (3) is screwed on to the *ball screw spindle* (4), which is fitted on the motor axle. Due to a fitting hole in this flange, the bearing-faces of this flange are perpendicular to the spindle axis. Two *axial needle roller bearings* (INA FAG AXK1024) (5) fix the spindle to the base-foot in x, ψ and θ. The axial needle bearings are held into place by a hardened steel *cover* (6) and a *axial bearing washer* (INA FAG AS1024) (7). The cover is screwed on to the base-foot with four *M3 bolts* (8).

The radial bearing inside the motor (Maxon, 2010) is used to fix the spindle in z and y because the motor is placed in the base-foot by a lead-in edge. The other end of the spindle is free, so, the only free DOF of the spindle is its rotation φ, which is controlled by the motor.

The *ball screw nut* (9) is screwed on and then secured with a set screw into a *nut holder* (10) with two axles, one on each side on a coinciding axis that intersects with the axis of the spindle. On each axle are subsequently mounted a *rod end* (11), a *single row yoke type track roller* (INA FAG LR604-2RSR) (12) and a *M3 hexagon nut* (12). This nut is screwed on to secure the ball of the rod end to the nut holder, which increases the bending stiffness of the axles of the nut holder.
Yoke type track rollers have outer rings with a crowned outside surface. The radius of the curvature is 500 mm. Consequently, the Hertzian contact between the track roller and the surface it rolls on remains unchanged, even if the track rollers runs skewed or tilted over the surface.
The track rollers can roll over a *track roller strip* (14), glued to the base-foot, to prevent the nut from rotating (φ) and to keep the spindle free from forces that are perpendicular to its axis. The required minimum thickness of the strip is 0.5 mm (if e.g. stainless steel ASTM 420 is used).
A little clearance between the strips and the track rollers, necessary to assemble the track rollers into the guide, like 0.05 mm, will allow the nut to rotate about 0.1°. This will result in imperceptible backlash at the toe joint.

The rod end is connected to a *push pull rod* (15). On the other end of the push pull rod, another *rod end* (16) is placed. The effective length of the push pull rod can be set to the right length (45 mm) by means of the two rod ends: each rod end has a different M3 thread, one left handed and one right handed, so they can be screwed into the push pull rod (which has corresponding thread on both ends). Each rod end's position is then locked with a *M3 nut* (17) (also with corresponding thread). Both rod ends (16) are mounted to the toe, eccentrically to the toe hinge axis, by means of *fitting bolts* (18). These fitting bolts also fit into the toe by lead-in edges drilled into the toe, see Figure 3.20 (below right) for this detail.

The design with two push pull rods comprises a major advantage. The forces induced by the toe are shared by the push pull rods, so less moment is applied to the spindle. Also the radial force to the spindle, induced by the push pull rods, is passed symmetrically into the base-foot by the track rollers.

In Figure 3.21, the extreme positions of the toe, with respect to the foot, are depicted.

Transmission ratio, transmission efficiency and joint torque
With this ball screw actuation a ratio, dependent on toe ψ, which is defined with $i = \psi_{toe}/\theta_{motor}$, is realized, see Figure 3.22. The efficiency of the actuation is assumed to be 90 %, because the transmission is a ball screw. The ball screw has a nominal diameter of Ø 8 mm and a lead of 2 mm. From this and the kinematics, the toe joint torque can be derived; nominal torque as well as stall torque. This is shown in Figure 3.23.

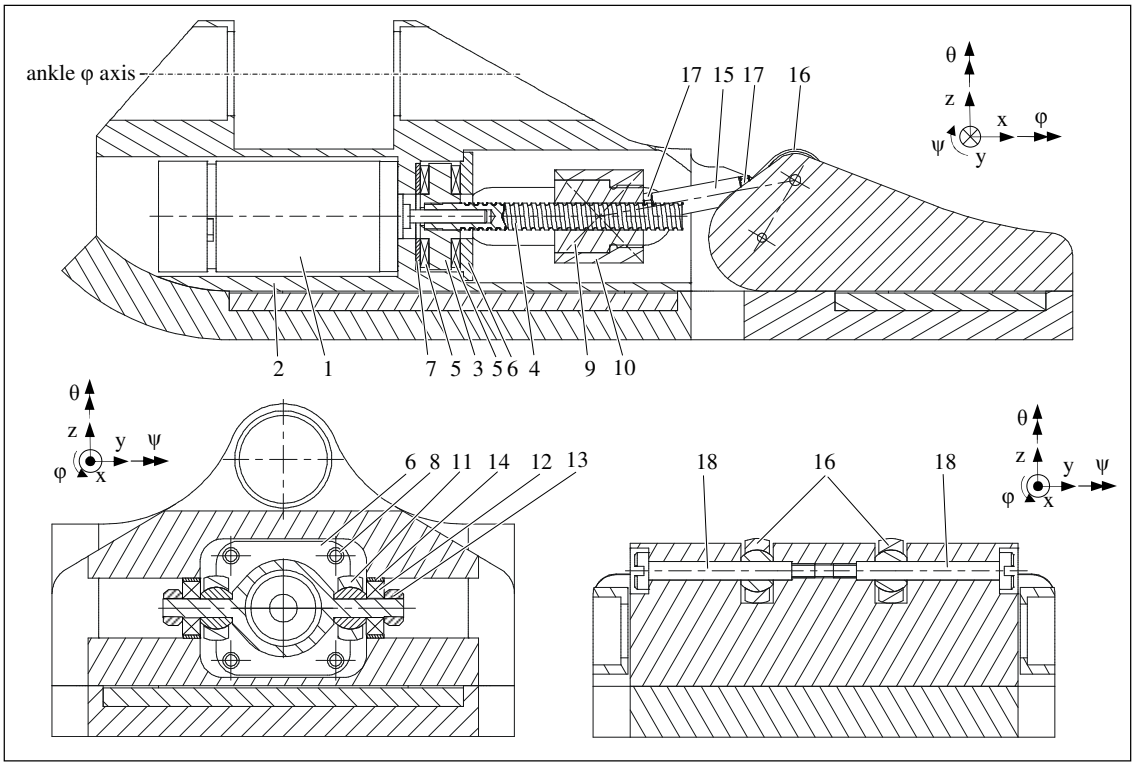

Figure 3.20: Toe section view in xz plane (above), yz plane section view through center of the ball screw nut (below left) and yz plane section view through the center of the eccentric holes of the toe (below right): DC motor (1), base-foot (2), flange (3), ball screw spindle (4), axial needle roller bearings (5), cover (6), axial bearing washer (7), M3 bolts (8), ball screw nut (9), nut holder (10), rod end (11), single row yoke type track rollers (12), M3 hexagon nut (13), track roller strip (14), push pull rod (15), rod ends (16), M3 nuts (17) and fitting bolts (18).

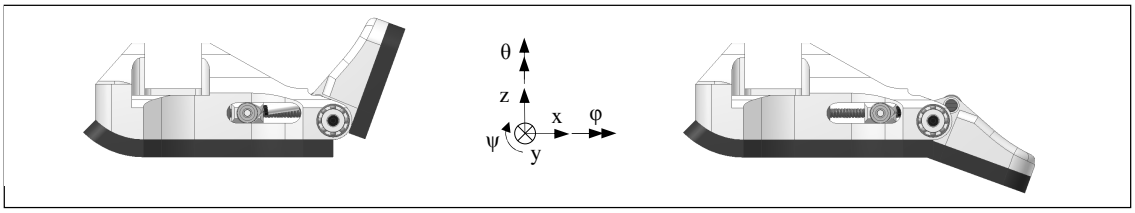

Figure 3.21: Extreme positions of the toe with respect to the base foot.

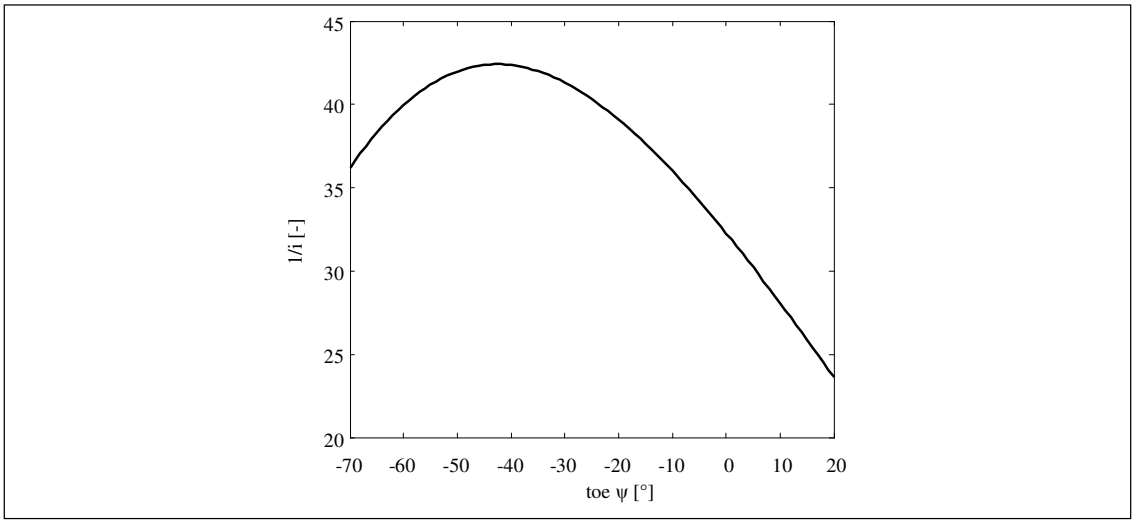

Figure 3.22: Reduction of the toe actuation in 1/i, dependent on toe ψ.

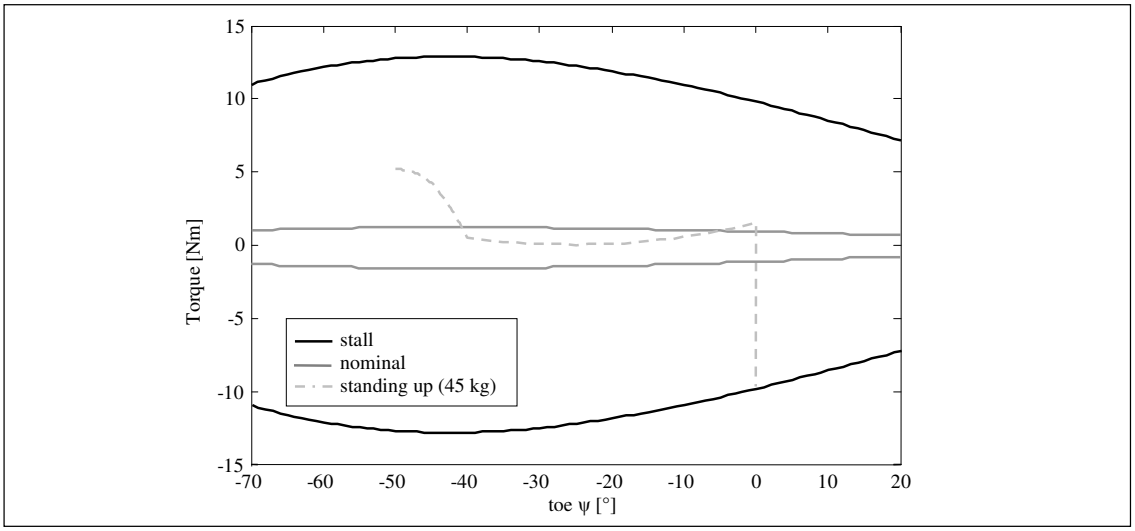

Figure 3.23: Toe joint torque: stall torque and nominal torque and standing up from a squatting position (from Appendix C).

Backlash

Like in the knee and ankle actuation, the backlash of the ball screw itself can be eliminated with a ball screw spindle with altered helical grooves. The clearance between the track rollers and the track rollers strip can be kept small by keeping tolerances fine (precise machining). Then, the backlash at the toe joint will be negligible.

Actuation stiffness

The ball screw indirectly acts on the toe axis; therefore, the axial spindle and nut stiffness has to be converted to a stiffness that is in line with the axial stiffness of the push pull rods. The decomposition of stiffness, with respect to an angle, is depicted in Figure 3.24.

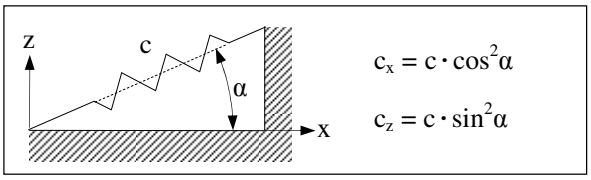

Figure 3.24: linear stiffness c_x and linear stiffness c_z; derived from (linear) stiffness c.

Then, the stiffness of the ball screw spindle, the stiffness of the ball screw nut and the stiffness of the push pull rod are in line and in series and can be added to each other, according to equation (3.1).
The stiffness of the axial needle roller bearing is assumed to be significantly higher than the three above mentioned stiffnesses, thus, the ball screw spindle is assumed to be rigidly attached to the foot in x, y, z, φ and ψ (obviously, it is free in θ). The nut stiffness is assumed on $10 \cdot 10^7$ N/m, the axial stiffness of the push pull rod is also $10 \cdot 10^7$ N/m and the stiffness of the spindle depends on its effective length. With the effective radius r from the push pull rod to the toe axis, the actuation stiffness is computed and depicted in Figure 3.25.

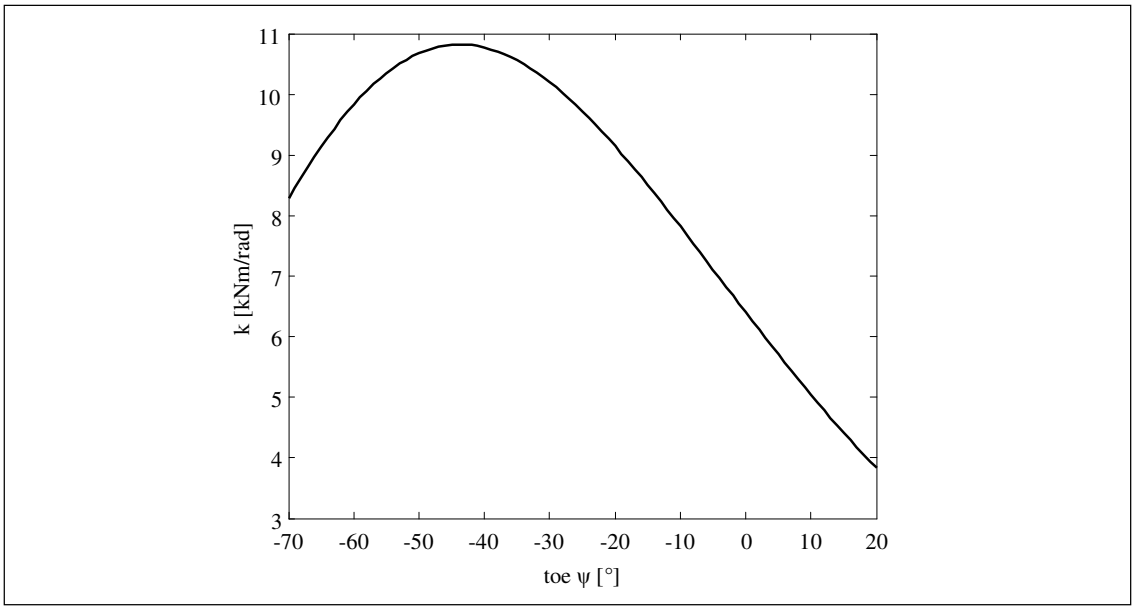

Figure 3.25: Toe actuation stiffness, dependent on toe ψ angle.

3.7 Foot sole and toe sole

According to the functions it fulfils, the design of the sole can be divided into two parts;
1. the heel,
2. the middle foot and toe sole.

The heel copes with ground impacts and the middle and toe sole support the robot while standing. An overview is shown in Figure 3.26. The *heel* (1) is curved to fit on the base-foot which has the same curvature. It is made from 10 mm thick rubber (properties, yet to be defined). The middle foot comprises a *rubber layer* (2) of 6 mm with raised edges up to 10 mm. In this, a 4 mm aluminum *pressure plate* (3), with four pads for force sensors, is inserted. The same holds for the toe sole: a *rubber layer* (4) and an aluminum *pressure plate* (5).
As can be seen in Figure 3.26, the middle sole is narrower on the sides. This will not decrease the SP, because the convex hull of the contact point will remain unchanged. Using these cut outs, the robot is able to place its feet closer to each other by placing the inner side of the toe of one foot, in the cut out of the other. Additionally, through these cut outs, the feet display more resemblance to human feet (or shoes).

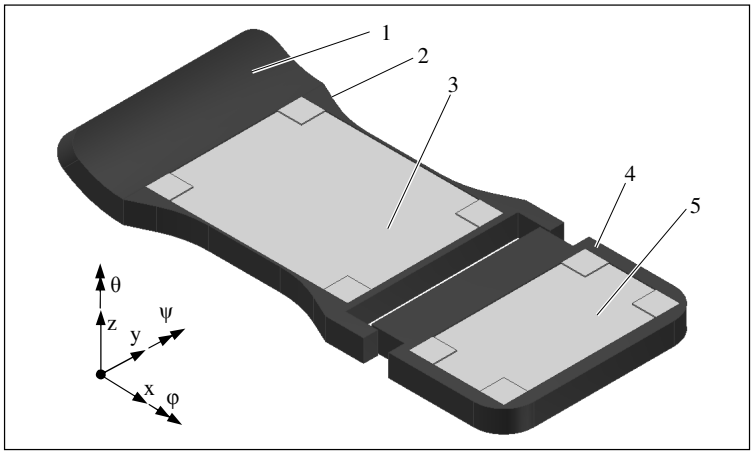

Figure 3.26: Sole design.

Heel

During walking, the heel of the foot encounters impacts. In human walking, the heel strikes the ground with a (almost completely horizontal) velocity of around 0.4 m/s if the walking velocity is 1.6 m/s (Winter, 1991), see Figure 3.27. When the foot touches the ground, the velocity drops, almost instantaneously, to 0 m/s.

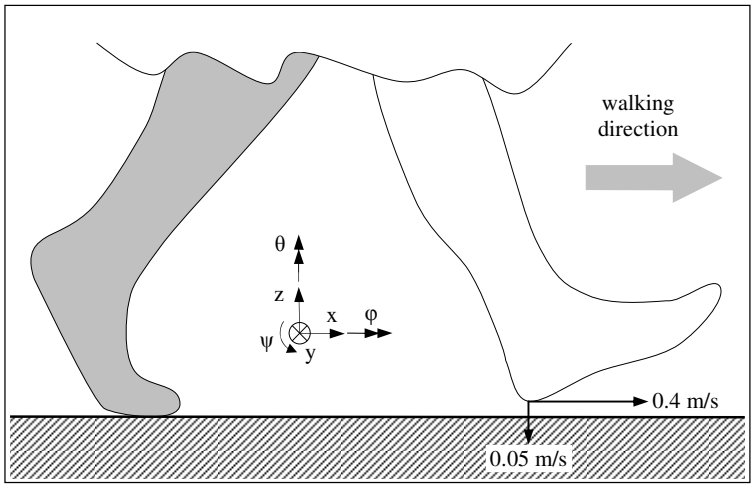

Figure 3.27: Impact velocity of the heel during a normal walking gait.

In (Winter, 1991), the ground reaction force during a *stride* is measured and normalized to the total human body mass, see Figure 3.28. The curvature of the lines is typical for human walking: the vertical force has a characteristic double hump. The first is related to the heel impact, the second is due to the toe push off. Thus, for the heel the first peak value is of importance.

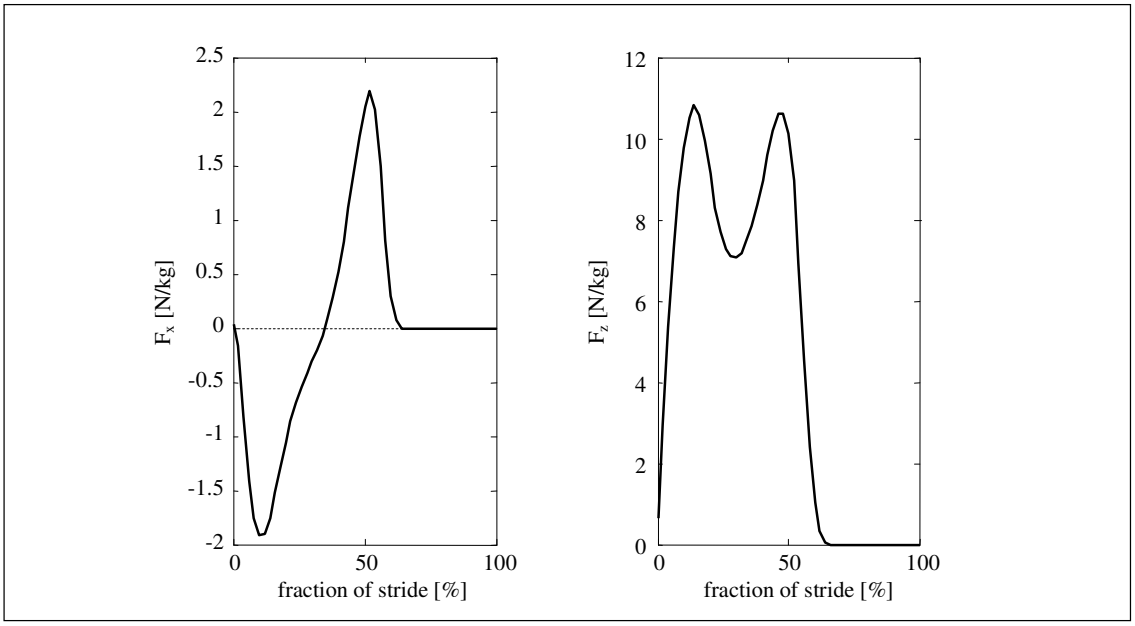

Figure 3.28: Normalized ground reaction forces (in x and z direction) of a 'normal' human walking gait (Winter, 1991). Note that the position where the force acts on the heel is not incorporated; it is just an implication of the normalized magnitude of these forces.

The estimation of an impact force, F_{impact}, is done with:

$$F_{impact} = v_{impact}\sqrt{mc} \tag{3.7}$$

with the impact velocity v_{impact}, the mass m and the impact stiffness c. To minimalize the impact force, all three parameters should be minimal. With the sole design, only the impact stiffness can be reduced. To facilitate this, a layer of 10 mm rubber is glued to the heel. Rubbers (natural or synthetic) have a Young's modulus between E = 10 MPa and E =100 MPa. This implies a contact stiffness between 100 N/mm and 1 kN/mm, supposing that a cross section of 1000 mm^2 (10 mm × 100 mm) contacts the ground on impact.
To predict the ground reaction forces from this, the mass should be determined. Walking implies that both feet are on the ground, at the moment when the heel strikes the floor, so: the actual mass that strikes the ground is unknown.
To predict the ground reaction force(s), the forces of Figure 3.28 can not be used either, because a robot is unable to achieve an identical gait. Masses, dimensions and inertias are always different. Therefore, it is advised to experiment in practice with different kinds of rubber and different designs of the heel, or to investigate this with dynamical models with incorporated impact dynamics. In Figure 3.29, there are some ideas that could be used for experiments.
In appendix E, a Matlab SimMechanics™ model for an impact point on the sole has been made that can be used as a starting point for a complete dynamical model.

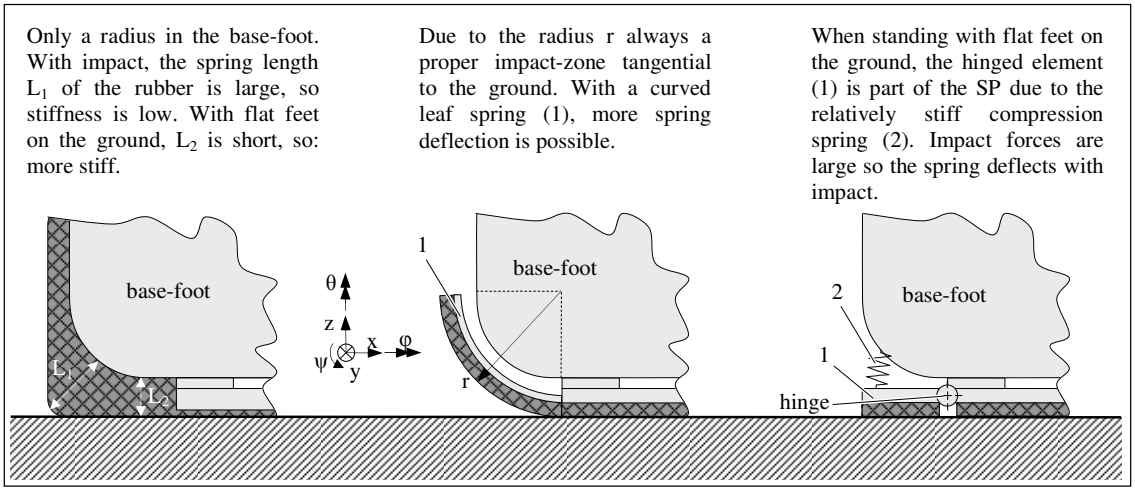

Figure 3.29: Possible concepts for heel design.

Another aspect of the heel is to roll over the ground, between the impact and the phase that the foot is flat on the floor. If the center of the radius of the heel is exactly in the center of the ankle's universal joint, the ankle will only move in x direction during this roll off, this is practical for kinematic computation. However, in this case the SP is reduced: the robot's COM can not be behind the ankles as in a human gait or otherwise the robot will tend to fall over, backwards. Again, experiments should enlighten this symptom and a solution can be found.

Middle foot and toe sole
A way to compute the location of the ZMP the *Center of Pressure* (acronym COP) has to be measured, see Appendix B. There are some methods to measure or compute this COP, but a simple and relatively cheap way is to measure with pressure sensors like the one shown in Figure 3.30. These pressure sensors are also incorporated in modified TUlip.
On the four corners of the pressure plates, the force sensors can be glued. The sensors must be coupled by this plate to be able to average the

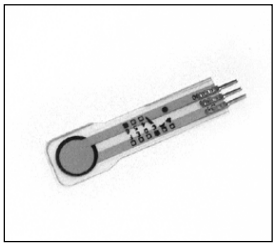
Figure 3.30: Pressure sensor from Flexiforce™

resultant force correctly. If the pressure sensors are not coupled and they are not the only contact points with the ground, a lot of force would be passed directly from the rubber layer into the base-foot without going through a sensor. This compromises the measurement and consequently, an inaccurate COP can lead to instability.

The rubber layer on the middle foot and toe sole can be different from the heel. The most important functionality of this rubber layer is: anti-slip. Again, experiments have to prove which rubber is suitable for different grounds. Maybe even a different rubber for each ground surface can be chosen.

3.8 Concluding remarks

The design of the left leg is identical to the right leg. This makes the legs interchangeable which is favorable with respect to cost. Parts that have to be fabricated come in identical pairs and the number of spare parts is less than if the legs were symmetric or totally different. Additional to this, possible chance of assembly errors is significantly reduced.

The toe axis, the ankle axis and knee actuation bearings are all the same: INA FAG 61800-2RSR (10 per leg), so again costs, number of spare parts and possible assembly errors are reduced through this. The same holds for the plain bearings of the knee actuation and the ankle ball screw actuators (20 per leg) and for the axial needle roller bearings (INA FAG AXK1528) of the knee actuation and the ankle ball screw actuators (6 per leg).

All parts that have to be fabricated are designed to be milled or turned. Only one exception: the universal joint (with elastic hinge) of the knee actuation has to be cut with wire EDM. The ring gear segment of the leg θ actuation, is a 110° segment, so, three segments could be made from one ring (one for each leg and a spare one).
The milled and turned parts have fillet edges to prevent notch effects (stress raisers).
The fabricated parts are occasionally glued together. This is to replace welding. Welding introduces internal stresses to the material which will often lead to warping. Consequently, tolerances are only met if the fabrication is remachined after welding; an extra fabrication process step, which will add costs. Additionally, a glue connection can be opened by heating or the glue can be dissolved applying e.g. chemical reactions or by applying loads that are larger than the regular forces the robot will encounter. Therefore, the parts can be removed from each other without damaging the parts.

The design incorporates many fitting edges. Although this make the fabrication of individual parts more expensive (precision machining), these fitting edges ensure that the assembly of the robot is easy and does not have to be adjusted to e.g. get correct lengths, coinciding or intersecting axes of rotation, etc. Moreover, the assembly is more suited for repeated disassembly, and therefore, less expensive.

Through the use of aluminum, approximately all fabricated parts are light weight while remaining relatively inexpensive. Materials that are more light weight with comparable stiffness (e.g. magnesium alloys or carbon fiber parts) are expected to be too expensive.

The joint actuations are designed to be statically constrained, to avoid internal stresses, which could compromise the behavior of the actuations.

The total mass of the leg is 7.7 kg, this is about 17 % of the expected total mass of the robot (45 kg). The mass of the foot is about 1 kg: 2 % of 45 kg. If a sole, or a set of soles are chosen, through the proposed experiments, the base-foot and the toe can be machined out to reduce the mass. The mass of the lower leg is about 2.4 kg: 5.3 % of 45 kg, and the mass of the upper leg is about 4.3 kg: 9.5 % of 45 kg. These mass fractions are comparable to the mass fractions of a human: 2 %, 5 % and 10 %, respectively (see Appendix A).

Chapter 4
Joints and joint actuations of the hips and waist

4.1 Design overview

The 'waist section', depicted in Figure 4.1; consists of a *waist* (1) a lower part of the *torso* (2) and the *hips* (3). It incorporates the following joints (and its actuations): torso φ, torso θ, hip ψ and hip φ. This, and some general dimensions of the leg, can also be observed in Figure 4.1.

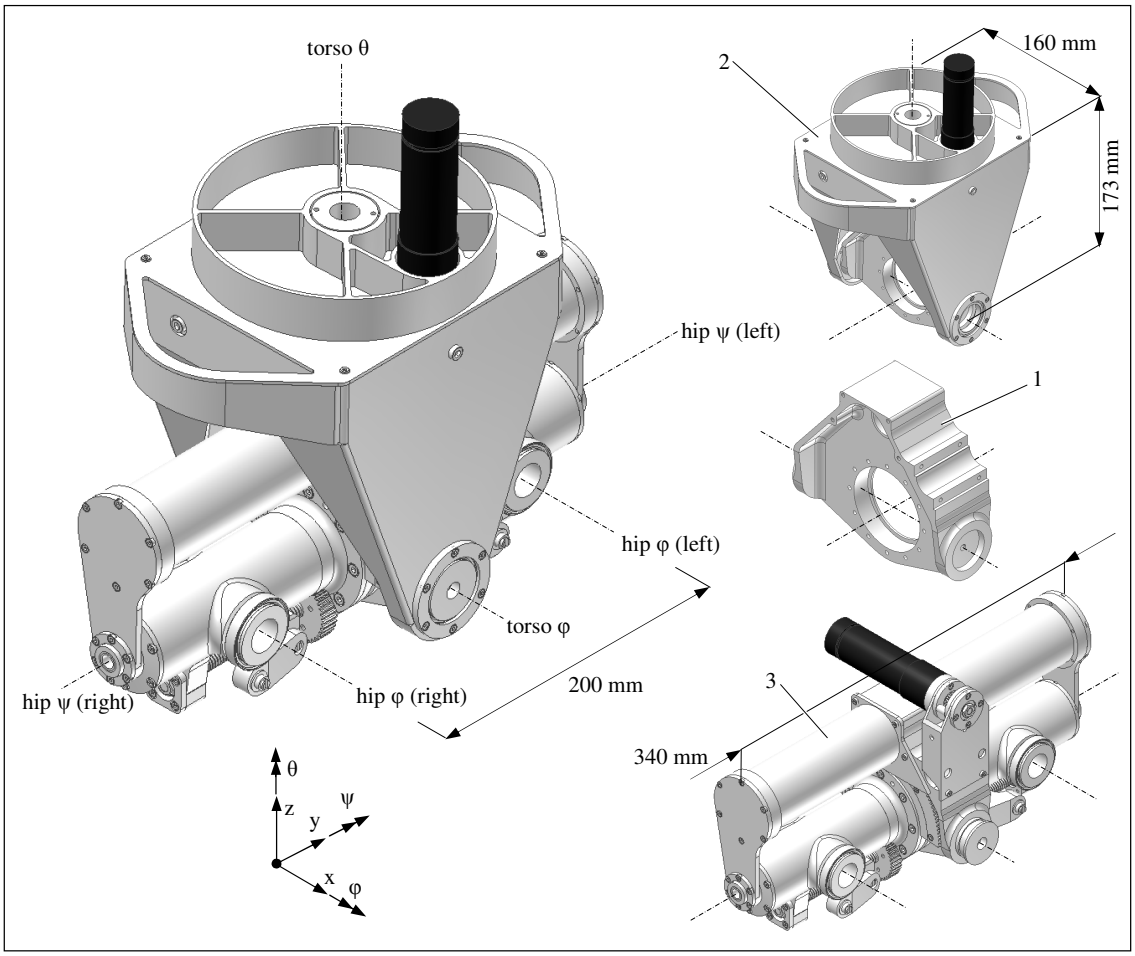

Figure 4.1: The waist section (left) and three sub-assemblies: waist (1), lower part of the torso (2) and the hips (3).

Waist
The waist (see Figure 4.1) is the 'core' of the robot. It can be considered as the equivalent to the pelvis bone of a human to which the waist, the hips and the upper body (beginning with a torso) are connected.
As can be seen in Figure 4.2, its xy plane cross section is I-shaped by the main wall with the anterior and posterior wall. To increase its bending stiffness (around z axis) the cross section is fixed with the three plates; the oblique anterior plate, the oblique posterior plate and the top plate.
To the main wall, both hip ψ joints (ψ-tubes) and joint actuations (ψ-motor tubes) are fixed. Hip φ is subsequently fixed to the hip ψ-tubes. To the anterior and posterior wall, the torso φ hood is fixed. and torso θ is subsequently fixed to this hood.

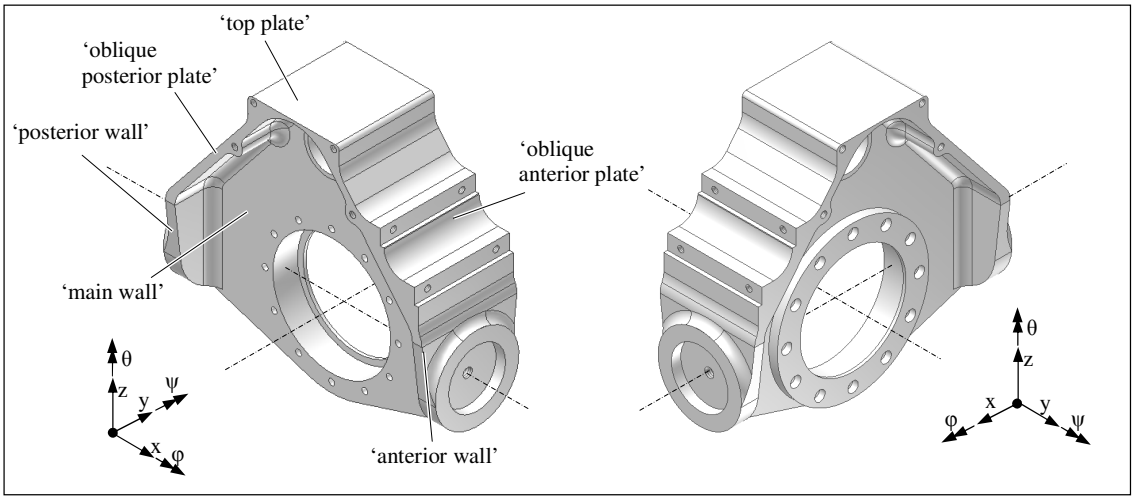

Figure 4.2: The waist of the robot, the equivalent to the pelvis bone of a human, with some designations.

Joints and joint actuations
The joints are each fully actuated over its entire ROM and actuated bi-directionally. Of every DOF, first the joint construction is explained, followed by a description of the actuation of this joint. After this detailed explanation of the design, the design is analyzed with respect to transmission ratio, transmission efficiency, joint torque, actuation stiffness and backlash.

Chapter outline
Section 4.2 explains the design of the DOF hip ψ, followed by the description of the design of hip φ, in section 4.3. This latter DOF is directly connected to the upper leg, explained in the previous chapter.

The waist DOFs to the torso, being torso φ and torso θ, are subsequently explained in section 4.4 and 4.5.

After the design of the joints and their actuations a proposal for the design of the upper body is given in section 4.6.

Just as in chapter 3, some concluding remarks, with respect to e.g. use of purchase components and the fabrication of parts as well as the total masses of the links are given in section 4.7.

4.2 Hip ψ

Joint construction

The hip ψ axis has to intersect with the hip φ axis and the leg θ axis, independent of any of these angles. Therefore it is chosen that the hip ψ axle is a tube so that the hip φ joint and its actuation can be placed inside it. From now on, such a tube is called a *ψ-tube*. A major advantage of a tube rather than e.g. an axle is it high stiffness with respect to mass. Other advantages of a tube are that components can be placed inside and concentric to the tube, thus; the inertia of these components is lower, components are protected and it easier to fix these components to the tube.

Figure 4.3 (above right) shows that the *waist* (1) supports the two tubes; *ψ-tube left* (2) and *ψ-tube right* (3). In reality, these tubes are identical (but for convenience, they are numbered differently). The two tubes above them, the ψ-motor tubes, contain the actuation of these ψ-tubes and are 'rigidly' fixed to the waist, which is explained later.

In the waist, a hole (Ø 62 mm) is machined. This hole contains a *four point contact bearing* (INA FAG QJ206-MPA) (4). Through a lead-in edge, the centerline of the bearing is perpendicular to the main wall of the waist. The outer ring of this bearing is fixed to the waist by means of a *retaining ring* (5) and twelve *M3 bolts* (6).

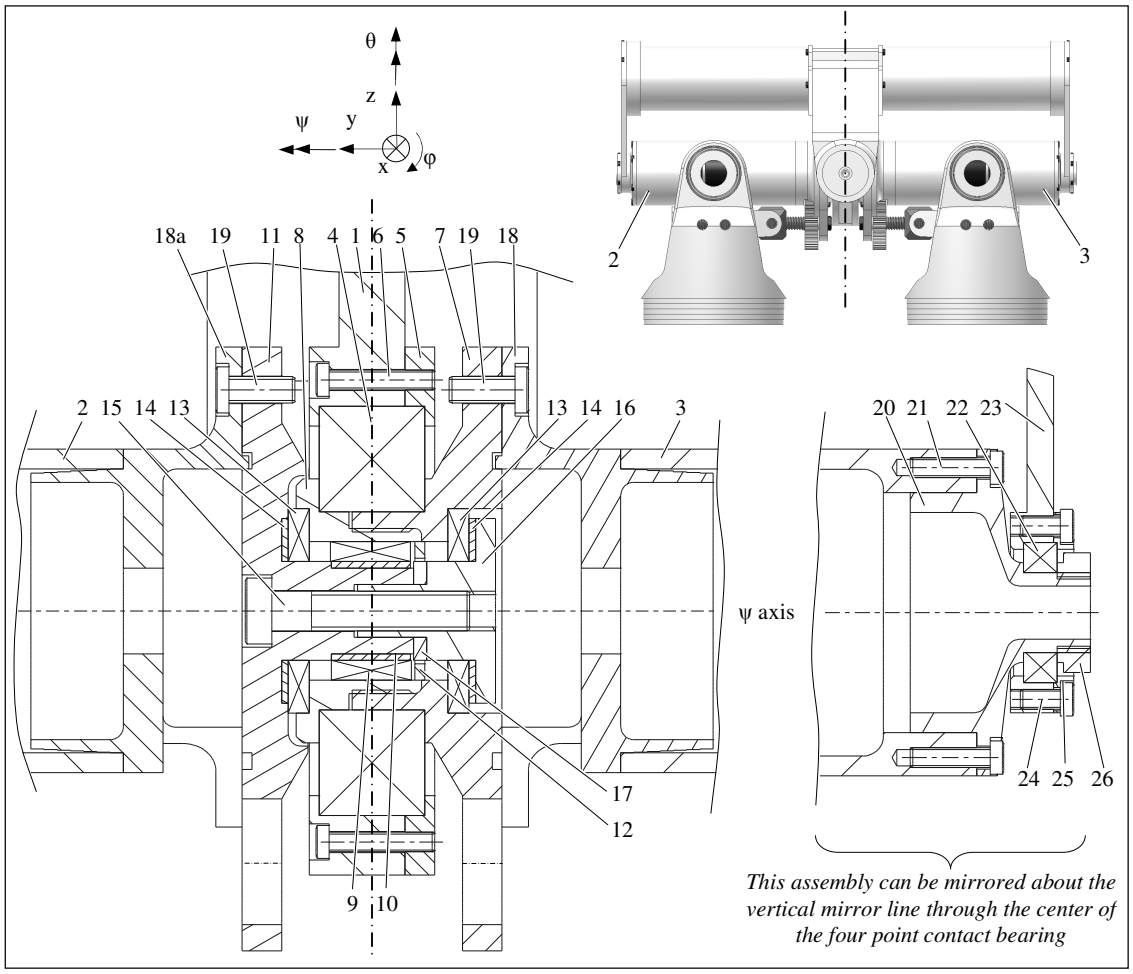

Figure 4.3: Posterior view and a section view of the waist and the hip ψ joint construction: waist (1), ψ-tube left (2), ψ-tube right (3), four point contact bearing (4), retaining ring (5), M3 bolts (6), bearing flange right (7), bearing cap right (8), drawn cup needle roller bearing with open ends (9), bush (10), bearing flange left (11), retaining ring (12), axial needle roller bearings (13), axial bearing washers (14), M6 bolt (15), bearing cap left (16), distance ring (17), φ-motor brackets (18,18a), M4 bolts (19), outside bearing flange (20), M3 bolts (21), deep groove ball bearing (22), end plate (23) M3 bolts (24), retaining ring (25), retaining nut (26). Note that the hip ψ and hip φ actuations are left out in the section view.

The extended axle of the *bearing flange right* (7) fits into the inner ring of this bearing. Then, this is fixed; a *bearing cap right* (8) is screwed into the extended axle of the bearing flange right. The centerlines of the bearing cap right and the bearing flange right, coincide by fitting edges on the axles, thus; the screwing thread (M25x1) is not used for alignment. As a result, the bearing flange right is fixed in x, y, z, φ and θ to the waist and its only free DOF is ψ.

The bearing cap right, has a hole, with a lead-in edge machined into it. Into this hole, a *drawn cup needle roller bearing with open ends* (INA FAG HK 1512) (9) is placed. Via a hardened steel *bush* (10), which functions as the inner ring of the drawn cup needle roller bearing, the *bearing flange left* (11) is inserted. The bearing flange is fixed in x and z with respect to the bearing flange right and a *retaining ring* (12) is used to prevent the drawn cup needle roller bearing to slide in y direction.

Theoretically, the drawn cup needle roller bearing also fixes φ and θ of the bearing flange left with respect to the bearing flange right, but due to its short length (12 mm) this is not the case. The fixation of φ and θ is done with two *axial needle roller bearings* (INA FAG AXW 15) (13), of which the needle rollers roll over an *axial bearing washer* (INA FAG AS1528) (14).
The axial needle roller bearings lie in round chambers of the bearing flange right and the bearing cap right. These round chambers ensure that the bearing faces of the axial bearing washers are parallel to each other, while being perpendicular to the ψ axis.

An *M6 bolt* (15) screws a *bearing cap left* (16), via a *distance ring* (17) onto the bearing flange left. Through this distance ring, the axial needle roller bearings are form-closed, so the M6 bolt can be screwed on with high tension. The combination of the two axial needle roller bearings also fixes y of the bearing flange left with respect to the bearing flange right.
The thickness of the distance ring must be bigger than its nominal thickness, by e.g. 0.5 mm. If this is assembled, this thickness can be machined to the correct thickness (and proper roughness) to eliminate play in y direction. Thus; allowing the axial needle roller bearings to rotate smoothly and without hindrance.

Now, the bearing flange left is free in ψ, with respect to the bearing flange right and subsequently, the bearing flange right is free in ψ, with respect to the waist. As a result, both can be considered free in ψ with respect to the waist and they share the same centerline (ψ axis).

To connect the ψ-tubes to the bearing flanges, on one end of each ψ-tube, a *φ-motor bracket* (18,18a) is glued, with a lead-in edge to ensure alignment. The glue-gap increases with six stages of 0.1 mm. Like in the lower leg: because of the increasing glue-gap the stress concentration in the glue reduces, and consequently, less shear stress will occur in the glue-gap if the ψ-tube is subjected to torsion due to applied torque.

Using seven *M4 bolts* (19), the φ-motor brackets (each with a ψ-tube) are mounted to the bearing flanges with fitting edges that fit into the lead-in edges of the bearing flanges (left and right). Accordingly, the centerlines of the ψ-tubes coincide with the centerlines of the bearing flanges and with the hip ψ axes.
The φ-motor brackets are screwed onto the bearing flanges to be able to (dis-) assemble quickly and easily (e.g. for maintenance).

The bearing flange left is supported by the combination of the drawn cup needle roller bearing and the two axial needle roller bearings into the bearing flange right. The bearing flange right is subsequently supported with the four point contact bearing into the waist. This would result in a relatively low tilting stiffness for both ψ-tubes (the ψ-tube right tilting stiffness even a little lower than the ψ-tube left tilting stiffness, because it is supported in the ψ-tube left, so the bearings work in series).

To increase the tilting stiffness of both ψ-tubes, the other end of each tube is supported as well: an *outside bearing flange* (20) is screwed onto the ψ-tube by means of six *M3 bolts* (21). Due to a lead-

in edge, the centerline of the flange coincides with the centerline of the ψ-tube. A *single row deep groove ball bearing* (INA FAG 61801-2RSR) (22) fits on the protruding axle of the outside bearing flange. The outer ring of this deep groove ball bearing fits in the *end plate* (23) and is secured with six *M3 bolts* (24) and a *retaining ring* (25). The inner ring of the bearing is fixed on the outside bearing flange, with a *retaining nut* (26).

The centers of the four point contact bearing and the drawn cup needle roller bearing lie in the midplane of the main wall of the waist (see Figure 4.3). Therefore, the forces are transmitted through the mid plane of the main wall of the waist. The same holds for the deep groove ball bearing; thus, the forces are transmitted through the midplane of the end plate.

The axial fixation of the ψ-tubes could be done at the outsides of the ψ-tubes. However, the end plates should have a significantly higher bending stiffness (k_φ) than it has now: if a ψ-tube is axially loaded, the end plate is loaded 'out of plane', so it acts like a leaf spring. To obtain a higher bending stiffness, the thickness of the plate could be increased or otherwise a component must be added.
A bad way to increase the bending stiffness is to increase the plate thickness: the stiffness increases proportional with the thickness, but the weight as well.
A component that has in plane stiffness over a length L, perpendicular to the plate, increases the stiffness proportional with L^3, while the weight increases proportional to L. However, this component with length L should be mounted on the outside of the end plate, because if it were placed on the inside, it would obstruct the ROM of the leg. Placement outside would increase the hip width (not hip joint width), which is not very human like.
The waist has a significantly higher bending stiffness due to its I-shape that is 'closed' (see Figure 4.2), so axial fixation is done to the main wall of the waist. Moreover, the end plates can remain with a low bending stiffness.

The design with the additional deep groove ball bearings in the end plates increases the tilting stiffness significantly. The support points of the ψ-tubes are lying far from each other (at the ends of the ψ-tubes).

The four point contact bearing has no seal on each side, so it will be subjected to contamination. Therefore, some self made seals or some purchased NILOS® rings (Nilos, 2010) could be used to prevent this.

Joint actuation
Some concepts to actuate the ψ-tubes were investigated; a brief description and a short discussion that evaluates these concepts can be found in Appendix F.

In Figure 4.4, the actuation of the ψ-tubes is displayed, this figure is on the next page.

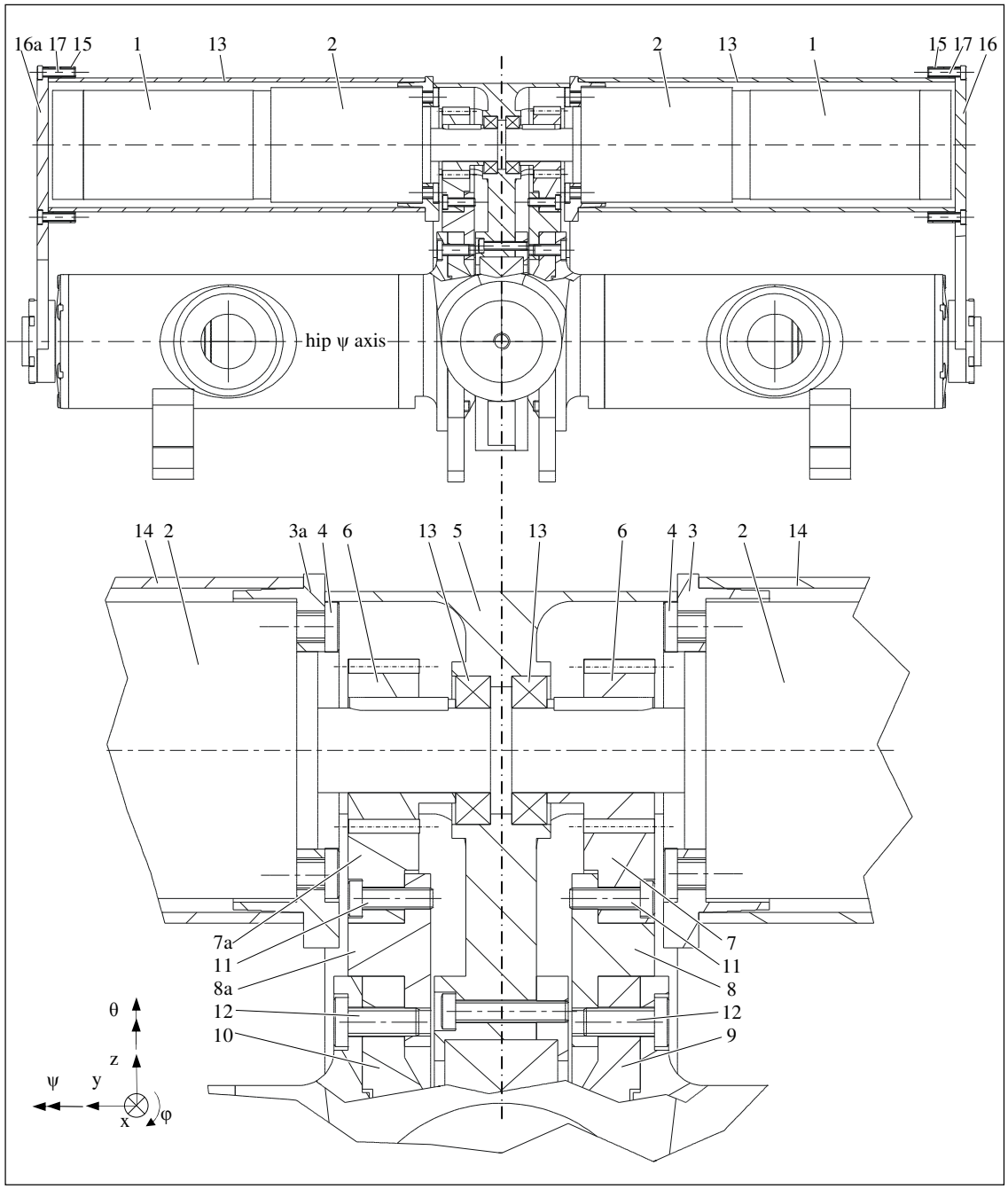

Figure 4.4: Actuation of the ψ-tubes in a posterior break out view (above) and a detail of this (below): DC Motor (1), planetary gearbox (2), ψ-motor bracket (3,3a), M4 bolts, waist (5), pinion gear (6), ring gear segment (7,7a), extension ring segment (8,8a), bearing flange (9,10), M3 bolts (11), M4 bolts (12), deep groove ball bearings (13), ψ-motor tube (14), end ring (15), end plate (16,16a) and M3 bolts (17).

The joint actuations of hip ψ are mirrored over the mid plane of the main wall of the waist, depicted with a center line in Figure 4.4. Identical parts have the same number, mirrored parts are indexed with an a.

A *150 W motor* (1), from Maxon (RE40), is placed (by Maxon) at the input side of a *gearbox* (2). The gearbox is fixed in x, z, φ and θ, to a *ψ-motor bracket* (3, 3a), through a fitting edge on the gearbox. Fixation of y and ψ of the gearbox is done with four *M4 bolts* (4). The ψ-motor bracket is fixed to the

waist (5) through four M4 bolts (not depicted) and alignment is ensured via a lead-in edge in the waist. Now the output shaft of the gearbox can rotate freely in ψ.

On the gearbox output shaft, a *pinion gear* (6) of m = 1 and z = 24 is placed. The rotation of the shaft is transmitted to the pinion gear by a parallel key (standard feature of this gearbox) and the axial position of the pinion gear on the axle is fixed with e.g. glue or a set screw. The pinion gear meshes with an external toothed, 145° *segment of a ring gear* (7,7a) of m = 1 and z = 120.
The pinion and the ring gear segment are made from hardened steel to increase the ultimate yield stress to let the teeth be able to withstand larger shear forces and to provide the teeth with harder contact surfaces to avoid unnecessary wear of the teeth.

A 145° *extension ring segment* (8,8a), is used to transmit the torque from the ring gear segment to the *bearing flange* (right 9, left 10) (which transfers it to the ψ-tube). The ring gear segment and the extension ring segment both have corresponding fitting edges, to ensure that the center lines coincide. Through a raised edge with threaded holes, the ring gear segment is screwed onto the extension ring segment with *M3 bolts* (11).
In the same way this extension ring segment is fixed to the bearing flange with *M4 bolts* (12) (in Figure 4.4; it can be seen that the bolts are not long enough; longer -standard- bolts machined to the right length, have to be used here).
The ring gear segments are mirrored; both can be made from one ring. The same holds for the extension ring segments.

Additional to torque, the output shaft of the gearbox encounters a radial force due to the final reduction. To reduce the moment that this radial force induces to the motor bearing, a *deep groove ball bearing* (INA FAG 61801-2RSR) (13) is placed on the shaft of the gearbox and fits in a hole made in the main wall of the waist.

The motor (and gearbox combination) is protected by the *ψ-motor tube* (14). This tube is glued onto the ψ-motor bracket, in four stages of 0.1 mm. As described in the previous chapter, this increases the shear strength of this assembly and is preferred over welding like described in section 3.7.

At the end of this tube, an *end ring* (15) is glued. Onto this end ring, the *end plate* (16,16a) is fixed through six *M3 bolts* (17). If the main wall of the waist and the end plates are considered as three, relatively thin, plates with two tubes in between (the ψ-motor tubes and ψ-tubes,) as depicted in Figure 4.5; the construction has one major weakness: the plates have low, out of plane stiffness, and can bend relatively easy.
However, if one of the planes has some additional stiffness in this direction, this bending stiffness is increased. This can be done, as illustrated in Figure 4.5 (middle below). This is applied on the waist with the anterior and posterior wall.

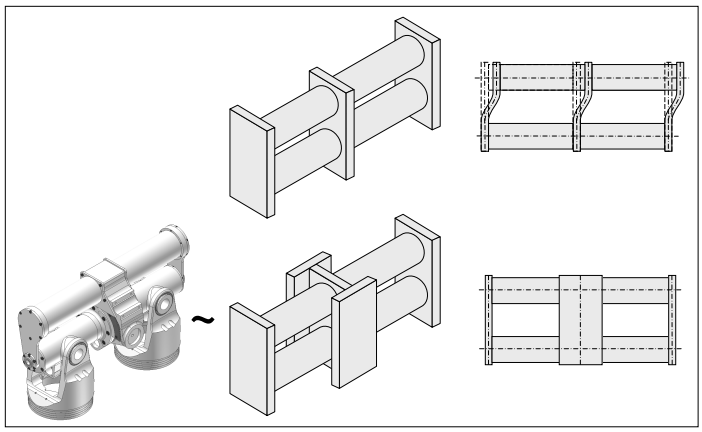

Figure 4.5: Three (thin) plates with tubes in between comprise a low stiffness out of plane of the plates, which will lead to bending of the plates (above). If some side plates are added to the middle plate to increase this bending stiffness (like the anterior and posterior walls of the waist) the construction becomes higher in stiffness (w.r.t. the bending of the plates).

The extreme positions of the hip ψ are depicted in Figure 4.6. If a larger angle segment of the ring gear segment is used, the ROM of hip ψ could be increased to e.g.: -110° to +110°, but it is expected that this is not necessary to perform 'regular' human like motions.

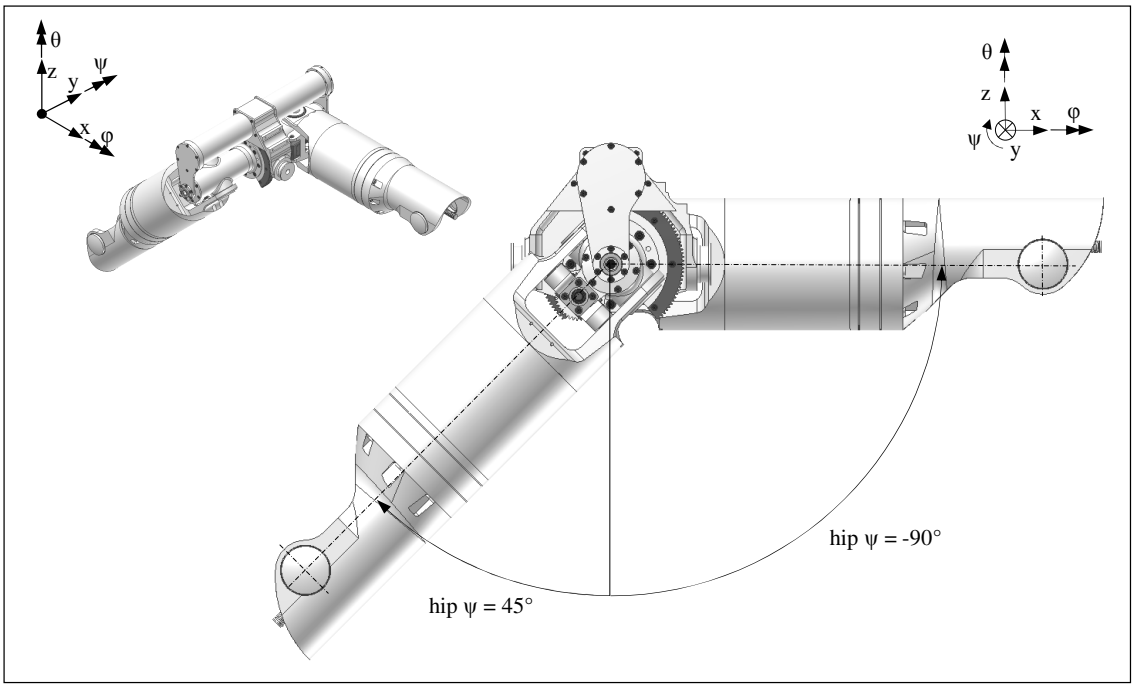

Figure 4.6: Extreme positions of the upper legs in ψ, as a result of the ROM of hip ψ: left leg in -90° and the right leg in 45°.

Transmission ratio, transmission efficiency and joint torque
The gearbox (Maxon: GP 42 C) is a three staged planetary gearbox with a transmission ratio of i = 1/43 (≈ 0.023), an efficiency of 71 % and the nominal torque is 15 Nm (the intermittently permissible output torque is 22.5 Nm). The total transmission efficiency drops to about 69 %, due to the final reduction gear. The absolute, total transmission ratio is i = 1/516 ($\approx 1.9 \cdot 10^{-3}$), which leads to a nominal joint torque of about 37.5 Nm and an intermittently permissible joint torque of about 112.5 Nm.

Actuation stiffness
Like the stiffness of the leg θ actuation, this actuation is considered very stiff due to the gear transmissions.

Backlash
Due to the final transmission, the backlash is reduced from 0.5° of the gearbox to 0.1° at the joint. Because of the length of the legs (780 mm), this results in a backlash of 1.4 mm at the tip of the toe.

4.3 Hip φ

Joint construction
The aforementioned ψ-tube is machined from a single piece of aluminum. In this way, fiting holes of the hip φ can be directly fabricated with the fitting holes of the hip ψ. Accordingly, intersection of the hip φ with the hip ψ is ensured. The ψ-tube is shown in Figure 4.7 (left). As can be seen in this figure, there are two 'protruding tubes' on this ψ-tube in the φ direction. Onto these protruding tubes, the upper leg is mounted.

In Figure 4.7 (right), a cross section of a hip φ joint is shown. The axes of the protruding tubes of the *ψ-tube* (1), both coincide with the hip φ axis.

The upper leg hip connector (2) (also no. 3 from Figure 3.2), has two 'ears'. In each ear, a pot hole is made. In these holes, *single row deep groove ball bearings* (INA FAG 61806-2RSR) (3) are inserted. These bearings fix y, z, θ and ψ of the upper leg hip connector through two *bushes* (4) that have lead-in edges, on which the inner rings of the bearings fit. The protruding tubes of the ψ-tube, have a lead-in edge and a M25x1 thread, in which the bushes can be screwed. The bushes have a fitting edge, which fits into the lead-in edge of the protruding tubes of the ψ-tube, and corresponding thread ensures that the bushes can be fixed to the ψ-tube.
The inner rings of the bearings are form-closed to the protruding tubes of the ψ-tube, by a raised edge on the bush and a *distance ring* (5). This fixes x of the upper leg with respect to the ψ-tube.

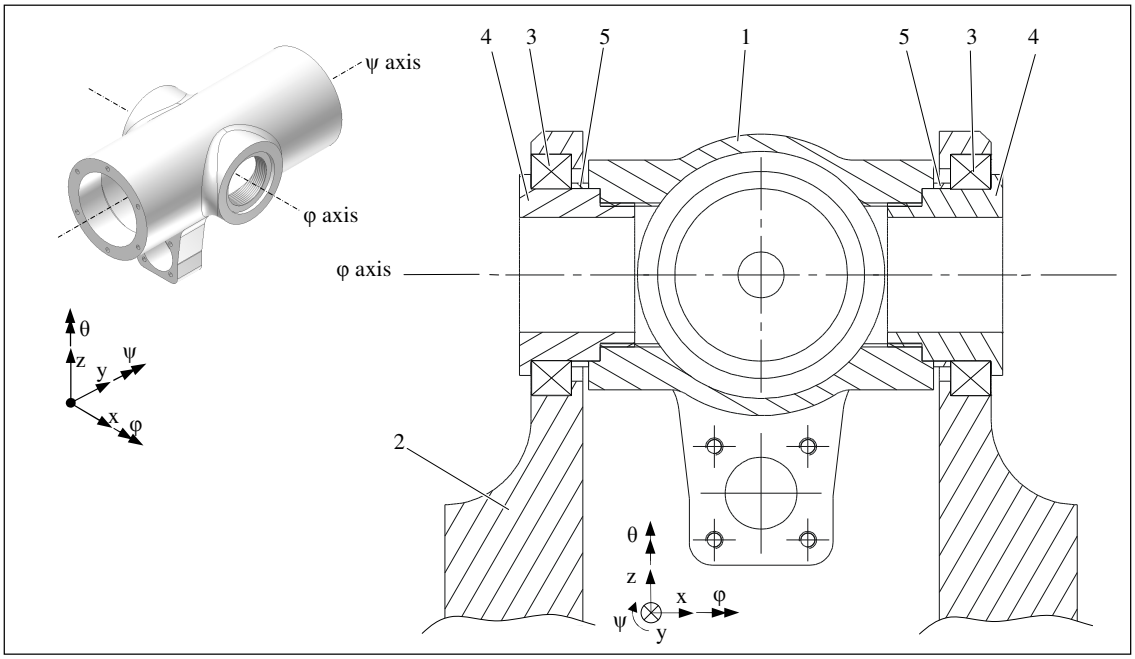

Figure 4.7: Isometric view of a right ψ tube (left). Section view of hip φ joint, actuation made invisible (right): ψ-tube (1), upper leg hip connector (2), single row deep groove ball bearings (3), bushes (4), distance rings (5).

Through the connection of the two ears by the protruding tubes of the ψ-tube, the bending stiffness of the ears is increased significantly because the ears now working in parallel.
The bushes are left open in this design. For esthetics, these bushes can be closed or a cap can be screwed on. The open structure can be used to insert an absolute encoder or a conduit for conductors from the actuation.

Joint actuation
The concept is as follows: a DC motor drives a pinion gear that meshes with a gear (ratio = 1) (parts 3 and 4 from Figure 4.8). This gear is fixed on a ball screw spindle. A ball screw nut can translate over the spindle, because it is prevented from rotating by a 'push pull arm'. This push pull arm, on one end mounted to the ball screw nut and on the other end mounted on the upper leg, (eccentric to the hip φ axis) transforms this linear motion into a rotation of the upper leg around the hip φ axis.

Figure 4.8 shows the actuation of the hip φ, mounted to the ψ-tube.
A lead-in edge and six M3 bolts (not depicted) fix a *90 W motor* (1) from Maxon (RE35) to the *φ-motor bracket* (2).

On the output shaft of this motor, a *pinion gear* (3) of m = 1 and z = 38 is glued. Four treaded holes on the pinion gear offer a grip when this pinion gear needs to be removed from the motor output shaft. The pinion gear meshes with an identical *gear* (4), which is glued to a *ball screw spindle* (5). This gear also has four threaded holes for removal.

Into a hole of a protrusion of the *ψ-tube* (6), an *single row angular contact ball bearing unit* (INA FAG ZKLR0624-2Z) (7) is fitted. The outer ring of this bearing unit is fixed between a raised edge of this hole and a *retaining ring* (8). This is fixed to the protrusion with four M3 bolts (not depicted).
The inner ring of the single row angular contact ball bearing unit is fixed to the ball screw spindle through a fitting edge. In y direction the ball screw spindle is fixed to the inner ring through a raised edge of the ball screw spindle and a *M6 washer* (9) and a *M6 hexagon nut* (10).

The mirror image of the single row angular contact ball bearing unit the fixes the ball screw spindle to the ψ-tube in x, y, z, φ and θ. The single row angular contact ball bearing unit has an X-arrangement which means that the apexes of the pressure cones (due to the angular contact), coincide. This implies that fixation of the ball screw spindle has no tilting stiffness. Therefore, a *single row deep groove ball bearing* (INA FAG 626-2RS) (11) is fitted into a hole of the *bearing flange* (12).
The single row deep groove ball bearing is fixed in y to the ball screw nut through a raised edge on the ball screw spindle, followed by a protruding edge on the gear and on the other side; a *M6 hexagon nut* (13). This single row deep groove ball bearing is not fixed in y to the bearing flange, because the single row angular contact ball bearing unit already fixes the ball screw spindle in y. To align the single row deep groove ball bearing with the angular contact ball bearing unit, a dowel pin (not depicted) is inserted into the φ-motor bracket and the bearing flange, after the φ-motor bracket is glued to the ψ-tube.

As a result, the ball screw spindle is free in ψ with respect to the ψ-tube. A *push pull arm* (14) is fixed to the *upper leg hip connector* (15), through a pair of *axles* (16) which are screwed into this push pull arm via lead-in edges. These lead-in edge ensures that both axles have coinciding axes. The axles are made of hardened steel to have a bearing surface that wears minimally and to increase the yield strength to be able to withstand more radial force and consequently, more ‘push pull’ force.
Into fitting holes of the upper leg knee connector, which are drilled in the same fixation to let the axes coincide, *plain bearings* (17) are placed. Plain bearings are used because they can withstand high radial forces and because the axles do rotate small angles (back and forth).

On the other end of the push pull arm, with identical plain bearings and axles, the push pull arm is connected to a *universal joint* (18). Like the universal joint of the knee actuation (no. 19 of Figure 3.4), the universal joint has an internal DOF; the θ axis, which intersects with the ψ axis, is created with an elastic hinge. Therefore, the nut has two DOFs: ψ and θ, and it functions as a universal joint.
Into the universal joint, a *ball screw nut* (19) is screwed. Through a fitting edge of the ball screw nut and a lead-in edge of the universal joint, the ball screw nut is fixed in six DOFs with respect to the universal joint (and secured with glue or a set screw).

Because the holes in the upper leg hip connector, to which the push pull arm is connected, are eccentric to the hip φ axis, the translation of the ball screw nut is, via the push pull arm, transformed into a rotation of the upper leg hip connector, and consequently of the whole leg, around the hip φ axis.

The push pull arm is H-shaped: both push pull ’rods’ are connected by a cross bar, to provide the ball screw nut with rotational stiffness around ψ. Into this cross bar, a hole is made that offers passage for the ball screw spindle. The hole is not cylindrical because the push pull arm runs through an angle range, dependent on the hip φ ROM.

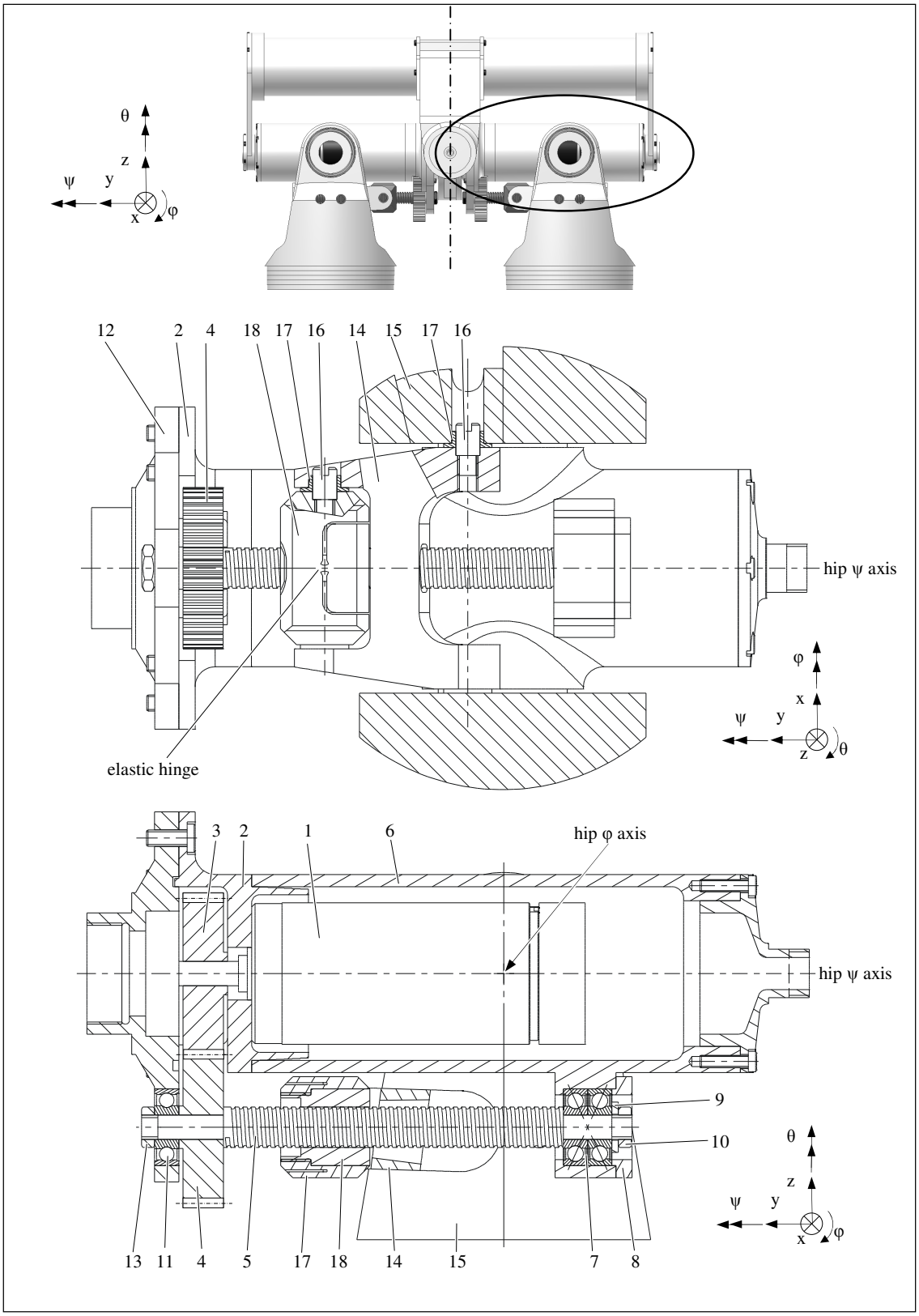

Figure 4.8: The right hip φ actuation encircled in a posterial overview of the hip section (above). Ventral section view with breakout view of universal joint and push pull arm (middle), posterior section view (below): DC motor (1), φ-motor bracket (2), pinion gear (3), gear (4), ball screw spindle (5), ψ-tube (6), angular contact ball bearing unit (7), retaining ring (8), M6 washer (9), M6 hexagon nut (10), deep groove ball bearing (11), bearing flange (12), M6 hexagon nut (13), push pull arm (14), upper leg hip connector (15), axles (16), plain bearings (17), universal joint (18) and ball screw nut (19).

The construction with the push pull arm is two fold over-constrained: θ and ψ of the push pull arm are forced twice through the upper leg hip connector. Because the ψ-tube and the upper leg hip connector, each are machined from a single piece of aluminum, and holes are drilled in the same fixture, the effects of this over-constrained design is kept to a minimum. The construction comprises a major advantage. Through the double shear principle, the axles encounter half of the push (or pull) force. Moreover, the push pull arm transmits force almost symmetrically, which induces less additional moments loads to the ball screw spindle. Another advantage is the simplicity of the construction: the H-shaped push pull arm can be (dis-) assembled for e.g. maintenance.

The elastic hinge has the following dimensions: D = 4 mm, h = 1.5 mm and t = 2 mm (dimension types as in Figure 3.10). Together with equation (3.5) and (3.6), the axial stiffness and bending stiffness are computed: $18.5 \cdot 10^7$ N/m and 40 Nm/rad (≈1.5 Nm/°), respectively.

The extreme positions of the hip φ joint are depicted in Figure 4.9.

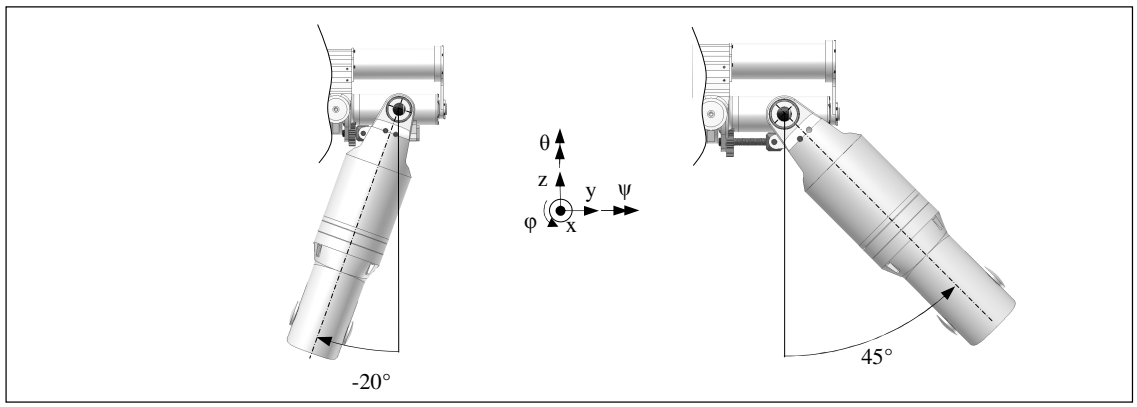

Figure 4.9: Extreme positions of the hip φ joint.

Transmission ratio, transmission efficiency and joint torque
With this ball screw actuation, which has a lead of 3 mm, a ratio dependent on hip φ, which is defined with $i = \psi_{hip}/\theta_{motor}$, is realized, see Figure 4.10.

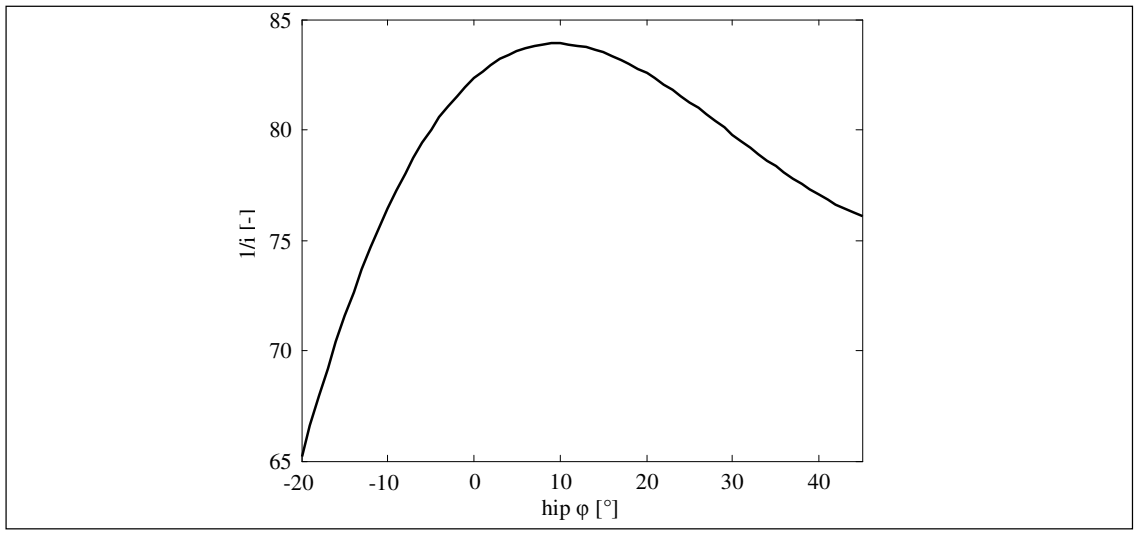

Figure 4.10: Reduction of the actuation in 1/i, dependent on hip φ.

Together with an 87 % estimated transmission efficiency, the joint torques are derived from the kinematics of the actuation, depicted in Figure 4.11.

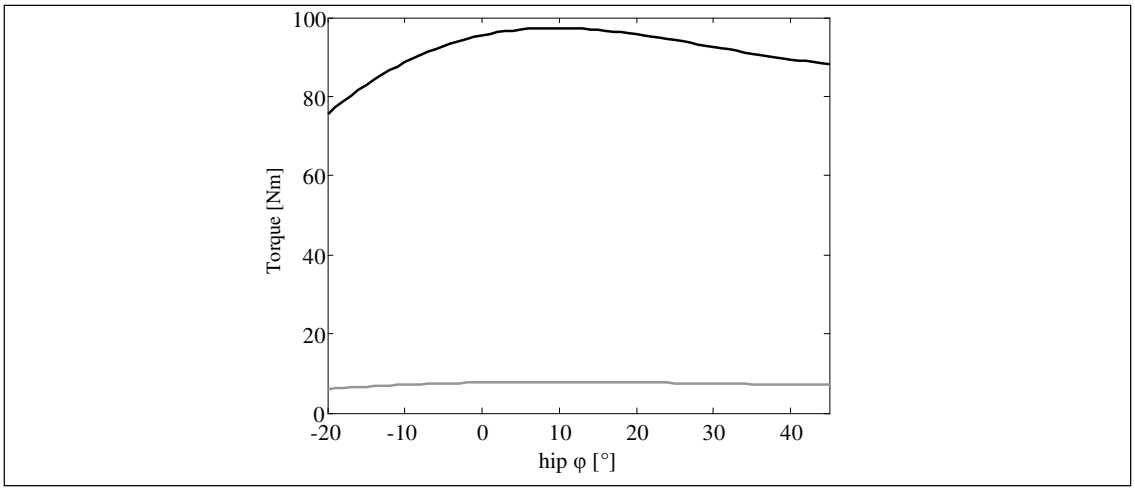

Figure 4.11: Absolute nominal (gray) and stall (black) joint torque of the hip φ join, dependent on hip φ.

Actuation stiffness

The axial stiffness of the ball screw spindle is dependent on hip φ (because it affects the effective length of the ball screw spindle). The contact stiffness between the ball screw spindle and the ball screw nut is estimated on $10 \cdot 10^7$ N/m, the axial stiffness of the push pull arm is estimated on $20 \cdot 10^7$ N/m. Like in the actuation of the toe, the stiffness of the ball screw has to be converted to a stiffness is in line with the push pull arm. The derived rotational stiffness is displayed in Figure 4.12.

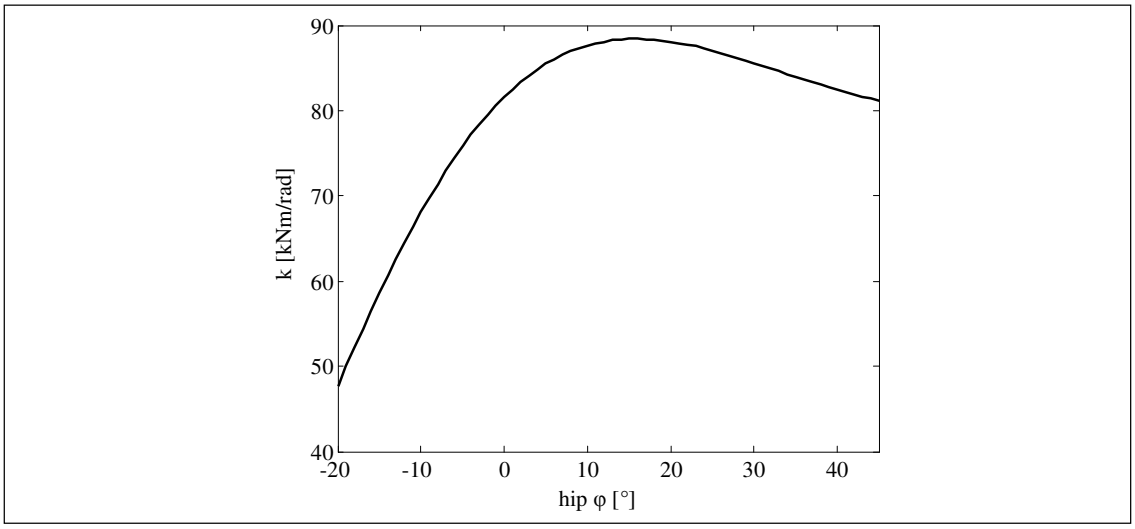

Figure 4.12: Hip φ actuation stiffness, dependent on hip φ.

Backlash

The meshing gears between the output shaft of the motor and the ball screw spindle comprise some (small) backlash. Through the ratio of the ball screw this backlash becomes imperceptible at the hip φ.

4.4 Torso φ

Hood and joint construction
Additional to the hips, the torso is also mounted to the waist. As can be seen in Figure 4.13 (left), the bottom component of the torso is a 'hood'.

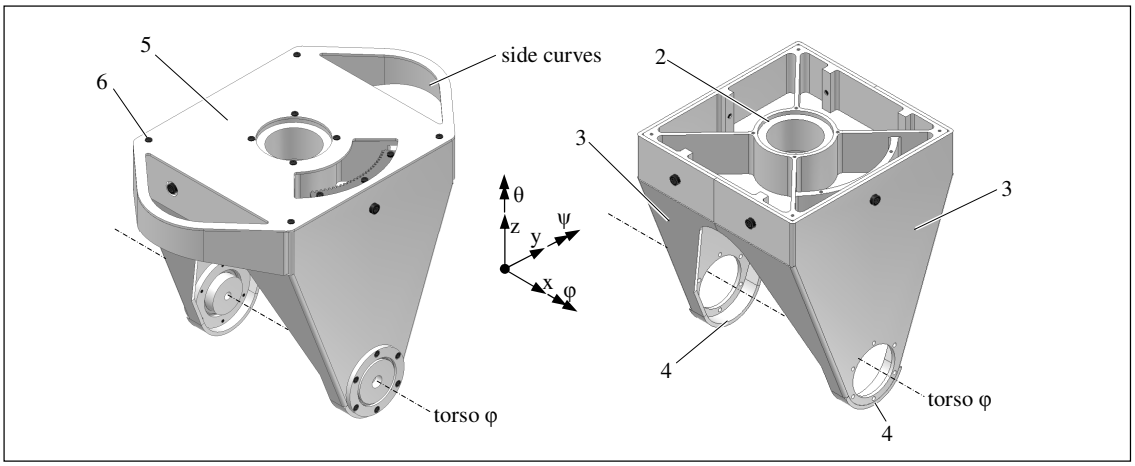

Figure 4.13: Overview of bottom part of the torso: a 'hood' (left). The same, with bearing parts, top plate and side curves made invisible (right): base (2), folded plates (3) and tube sections (4).

This hood is supported by the *waist* (1), on the torso φ axis. As can be seen in Figure 4.13 and Figure 4.14, the hood basically consists of a *base* (2), two *folded plates* (3) and two *tube sections* (4).

Around a central hole for the torso ψ axis, pockets are machined into the base to decrease its mass. A *top plate* (5) is placed on it, with eight *M3 bolts* (6) to create a closed box effect.
The top plate is wider than the base to be able to connect two side curves (see Figure 4.13 left) with e.g. some M3 bolts. These curves are just to provide guidance and passage for conductors from the leg to the torso. Now, the conductors do not have to pass through along torso ψ axis, so they bend less when the robot is moving. More functionality of these side curves is given in section 4.5.

Onto the folded plates, the tube sections are welded to connect one side to the other, so, the bending stiffness increases. Each side of the folded plate is cut out oblique with an end curve, to provide space for the ψ-motor tubes of the hip ψ actuation. At the top, each folded plate is screwed on the base through three *M5 bolts* (7).

The folded plates are relatively compliant with respect to impacts with possible dents as a result. Therefore, components should be added to give the folded plates more stiffness to this. For example, plates perpendicular to the folded plate (parallel to the xz plane) can be added. Another advantage of these plates is that they increase the bending stiffness of the hood.

On the bottom of each folded plate, a bearing is fixed to support the hood to the waist. A *retaining ring A* (8) is placed at the inside of a hole in the folded plate. This retaining ring has six M3 holes and a lead-in edge, in which the outer ring of a *single row deep groove ball bearings* (INA FAG 61806-2RSR) (9) is placed. A *retaining ring B* (10) with a lead-in edge is placed at the other side of the folded plate, prior to fixating the outer ring of the single row deep groove ball bearing using six *M3 bolts* (11). The retaining rings are dimensioned in such way that the center of the ball coincides with the mid plane of the folded plate.

Each folded plate is fixed in y, z ψ and θ to the waist by means of a *bush* (12) that has a fitting edge that fits into a lead-in edge of a hole in the waist. The inner ring of the single row deep groove ball bearing is fixed in y to the waist by means of a *distance ring* (13) and a raised edge of the bush. This is fixed by a *M6 bolt* (14).

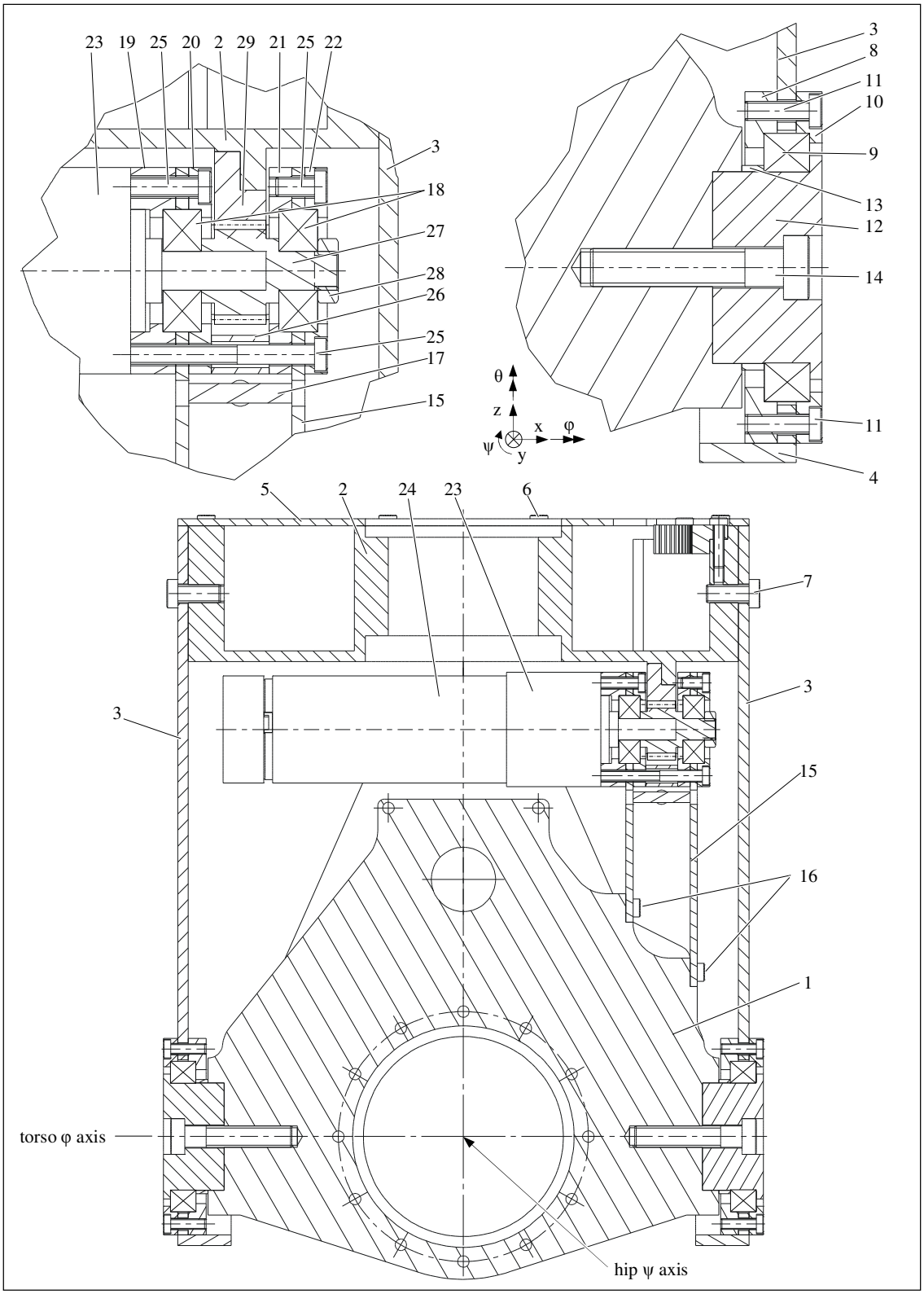

Figure 4.14: Sagittal section view of waist with bottom part of the torso (left) and a detail of the hip φ joint construction (right): waist (1), base (2), folded plates (3), tube sections (4), top plate (5), M3 bolts (6), M5 bolts (7), retaining ring A (8), single deep groove ball bearing (9), retaining ring B (10), M3 bolts (11), bushes (12), distance ring (13) and M6 bolts (14), rectangular tube (15), M3 bolts (16), plate (17), single row deep groove ball bearing (18), retaining rings (19,20,21,22), planetary gearbox (23), DC motor (24), M3 bolts (25), distance bush (26), pinion gear (27), M6 hexagon nut (28), ring gear segment (29).

Joint actuation
Onto the 'oblique anterior plate' of the waist, a *rectangular tube* (50×20×2 mm) (15) is fixed with four *M3 bolts* (16) and fitting edges, or alternatively, a dowel pin could be used. To increase the torsion stiffness of the rectangular tube, a *plate* (17) is plug welded in its core.

On opposite walls of the rectangular tube, the outer rings of *single row deep groove ball bearings* (INA FAG 626-2RS) (18) are fixed, by means of four (non-identical) *retaining rings* (19, 20, 21, 22). These rings have the same hole pattern as the Maxon *planetary gearbox* (23). A *60 W motor* (24), from Maxon (RE30), is placed (by Maxon) at the input side of the gearbox.

The left single row deep groove ball bearing is fixed between two retaining rings (19, 20) to the wall of the rectangular tube together with the gearbox. The other single row deep groove ball bearing is fixed between the other two retaining rings (21, 22).
The retaining rings are fixed by means of five *M3 bolts* (25). Three of these M3 bolts run through all retaining rings and are screwed in the gearbox. Two M3 bolts are screwed in only two retaining rings (the upper hole) to provide space for the final gear (explained later). To maintain the correct distance between the bearings, each of the lower three holes of the hole pattern are interconnected through a *distance bush* (26) with the correct length. Lead-in edges of the retaining rings and a fitting edge on the gearbox ensure that the centerlines of the bearings and the gearbox coincide.

On the output shaft of the gearbox, a *pinion gear* (27) of m =1 and z = 14 is placed. Through a flat side on the output shaft and a flat side in the fitting hole of the pinion (fabricated with sinker EDM), the position of the pinion gear is controlled by the motor.
The pinion gear has a protruding axle, which fits into the inner ring of the (right) single row deep groove ball bearing. This inner ring is closed between a raised edge of this axle and a *M6 hexagon nut* (28). The pinion gear meshes with a 50° *segment of a ring gear* (29) of m = 1 and z = 240. This ring gear segment is fixed to the base through a lead in edge and three *M3 bolts* (not depicted).

The extreme positions of the torso φ axis are depicted in Figure 4.15.

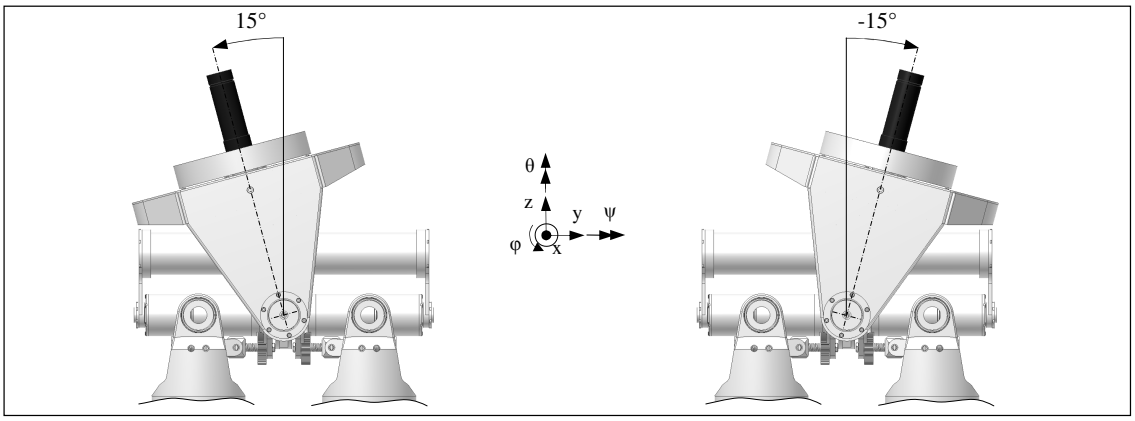

Figure 4.15: The extreme positions of the torso φ.

Transmission ratio, transmission efficiency and joint torque
The planetary gearbox (GP 32 A) is two staged, has a ratio of i = 1/14 (≈ 0.07) and an efficiency of 75 %. The final gear has a ratio of 7/120 (≈ 0.06) and an efficiency of 97 %. Therefore, the transmission has a total ratio of 1/240 ($\approx 4.2 \cdot 10^{-3}$) and a total efficiency of 73 %.
The nominal output torque of the gearbox is 2.25 Nm and the intermittently permissible output torque is 3.4 Nm. Together with the final gear, the nominal joint torque is 38.6 Nm and an intermittently permissible joint torque of 58.3 Nm.

Actuation stiffness and backlash
Like the stiffness of the hip ψ actuation, this actuation is considered very stiff due to the gear transmissions. The backlash of the planetary gearbox is 0.8°, which is reduced by the final reduction to 0.05°.

4.5 Torso θ

Joint construction

As can be seen in Figure 2.1 (right), the torso θ axis intersects with the torso φ axis at the point where also the hip ψ axis intersects. Together with to the construction of the hip ψ joints (the ψ axes of the hips are always coinciding), the torso is able to move independently of the legs in φ, θ and ψ. So, a ball joint is constructed, which gives the torso more freedom in moving the COM to a desired location.

The construction of the torso θ joint is depicted in Figure 4.16.
The central hole of the *base* (1) of the hood, as described in the previous section, is a potted hole wherein two *axial needle roller bearings* (INA FAG AXW 35) (2) are fitted. On top the upper axial needle roller bearing, subsequently are placed: an *axial bearing washer* (INA FAG AS3552) (3), a *flange* (4) and the *round base* (5). This round base is the bottom of the rest of the torso (which is not detailed in this design). In this base, pockets are machined, to reduce its mass. Consequently, it has low torsion stiffness. This torsion stiffness needs to be increased by the rest of the torso.

As a result, the round base is fixed in z, φ and ψ by screwing *tube 1* (6) into *tube 2* (7). The flange (4) can be ground to the right (axial) length to ensure that there is no (or imperceptible) play between the two axial needle roller bearings, and the tension force between tube 1 and tube 2 can be high. Both tube 1 and tube 2 have holes in the flange to offer grip while screwing these two onto each other.

Tube 1 has a fitting edge that fits into the lead-in edge of the central hole of the round base, so they have a coinciding θ axes. Tube 1 also has a fitting edge that fits into the lead-in edge of tube 2; consequently, this axis coincides too. Therefore, this axis can be fixed in x and y by means of the *drawn cup needle roller bearing with open ends* (INA FAG HK3520) (8) and a hardened steel *inner needle roller ring* (9). The drawn cup needle roller bearing fits into the lead-in edge of the base, the inner needle roller ring fits onto the fitting edge of tube 2.

Now, the round base is fixed in x, y, z, φ and ψ with respect to the base and its only free DOF is θ.

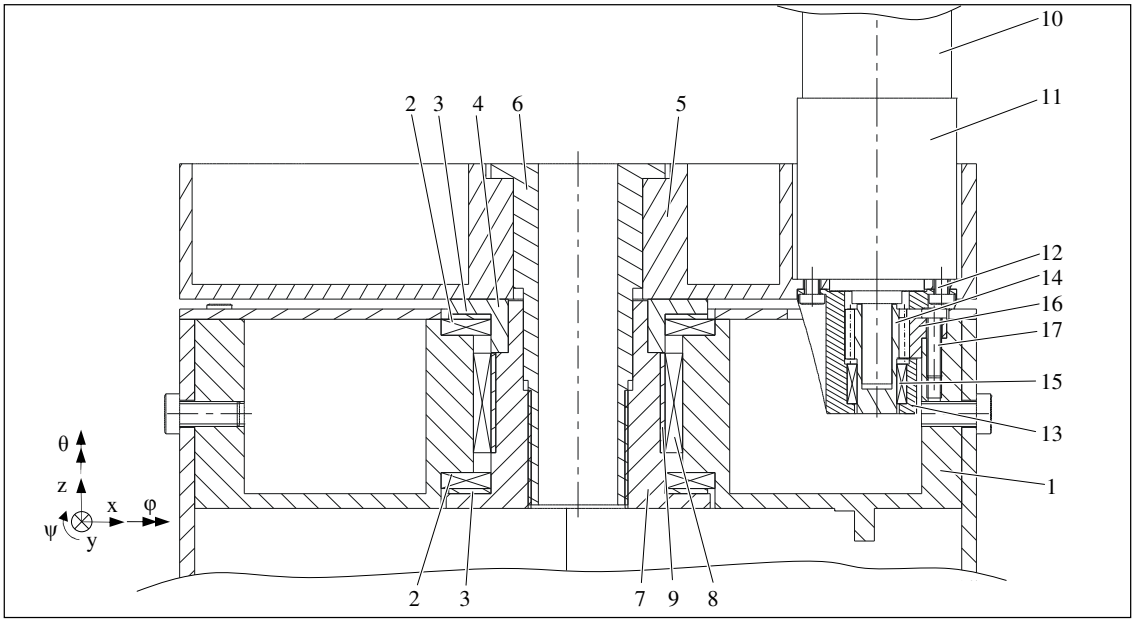

Figure 4.16: Anterior view of torso θ construction (above left) and a xz plane section view of this (below): base (1), axial needle roller bearings (2), axial bearing washers (3), flange (4), round base (5), tube 1 (6), tube 2 (7), drawn cup needle roller bearing with open ends (8), inner needle roller ring (9), DC motor (10) planetary gearbox (11), M3 bolts (12), con (13), pinion gear (14), drawn cup needle roller bearing with open ends (15), ring gear segment (16) and M3 bolts (17).

Joint actuation
A *60 W motor* (10), from Maxon (RE30), is placed (by Maxon) at the input side of a *planetary gearbox* (11). The gearbox is fixed in x, y, φ and ψ by a lead-in edge that fits into a fitting hole in the round base. The gearbox is fixed in z and θ through four *M3 bolts* (12). These M3 bolts, also fix a *cone* (13) with a hole, concentric to the output shaft of the gearbox.

The output shaft of the gearbox can now rotate freely in θ. On this output shaft, a *pinion gear* (14) of m = 1 and z = 10 is fixed with glue or alternatively a set screw. The pinion gear has a protruding axle. Through a *drawn cup needle roller bearing with open ends* (INA FAG HK0808) (15) this protruding axle fits into a concentric hole of the cone. The pinion gear meshes with a 90° *segment of a ring gear* (16) of m = 1 and z = 120. This ring gear segment is fixed to the round base through a lead-in edge and three *M3 bolts* (17). The cone is cut out to provide space for the meshing gears.

The final gear allows the extreme positions of the torso θ joint, depicted in Figure 4.17.

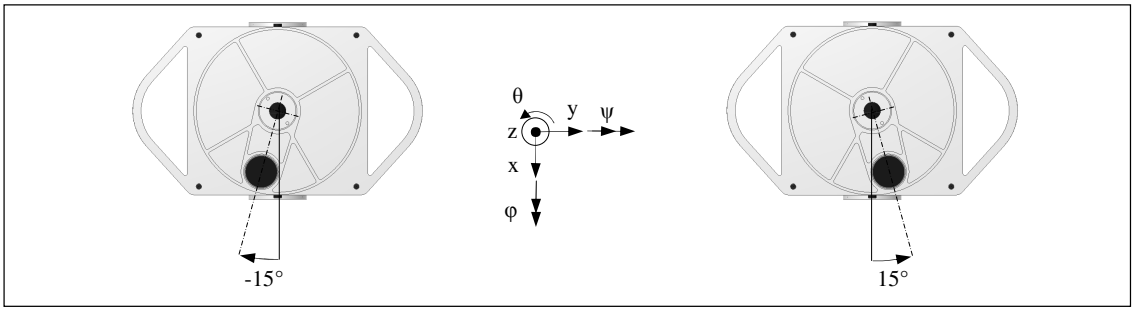

Figure 4.17: Extreme positions of the torso θ joint.

Transmission ratio, transmission efficiency and joint torque
The planetary gearbox (GP 32 A) is identical to the planetary gearbox of the torso φ joint, and therefore, it has a ratio of i = 1/14 (≈ 0.07) and an efficiency of 75 %. The final gear has a ratio of 10/120 (≈ 0.08) and an efficiency of 97 %. So, the transmission has a total ratio of 1/168 (≈ $6 \cdot 10^{-3}$) and a total efficiency of 73 %.
The nominal output torque of the gearbox is 2.25 Nm and the intermittently permissible output torque is 3.4 Nm. Together with the final gear, the nominal joint torque is 27 Nm and a intermittently permissible joint torque of 40.8 Nm.

Actuation stiffness and backlash
Like the stiffness of the torso φ actuation, this actuation is considered very stiff due to the gear transmissions. The backlash of the planetary gearbox is 0.8°, which is reduced by the final reduction to 0.07°.

4.6 Upper body

Configuration
Without an upper body, the robot is a biped rather than an anthropomorphic humanoid. If the design is intended for a biped, the torso θ base (see Figure 4.16) can be mounted to a torso without DOFs. In this torso, the power (e.g. batteries) and the intelligence (computer) of the robot can be placed.

If the new robot is intended to be a full anthropomorphic humanoid, the upper body is much more complex. It has to consist of a torso, neck with head and arms with hands.
An equivalent configuration to a human neck consist of four DOFs: a ball joint (3 DOFs) and an extra ψ joint in the bottom of the neck to let the human look to its feet, while standing straight up. The arms comprise seven DOFs: a universal joint (φ and ψ) in the shoulder, θ in the upper arm, ψ in the elbow, θ in the lower arm and the wrist is a universal joint (φ and ψ) too. Then, the torso has a

universal joint (φ and ψ) in the diaphragm (Takanishi et al., 2005). All these DOFs are displayed in Figure 4.18 (left).
Hands have 20 DOFs, 4 in each finger. This is shown in Figure 4.18 (right).

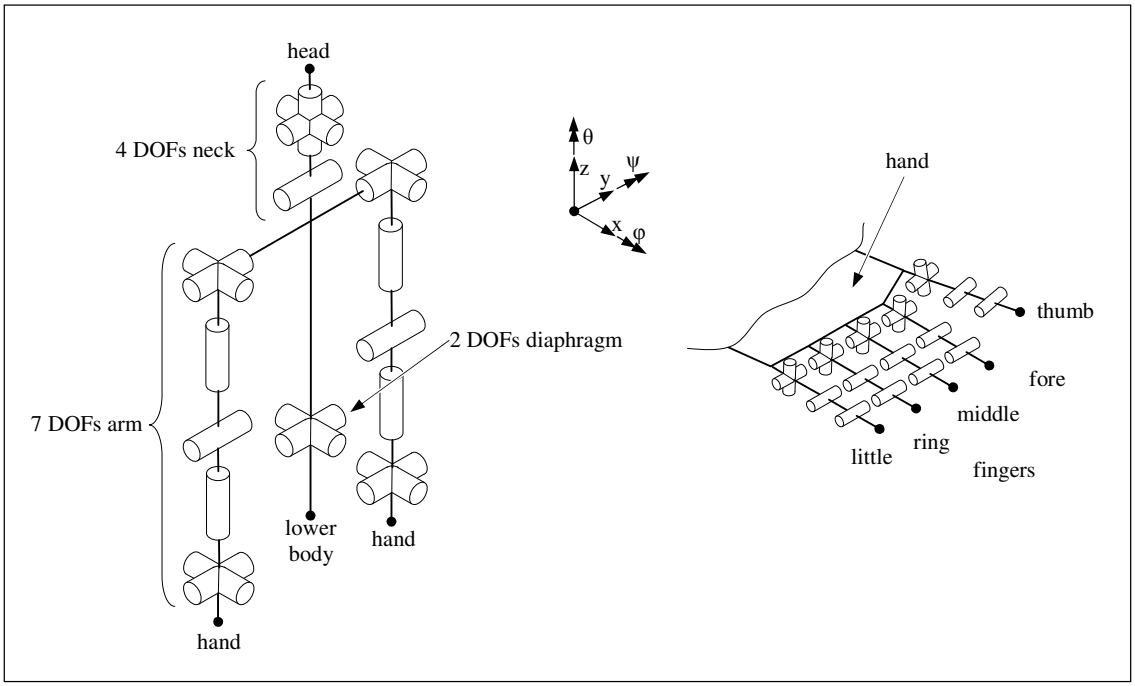

Figure 4.18: The DOFs that represent a human's upper body (left) and the DOFs of a hand with fingers (right).

A human head comprises many DOFs. To imitate all these DOFs would be too progressive, for now. A simple imitation of a head can incorporate a jaw joint (DOF: ψ) and one universal joint (ψ and θ) for both eyes, so a 3 DOF face. This will be able to have the same expression (mimicry) as a ventriloquism doll, which will leap to the eye because only a few anthropomorphic robots have this.

Torso
There are some remarks with respect to the torso (that would contain the power and intelligence of the robot):

- The torso must be stiff from the waist to the neck and arms. The stiff connection from waist to neck is necessary for self localization, the stiff connection to the arms for hand-eye coordination.
- All PCB's should be placed in a vertical arrangement for natural convection of the air.
- The connectors to the PCB's, should not be mounted to the PCB's perpendicular. This adds an extra curve to the conductor and it takes more space (that could be used for other PCB's).
- It must be possible that the front, back and the sides of the torso can be opened and closed. Open to perform maintenance and replacement of e.g. batteries, closed to protect the components in the torso.

The (stiff) torso must be mounted on the round base of Figure 4.16. This could be done as depicted in Figure 4.19. Conductors from the legs that pass through the holes in the side curves (2) can be protected and hidden with a (thin) rubber fold that is on one end mounted to the side curves and on the other end to the (stiff) torso. These folds can wrinkle (like human skin) when the torso θ axis is nonzero.

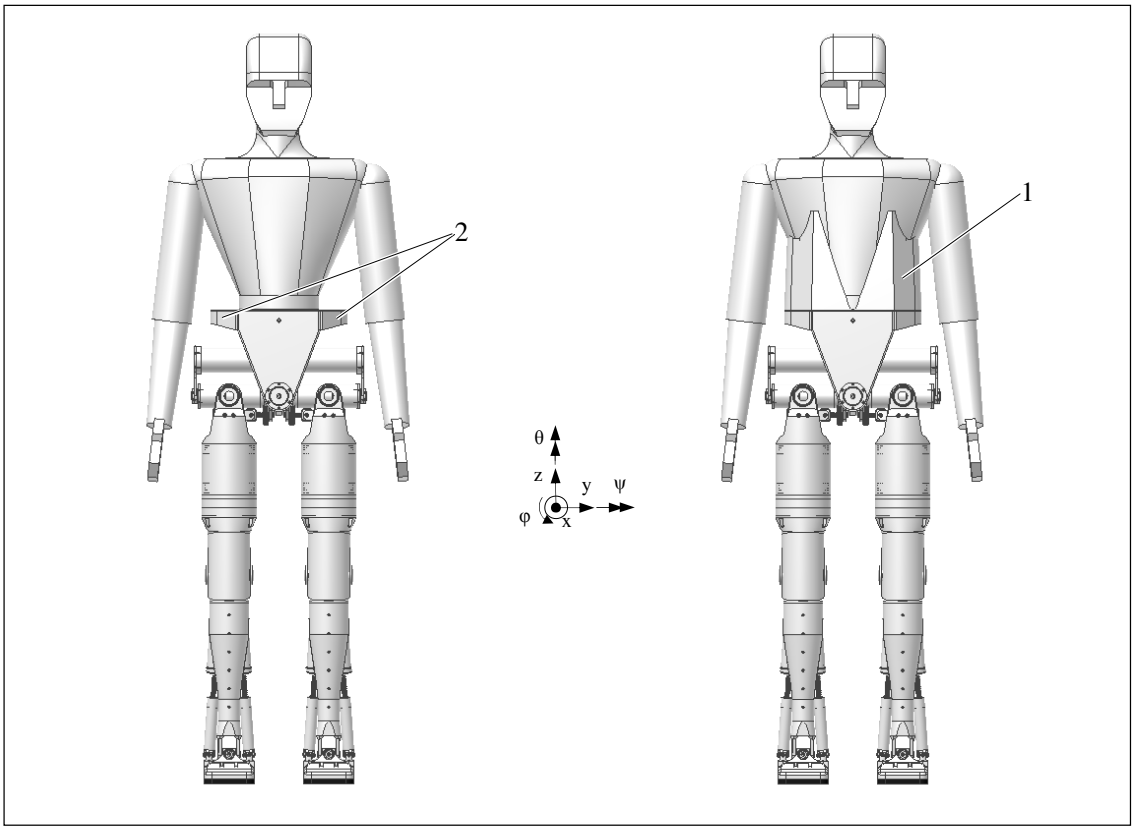

Figure 4.19: Anterior view of a possible anthropomorphic robot. Stiff upper body (left) and a rubber fold (1) that shapes the torso more human like is mounted on the side curves (2) (right).

4.7 Concluding remarks

The design of the hips and waist is not completely symmetric in the Sagittal plane, due to the four point contact ball bearing construction. Therefore, the assembly of the parts should be done with some care.

Like in the leg, bearings of the same type are used in multiple functions to reduce costs, number of spare parts and assembly errors. The hip ψ comprises the same bearing in the joint as in the joint actuation: INA FAG 61808-2RSR. INA FAG 626-2RS is used in the hip φ actuation as well in the torso φ actuation.

Apart from the universal joint in the hip φ actuation and the folded plates of the torso 'hood', the parts that have to be fabricated are designed to milled or turned. The universal joint can be fabricated with cut with wire EDM, the pinion gear of the torso φ actuation with sinker EDM and the folded plates have to be bent.
The milled and turned parts have fillet edges to prevent notch effects (stress raisers).

The design incorporates many fitting edges. Although this make the fabrication of individual parts more expensive (precision machining), these fitting edges ensure that the assembly of the robot is easy and does not have to be adjusted to e.g. get correct lengths, coinciding or intersecting axes of rotation, etc. Moreover, the assembly is more suited for repeated disassembly, and therefore, less expensive.

Through the use of aluminum, approximately all fabricated parts are light weight while remaining relatively inexpensive. Materials that are more light weight with comparable stiffness (e.g. magnesium alloys or carbon fiber parts) are expected to be too expensive.

The joint actuations are designed to be statically constrained, to avoid internal stresses, which could compromise the behavior of the actuations.

The mass of the waist and the hips (Figure 4.1 below right), has an approximate mass of 5.9 kg, which is 13 % of 45 kg. This mass fraction is the same as the average mass fraction of a human waist (according to Appendix A). The torso parts have a total mass of 2.9 kg. According to Appendix A, the torso should have a mass of 14.9 kg (33 % of 45 kg). Therefore, the remainder of the torso can have a mass of 12 kg, whereas the remainder of the total upper body can have a mass of 21.4 kg.

The masses of the individual links of the robot with respect to the total mass of the robot, which is 45 kg, are comparable to the average human mass fractions. Comparable masses for the upper body would be:

- torso 14.9 kg (2.9 kg already in use),
- upper arm 1.4 kg,
- lower arm 1 kg,
- hand 0.5 kg,
- head and neck 3.6 kg.

With these masses, the robot has a mass which is scaled from a human being with a total height of 1.8 m and a mass of 80 kg.

Chapter 5
Conclusion and recommendations

5.1 Conclusion

The goal of this thesis was: *To design a human like robot's lower body suitable for humanoid walking*. The new robot is human like because it is anthropomorphic: the configuration, link dimensions, ROMs and the link masses are comparable to human beings. The new robot is suitable for humanoid walking because the new robot's joints and actuations are able to provide ample torque, are stiff and comprise no backlash. These aspects are explained below.

A human like robot

In Table 5.1, the incorporated DOFs of these robots as well the new robot as the modified TUlip are given. As can be seen in this table, the new robot could be a humanoid with similar DOFs as Asimo and Wabian-2.

Table 5.1: Overview of the DOFs of current anthropomorphic robots (Asimo and Wabian-2) and of the new design. For comparison, modified TUlip is added as well. DOFs of the hands are left out, this would give a disproportional comparison.

Link	**Asimo***	**Wabian-2****	**New robot**	**Modified TUlip**
Face/Head	0	0	3#	0
Neck	3	3	4#	3
Torso	1	2	2#	0
Waist	0	2	2	0
Arm	2x7	2x7	2x7#	2x1
Leg	2x6	2x7	2x6	2x6
Foot	0	0	2x1	0
Total	**30**	**35**	**37**	**17**

* from (Sakagami et al., 2002), ** from (Takanishi et al., 2005), #proposed in section 4.6.

Together with an upper body as proposed as in section 4.6, the robot can be one of a few 'full' anthropomorphic robots, like the robots shown in Figure 1.1.

The new robot is able to perform more human like movements because the kinematic chain of the lower body has redundancy. Thereby, the robot is more agile than the initial and modified TUlip. Intersecting axes of rotation ensure that the computation of (inverse) kinematics is relatively simple. Moreover, the dimensions of the robot are comparable to an average human, according to Appendix A.

The link dimensions and masses are scaled from a human being of 1.8 m and 80 kg. The ROM of the robot is human like and for some joints it can be increased easily (e.g. by enlarging the ring gear segment) when this is desired for e.g. (inverse) kinematic computation for trajectory generation.

Improved walking and posture dynamics
The joint actuations of the new design are capable to provide ample torque. The robot should walk perform tasks while standing on its feet, according to the ZMP stability criterion. This criterion implies that the robot should be (dynamically) stable at all time instances. Relatively high torques are necessary to satisfy to this criterion. Thus; the new robot can provide sufficient joint torque to walk and perform tasks while standing on its feet, according to the ZMP criterion. In addition, the new robot joint actuations can even provide sufficient torque for standing up from a squatting position.

The (significant) improvement with respect to modified TUlip can be observed in Table 5.2.

Table 5.2: Joint torque with respect to the robot's overall mass in [N/kg].

		New robot (≈45 kg)		**Modified TUlip (≈30 kg)**	
joint		nominal [Nm/kg]	stall [Nm/kg]	nominal [Nm/kg]	stall [Nm/kg]
torso	φ	0.9	1.3	-	-
	θ	0.6	0.9	-	-
hip	φ	0.2*	2.2*	0.2	0.3
	ψ	1.7	2.5	1.3	2.0
leg	θ	0.6	0.9	0.2	0.3
knee	ψ	0.2*	3.8*	1.3	2.0
ankle	φ	0.4*	5.2*	0.2	0.3
	ψ	0.3*	4.8*	0.7	0.8
toe	ψ	0.02*	0.3*	-	-

* These actuations have angle dependent torque: minimal nominal torque and maximum stall torque are given.

Another aspect of the ZMP criterion is position control of the joints. This kinematic computation assumes rigid links, rigid joints and rigid joint actuations. The links, joints and joint actuations of the new robot are stiff. Moreover, the joint actuations are significantly stiffer than the joint actuations of the modified TUlip.
Furthermore, the robot comprises no backlash (either no backlash or imperceptible backlash). Together with the stiff joint actuations the new robot is suitable to use forward kinematics to 'predict' the movements of the new robot and consequently, the foot placement can be accurate and the robustness of walking and posture control is improved.

5.2 Recommendations

The design of the new robot has to be finished for fabrication. An upper body has to be designed and subsequently, fabricated. A new robot with a different configuration implies that the trajectory generation and the posture control has to be adapted to the new robot as well. These aspects are explained below.

Finalize design for fabrication
To finalize the design for fabrication, some parts can be optimized with Finite Element Methods (FEM) to reduce the weight while stiffness is not affected. Critical parts are the hood assembly of the torso φ and the lower leg base.

The electronics of the robot must be designed too. Some remarks:
- Absolute encoders (on the joint side) can be purchased or designed. Designed absolute encoders are dedicated and can be integrated in the new robot, whereas purchased encoders are less expensive.
- Local PCB's can be used to control the motors. The mass added to the links is minimal and the torso has more space for e.g. batteries.

– A CAN (Controller Area Network) bus can be used to transfer signals from, and to, the local PCB's. One power conductor can be used to provide power to the motors and local PCB's (in a parallel way).

When the lower body of the robot is finished, experiments on the sole of the feet have to result in a sole that fulfils the functions described in section 3.6.

Upper body
The design of the upper body, either a torso (biped) or a complete upper body (a torso, arms with hands and a head with a neck), has to be designed before, or during, the fabrication of the lower body. The torso will most likely contain the intelligence of the robot, so it is important that the torso is mounted to the robot, before testing. Moreover, the mass of the upper body is 53 % of the total mass (see Appendix A), and therefore, the weight of the upper body is of great importance for trajectory generation

It is recommended that the upper body consist of the DOFs described in section 4.5. With this configuration, the robot will leap to the eye and e.g. sponsors can be attracted to raise money for further research and development.

Trajectory generation and posture control
The new robot is more agile than modified TUlip but its feet have soles that have a smaller contact area. Moreover, the Support Polygon (SP) is definitely smaller when standing on one foot and most likely also smaller when standing on both feet (the feet are closer to each other). As a result, trajectory generation and posture control are of more importance because robustness is less. A redundant kinematic chain can be used to perform tasks while maintaining stability as in Figure 5.1 right.

Humans are capable of performing many different tasks and simultaneously move their limbs and torso implicitly to minimize effort. For example: When humans bend over to lift up an object, they implicitly maintain postural stability by moving their pelvis backwards as depicted in Figure 5.1 left. As a result, trajectory generation and posture control can also be used to reduce moment loads on the joints. Therefore, it reduces the power needed, which increases the time the robot can perform tasks.

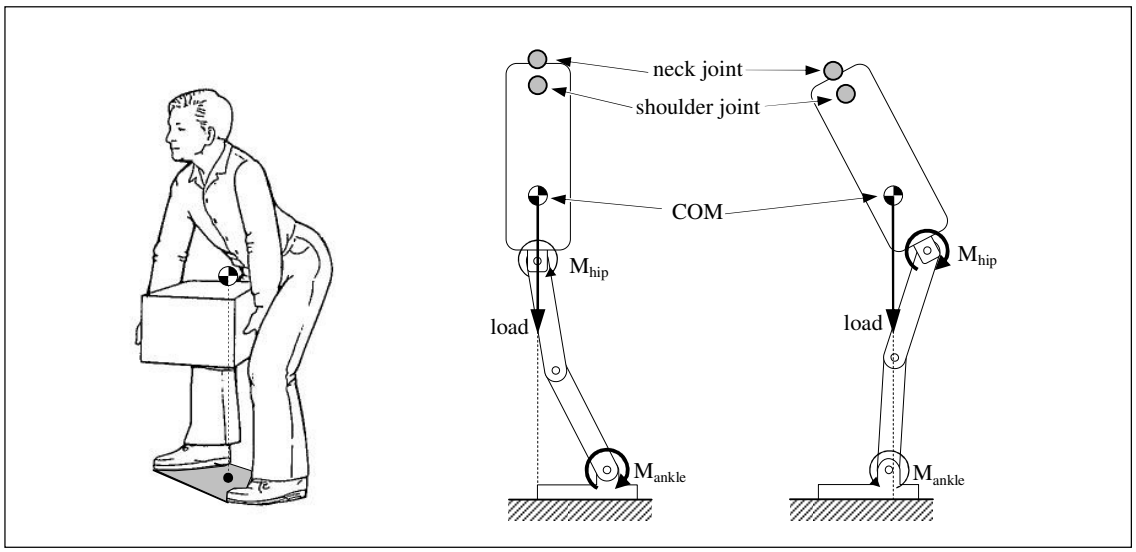

Figure 5.1: A human implicitly reduces the joint loads while performing tasks (left). Two robot that can perform similar tasks with the head and arms (neck and shoulder on approximately the same position): a robot that is at the edge of stability (middle) and a robot that is robust against perturbations (right). Both robots need approximately the same power: the middle robot must provide more torque in the ankle, whereas the right robot must provide more torque in the hip joint.

Bibliography

(Artas, 2010)
www.artas.nl

(Borovac & Slavnic, 2009)
Borovac, B., Slavnic, S., '*Design of Multi-segment Humanoid Robot Foot'*. Serbia: Novi Sad. University of Novi Sad, Faculty of Technical Sciences. 2009.

(Buschmann et al., 2009)
Buschmann, T., Lohmeier, S., Ulbrich, H., *'Humanoid robot Lola: Design and walking control'*. France: Paris. Journal of Physiology 103. 2009.

(Chevallereau, et al., 2009)
Chevallereau, C., Bessonet, G., Abba, G., Aoustin, Y., *'Bipedal Robots - Modeling, design and Walking Synthesis'*. United Kingdom: London. ISTE Ltd. 2009.

(De Haas, 1991)
De Haas, E., '*Mikroniek nummer 1 - Harmonic Drive als UHV-draaidoorvoer'*. Netherlands: Zoetermeer. Dutch Society for Precision Technology. 1991.

(Dekker, 2009)
Dekker, M.H.P., *'Zero-Moment Point Method for Stable Biped Walking'*. Netherlands: Eindhoven. Eindhoven University of Technology, Mechanical Engineering. DCT 2009.072. 2009.

(Dirken, 1999)
Dirken, J. M., *'Productergonomie - ontwerpen voor gebruikers'*. Netherlands: Delft. Delft University Press. 1999.

(HarmonicDrive, 2010)
www.harmonicdrive.com

(Hobbelen et al., 2008)
Hobbelen, D., De Boer, T., Wisse, M., *'System overview of bipedal robots Flame and TUlip: tailor-made for Limit Cycle Walking'*. France: Nice. IEEE/RSJ International Conference on Intelligent Robots and Systems. 2008.

(Kaneko et al., 2002)
Kaneko, K., Kajita, S., Kanehiro, F., Yokoi, K., Fujiwara, K., Hirukawa, H., Kawasaki, T., Hirata, M., Isozum, T.,'*Design of Advanced Leg Module for Humanoid Robotics Project of METI'*. IEEE Int. Conference on Robotics and Automation. USA: Washington DC. 2002

(Maxon, 2010)
www.maxonmotor.com

(McGeer, 1988)
McGeer, T., *'Passive dynamic walking'*. Canada: Burnaby, British Columbia. Simon Fraser University. 1988.

(Menzel & D'Aluisio, 2002)
Menzel, P., D'Aluisio, F., *'Robo Sapiens - Evolution of a New Species'*. USA: Napa, California. A Material World Book. 2002.

(Nilos, 2010)
www.nilos-ring.com

(Pratt & Williamson, 1995)
Pratt, G. A., Williamson, M. M., *'Series Elastic Actuators'*. Proceedings of IEEE International Conference on Intelligent Robots and Systems. 1995.

(Robocup, 2010)
www.robocup2010.org

(Rosheim, 1994)
Rosheim, M. E., *'Robot Evolution - The Development of Anthrobotics'*. USA: New York, New York. John Wiley & Sons, Inc. 1994.

(Rosielle, 2007)
Rosielle, P. C. J. N., *'Constructieprincipes - Bedoeld voor het nauwkeurig bewegen en positioneren'*. Netherlands: Eindhoven. Eindhoven University of Technology, Mechanical Engineering. 2007.

(Rosielle, 2010)
Rosielle, P. C. J. N., [private communications].

(Sakagami et al., 2002)
Sakagami, Y., Watanabe, R., Aoyama, C., Matsunaga, S., Higaki, N., Fuijmura, K., *'The intelligent Asimo: System overview and integration'*. Proc. IEEE/RSJ Int. Conference on Intelligent Robots and Systems, pp. 2478-2483. 2002.

(Sardain & Bessonet, 2004)
Sardain, P., Bessonnet, G., *'Forces Acting on a Biped Robot. Center of Pressure - Zero Moment Point'*. IEEE Transactions on Systems, Man, and Cybernetics - Part a: Systems and Humans, vol. 34, no. 5. 2004.

(Siciliano & Khatib, 2008)
Siciliano, B., Khatib, O., *'Springer Handbook of Robotics'*. Germany: Berlin. Springer-Verlag Berlin Heidelberg. 2008.

(SKF, 2010)
www.skf.com

(Takanishi et al., 2005)
Takanishi, A., Ogura, Y., Itoh, K., *'Some Issues in Humanoid Robot Design'*. USA: San Francisco, CA. Results of the 12th Int. Symposium ISRR. 2005.

(Van Zutven, 2009)
Van Zutven, P.W.M., *'Modeling, identification and stability of humanoid robots with a case study on humanoid robot TUlip'*. Netherlands: Eindhoven. Eindhoven University of Technology, Mechanical Engineering. 2009.

(Vukobratović & Borovac, 2004)
Vukobratović, M., Borovac, B., *'Zero-Moment Point - Thirty five years of its life'* [Journal]. Int. Journal of Humanoid Robotics. Vol. 1, No. 1, pp. 157-173. World Scientific Publishing Company. 2004.

(Vukobratović et al., 2007)
Vukobratović, M., Borovac, B., Potkonjak, V., *'Towards a unified understanding of basic notions and terms in humanoid robotics'*. Robotica. Vol 25, pp. 87–101. Cambridge University Press. 2007.

(Weston, 1985)
Weston, T., *'Atlas of Anatomy'*. Great Britain: London. Marshall Cavendish Books Limited. 1985.

(Whittle, 1996)
Whittle, M. W., *'Gait Analysis - An Introduction'*. Great Britain: Bristol. Reed Educational and Professional Publishing Ltd. 1996.

(Williams & Lissner, 1962)
Williams, M., Lissner, H., R., *'Biomechanics of Human Motion'*. Great Britain: London.W.B. Saunders Company. 1962.

(Winter, 1991)
Winter, D. A., *'Biomechanics and Motor Control of Human Gait: Normal, Elderly and Pathological'*. Canada: Waterloo, Ontario. University of Waterloo Press. 1991.

Appendix A
Anthropometry

A.1 Link Dimensions

The human skeleton can be taken as an example for the link dimensions of a humanoid robot. In Figure A.1, the key dimensions of the human skeleton are illustrated.

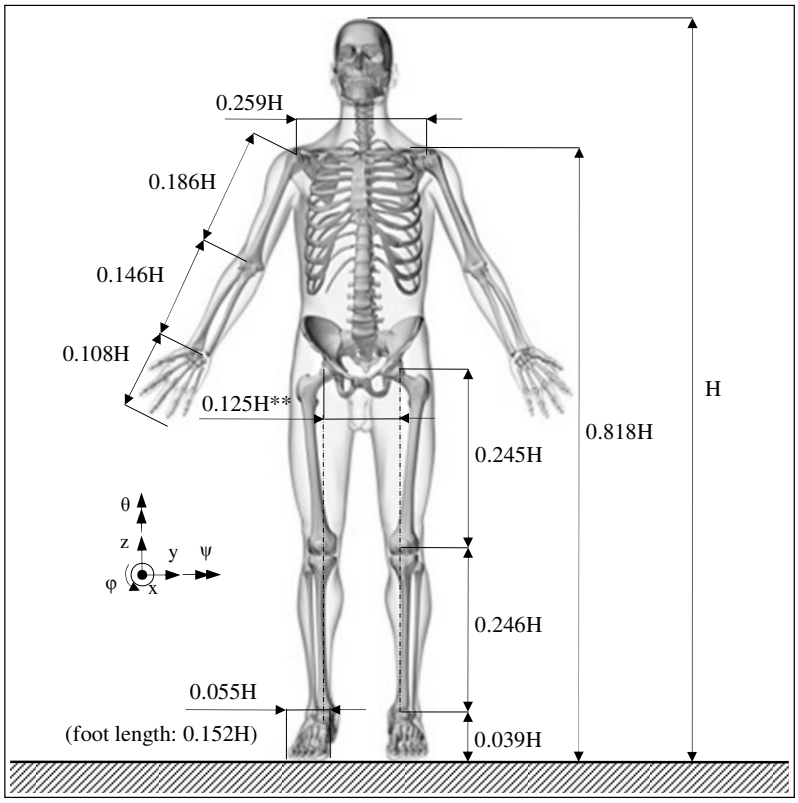

Figure A.1: Major body segment lengths of the human body, expressed as a fraction of total height H (Winter, 2005).
** From (Williams & Lissner, 1962).

Note that the hip joint, knee joint and ankle joint are vertically aligned.

A.2 Mass Distribution

To obtain a similar dynamical response to movements as a human, a robot should have a similar body mass distribution. This distribution is given in Table A.1.

Table A.1: Mass distribution of human beings, expressed as a fraction of total mass (Dirken, 1999).

body segment	**mass fraction [%]**
head and neck	8
torso	33
upper arm	3
lower arm	2
hand	1
arm	6
upper body	53
waist	13
upper leg	10
lower leg	5
foot	2
leg	17
lower body	47

Appendix B
Zero-Moment Point criterion

This Appendix is taken from (Dekker, 2009).

The ZMP could be defined as: *As the load has the same sign all over the surface, it can be reduced to the resultant force, the point of attack of which will be in the boundaries of the foot. Let the point on the surface of the foot, where the resultant force passed, be denoted as the Zero-Moment Point* (Siciliano & Khatib, 2008).

There are two major ways to compute the ZMP: via forward dynamics or by measuring the *Center of Pressure* (COP).

B.1 ZMP by Forward dynamics

An extremely simplified model to compute the ZMP is the so-called Cart-Table (Siciliano & Khatib, 2008). Figure B.1 illustrates a simplified model of a biped robot, which consists of a moving cart on a mass-less table. The cart has mass m and its position (x, z) corresponds to the equivalent COM of the robot. Also, the table is assumed to have the same *Support Polygon* (SP) as the robot.

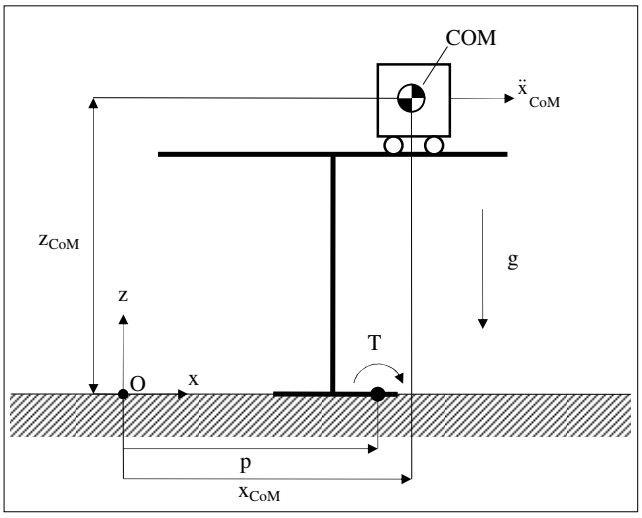

Figure B.1: Cart-table model.

In this case, the torque T around point P can be written as:

$$T = -mg\left(x_{COM} - p\right) + m\ddot{x}_{COM} z_{COM}\,. \tag{B.1}$$

Now, using the ZMP definition: T = 0 and thus $x_{ZMP} = p$, this results in:

$$x_{ZMP} = p = x_{COM} - \frac{\ddot{x}_{COM}}{g} z_{COM} \tag{B.2}$$

For the y direction the derivation is similar, so:

$$y_{ZMP} = p = y_{COM} - \frac{\ddot{y}_{COM}}{g} z_{COM} \cdot \tag{B.3}$$

B.2 ZMP by measuring COP

The *Center of Pressure*, in short COP, is the point on the ground where the total sum of the contact forces acts, causing a force but no moment. When the robot is walking, the feet are the only contact with the ground and encounter normal forces F_{Ni} and friction forces F_f. If the resultant force is within the funnel of apex 2α (α is the friction angle with the floor, so tan α < μ), the robot will not slide over the ground, so the location where this resultant force acts, can be found through the location of the resultant F_{RN} of the normal forces (see Figure B.2):

$$F_{RN} = \sum_{i=1}^{n} F_{Ni} \tag{B.4}$$

This resultant acts on the COP. So the position of the COP, denoted with (x_{COP},y_{COP}), with respect to the origin O_{xyz}, can be calculated with the equation:

$$x_{COP} = \frac{\sum_{i=1}^{n} x_{FNi} \cdot F_{Ni}}{F_{RN}}, \tag{B.5}$$

and

$$y_{COP} = \frac{\sum_{i=1}^{n} y_{FNi} \cdot F_{Ni}}{F_{RN}}. \tag{B.6}$$

The graphical representation of (B.5) and (B.6) is depicted in Figure B.2 right. If the COP is outside the SP, the biped tends to tip over, i.e. the biped will fall.

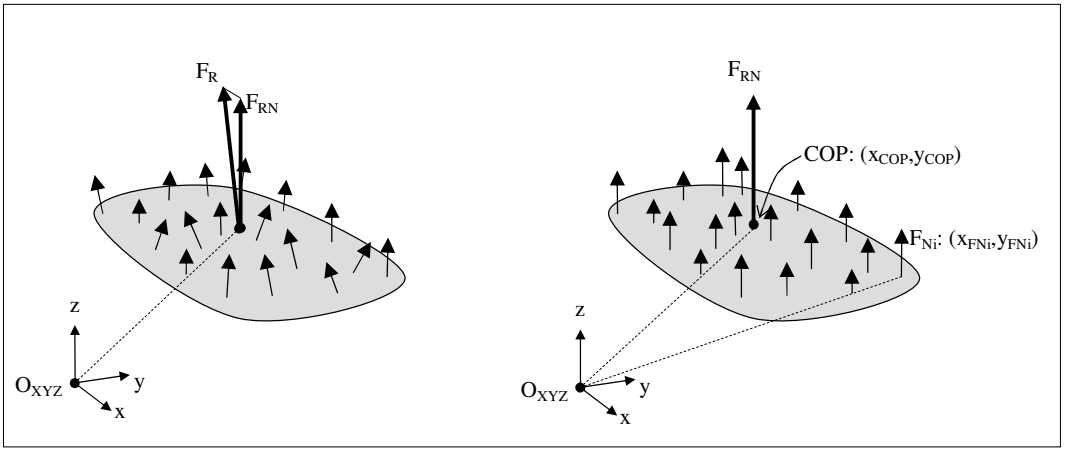

Figure B.2: The resultant force $\mathbf{F}_R$ (left) and the position of the COP (right).

B.3 ZMP Stability criterion

In order to achieve a dynamically stable gait the ZMP should be within the support polygon, at every time instance.

More information, definitions and calculation of the ZMP, COP and the ZMP criterion can be found in: (Dekker, 2009), (Sardain & Bessonet, 2004), (Siciliano & Khatib, 2008), (Van Zutven, 2009), (Vukobratović & Borovac, 2004) and (Vukobratović et al., 2007).

Appendix C
Static trajectories for ψ joint torques

To get an idea on the maximal required joint torques, a two dimensional model of a lower body is made. This is a Sagittal plane model (xz plane) and incorporates hip ψ, knee ψ, ankle ψ and toe ψ (and thus: a toe, a foot, a lower leg, an upper leg and a torso). The link dimensions match with new robot's dimensions and inertias are not taken into account because the movements are assumed to be slow (quasi-static).

From this, 'statically stable' trajectories for the joints have been generated, by means of trial and error. Together, the trajectories form the movement: *from: a squatting position with both toes on the ground and heels lifted, to: standing up straight with both feet flat on the ground.* In Figure C.1 this movement and the static stability check are shown.

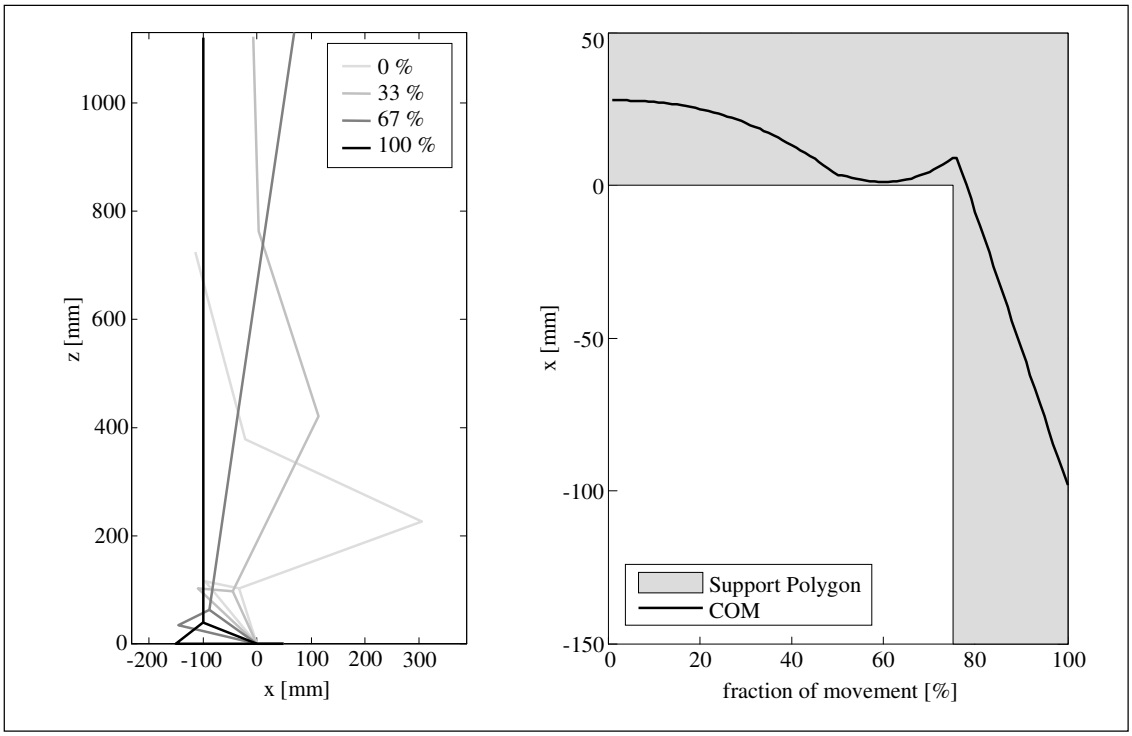

Figure C.1: Movement in Sagittal plane: *from: a squatting position with both toes on the ground and heels lifted, to: standing up straight with both feet flat on the ground.* (left). Stability check of the movement (right); The COM stays in the SP, so movement is considered to be statically stable.

From this, the required joint torques are derived, depicted in Figure C.2.

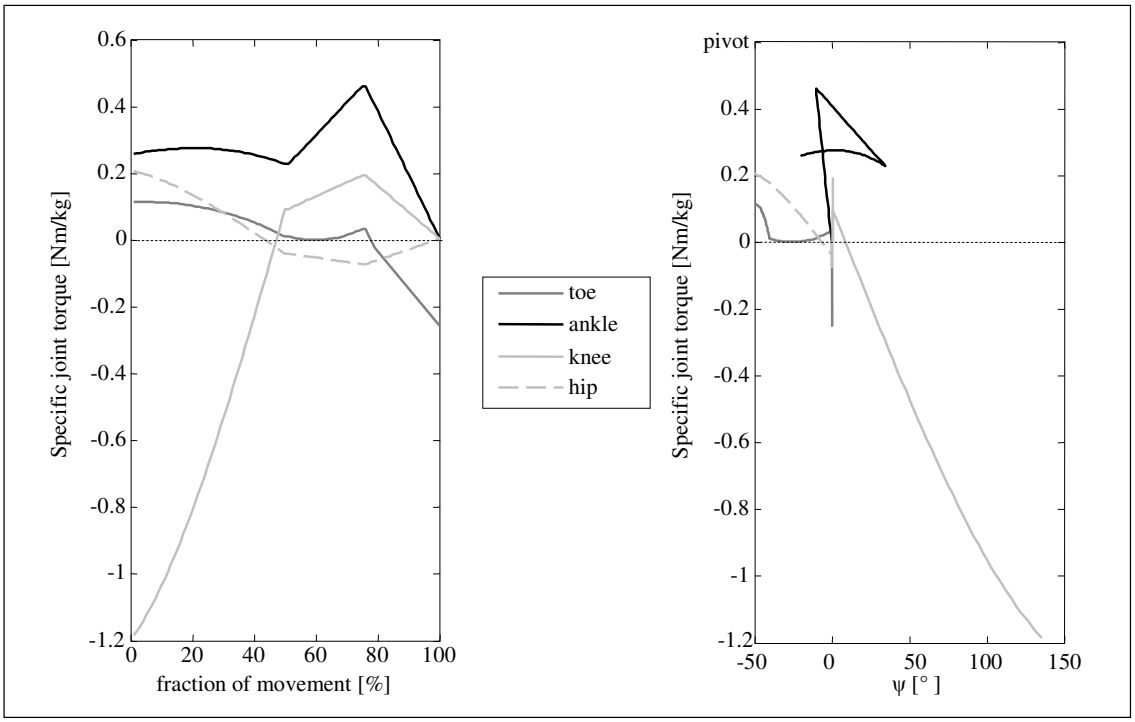

Figure C.2: Required specific ψ joint torques (w.r.t. the total body mass) as a result from the movement of Figure C.1.

Appendix D
Knee ψ joint actuation concepts

In this Appendix, sixteen concepts for the knee joint actuation are shortly mentioned, prior to the elaboration on four concepts after which arguments for the chosen concept are given. Note that the figures in this Appendix are schematic, just to give an idea of the concept, rather than proper scaled kinematic figures.

D.1 Direct ball screw

This concept utilizes a linear actuation, to rotate the lower leg. Because brushed DC motors are used, a ball screw transforms the rotary motion from the motor into a linear motion. For reasons described in section 2.4, the ball screw is chosen, contrary to power screws or roller screws.

Posterior direct ball screw actuation.
In Figure D.1, four (schematic) constructions of a direct ball screw actuation are shown.

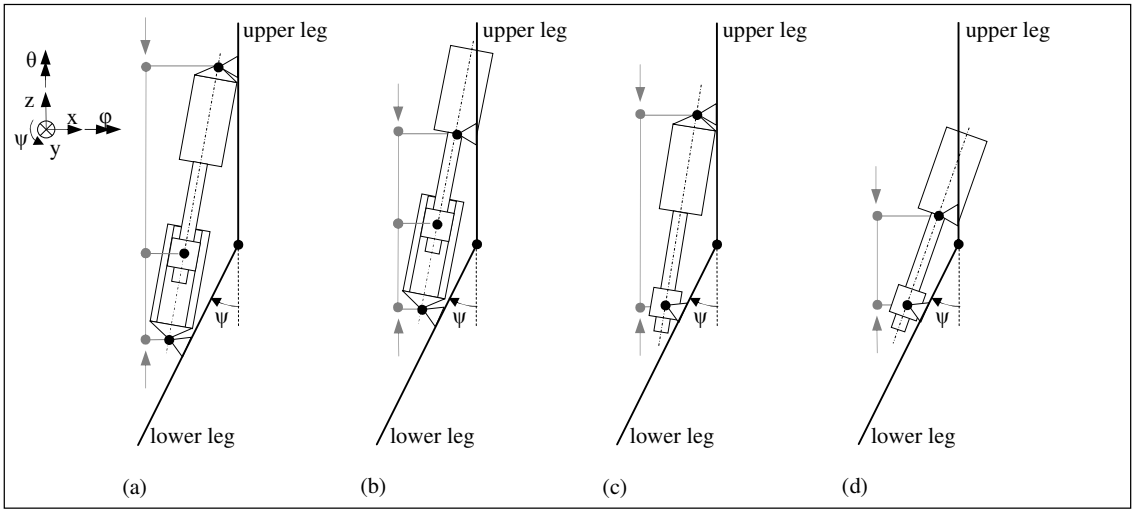

Figure D.1: Schematic views of the knee joint actuation with a direct ball screw at the back of the leg. (a) and (b) consist of a motor, spindle, nut and nut sleeve, (c) and (d) consist of a motor, spindle and nut. In (a) and (b), the nut sleeve is supported at the bottom to the lower leg, in (c) and (d), the center of the nut is fixed to the lower leg. In (a) and (c), the motor is supported at the top, in (b) and (c) the motor is supported at the location where the spindle is fixed to the motor. If the actuation is regarded as a chain; (a) and (b) consist of two links and (c) and (d) of one link, all shown in gray (arrows represent a compression force).

As can be seen, Figure D.1d is the best concept to withstand compression forces; it is stiffer with respect to buckling of the construction than the others. Nevertheless, this concept has a larger roll movement than a, b and c, as knee ψ passes through its ROM, because the effective length between the pivots on the upper and lower leg is small. This implies that this concept needs more space in the upper leg than e.g. concept a, which needs the least of roll movement, because the effective length between the pivots is the largest.

Anterior direct ball screw actuation.
Equivalent to the posterior direct ball screw actuation, there are also four concepts with an anterior ball screw actuation.

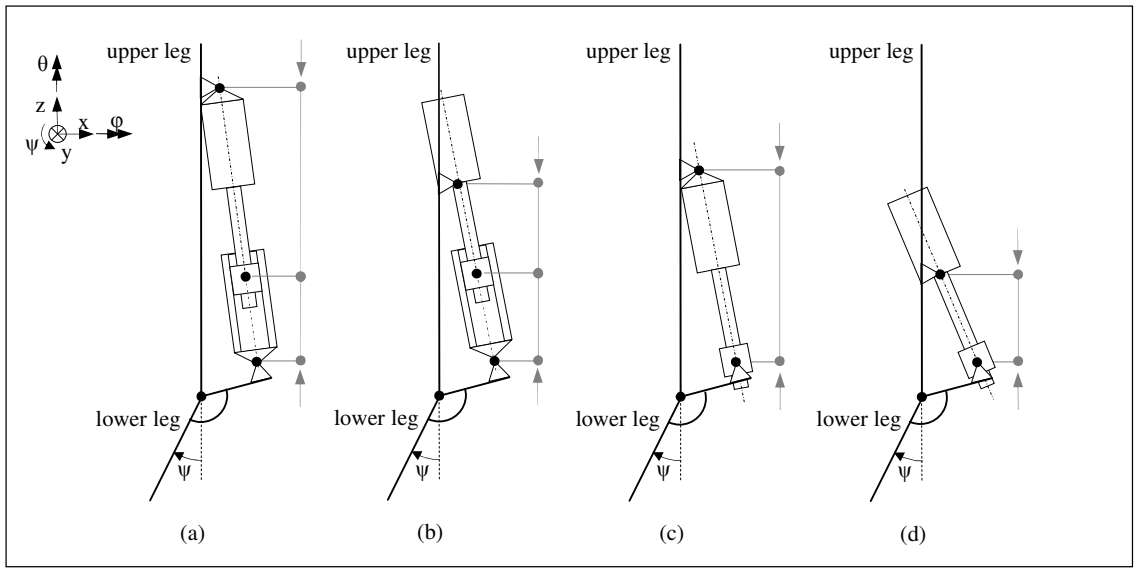

Figure D.2: Schematic views of the knee joint actuation with a direct ball screw at the front of the leg. (a) and (b) consist of a motor, spindle, nut and nut sleeve, (c) and (d) consist of a motor, spindle and nut. In (a) and (b), the nut sleeve is supported at the bottom to the lower leg, in (c) and (d), the center of the nut is fixed to the lower leg. In (a) and (c), the motor is supported at the top, in (b) and (c) the motor is supported at the location where the spindle is fixed to the motor. If the actuation is regarded as a chain; (a) and (b) consist of two links and (c) and (d) of one link, all shown in gray (arrows represent a compression force).

Again, concept d, is the best concept to withstand compression forces and concept a has the least roll movement.
The concept of placing the actuation anterior has two major advantages with respect to posterior actuation:
- High forces in the spindle, as a result of e.g. standing up from a squatting position, are under tension rather than compression. So, buckling is less critical.
- Anterior actuation does not obstruct the movement of the lower leg and thus; upgrading the actuation to more power, implying a larger motor, is much easier.

D.2 Indirect ball screw

Figure D.3 shows five concepts with a ball screw that, via a secondary transmission, actuates the knee joint.

Ball screw with linear guide
These concepts (a, b and c) focus on the fixation of the motor in six DOFs. From the (center of the) nut, the force is transmitted to the lower leg by means of a push pull rod (a and b) or a disc with a slot in which a track roller rolls (c). These constructions introduce forces that are perpendicular to the spindle. In order to withstand this, the nut is linearly guided and the linear guide needs to absorb these perpendicular forces. Now, the spindle only gets axial forces which is favorable.
A major advantage of these kind of actuations is that the spindles can be supported at the location where it is also fixed to the motor and the push pull rods (a and b) or the track rollers (c) coincide with the center of the nut and thus; compression forces are not critical.

Ball screw stroke reduction
These concepts (d and e) focus on ball screw stroke reduction. So, however the ball screw actuation stroke is small, the full ROM of the knee ψ can be obtained. Concept (d) has an ‘excavator’ bar linkage and concept (e) has a disc with a slot, in which a track roller rolls. The rotation of this disc is

then transmitted to a (smaller) disc with e.g. a steel belt. Both secondary transmissions have a ratio i > 1.

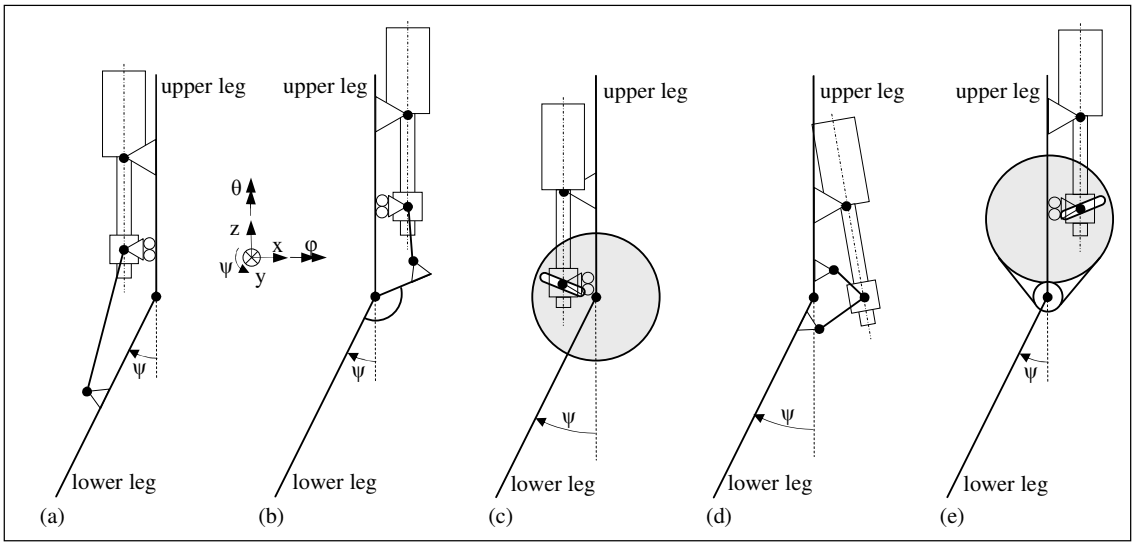

Figure D.3: Schematic views of the knee joint actuation, with a ball screw and a secondary transmission: (a) and (b) a push pull rod, (c) a disc with a slot connected to the lower leg, (d) an excavator bar linkage and (e) a disc with a slot and a steel belt to a disc connected to the lower leg.

D.3 Other concepts

In Figure D.4 three other concepts of knee actuation are shown.

Bevel gear in combination with a planetary reduction

This concept (a) incorporates a planetary reduction in combination with a bevel gear. This bevel gear is placed between the motor and the planetary reduction because bevel gears introduce perpendicular forces which have to be supported to the upper leg; these forces are small if it is placed directly on the motor. Now, the secondary transmission is the planetary reduction which has the advantage that is does not introduce perpendicular forces, because it is a concentric reduction.

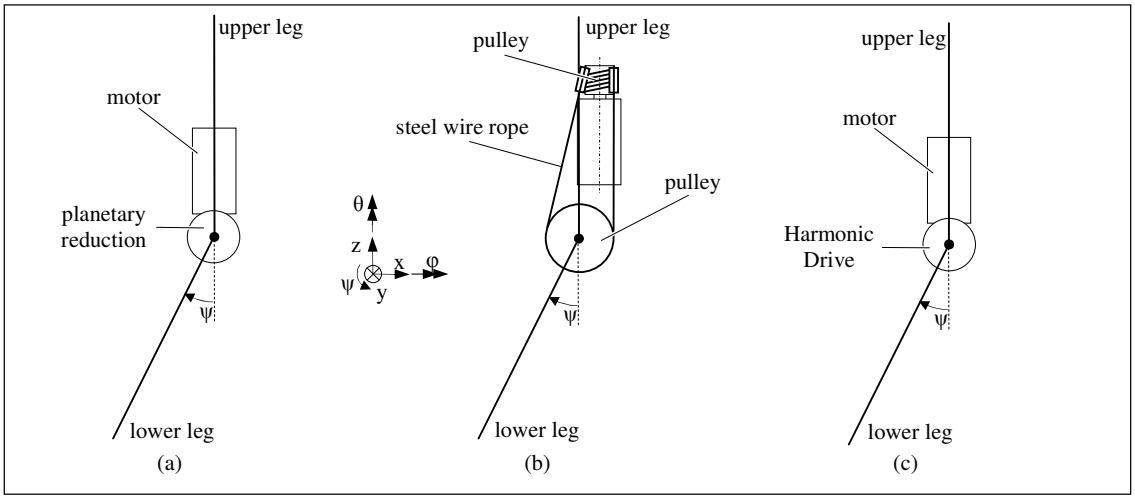

Figure D.4: Schematic views of concepts for knee actuation without a ball screw: (a) planetary reduction with a bevel gear, (b) planetary reduction with a steel wire rope on pulleys and (c) a Harmonic Drive.

Planetary reduction in combination with a steel wire rope on pulleys
This concept (b) is used in modified TUlip to actuate the knee (and hip ψ and ankle ψ). The steel wire rope on pulleys is the secondary reduction which increases the torque. Because the motor with a planetary reduction has a length that is larger then the leg width, it has to be placed vertically in the leg. Because of this, the steel wire rope has to incorporate a perpendicular transmission due to the fact that the knee axis is perpendicular to the vertical centerline of the leg. This is disadvantageous with respect to stiffness and efficiency.

Harmonic Drive
The Harmonic Drive (concept c) can withstand high torques. Therefore, it can directly actuate the knee joint. It is small so it provides much space for other functionality like e.g. a leg θ actuation or electronics.

D.4 Final choice from four concepts

Because of the large ROM of the lower leg (from 0° to 135°), from each section, concepts which incorporate the anterior actuation, are chosen:
- a direct ball screw actuation,
- an indirect ball screw actuation with a push pull rod as a secondary transmission,
- an indirect ball screw actuation with an 'excavator' bar linkage as a secondary transmission,
- an Harmonic Drive actuation.

The kinematics of these concepts are designed in SAM[E] and then, checked in CAD. With these kinematics, the transmission ratio and the provided joint torques are computed. With the stiffness of bearings, ball screws, bars and push pull rods; an estimate for the actuation stiffness is computed. After this, some other aspects of the concepts are evaluated.

Ratio and joint torque
The transmission ratios of the concepts can be seen in Figure D.5, The joint torques are displayed in Figure D.6.

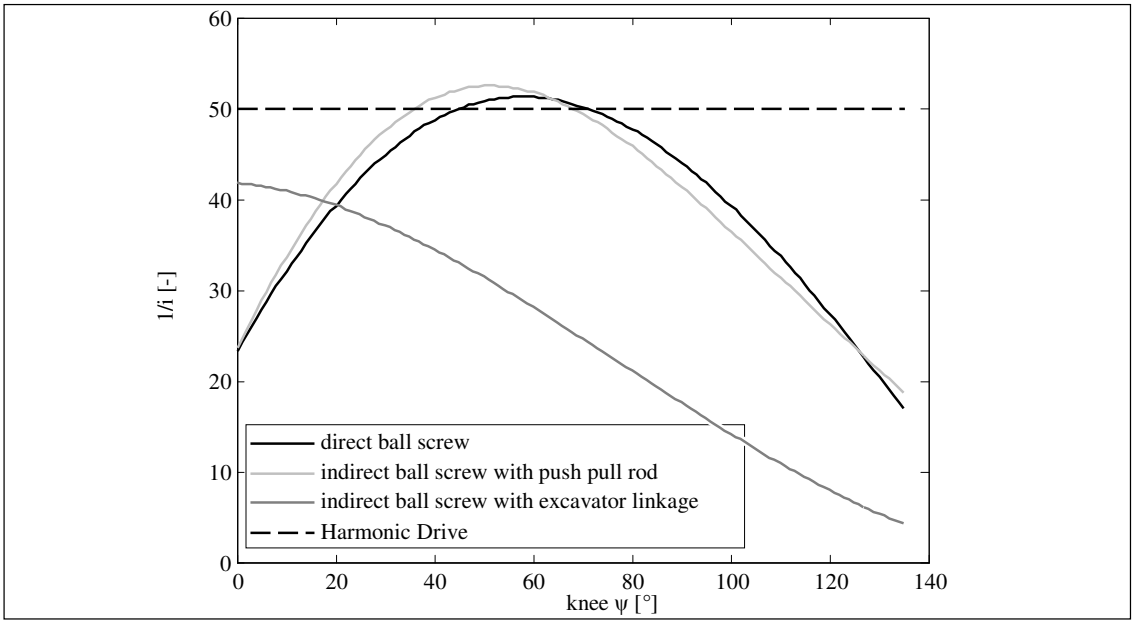

Figure D.5: Transmission ratio in comparison for four knee actuation concepts in 1/i.

[E] SAM (Synthesis and Analysis of Mechanisms) is an interactive PC-software package for the design, analysis (motion and force) and optimization of arbitrary planar mechanisms (Artas, 2010).

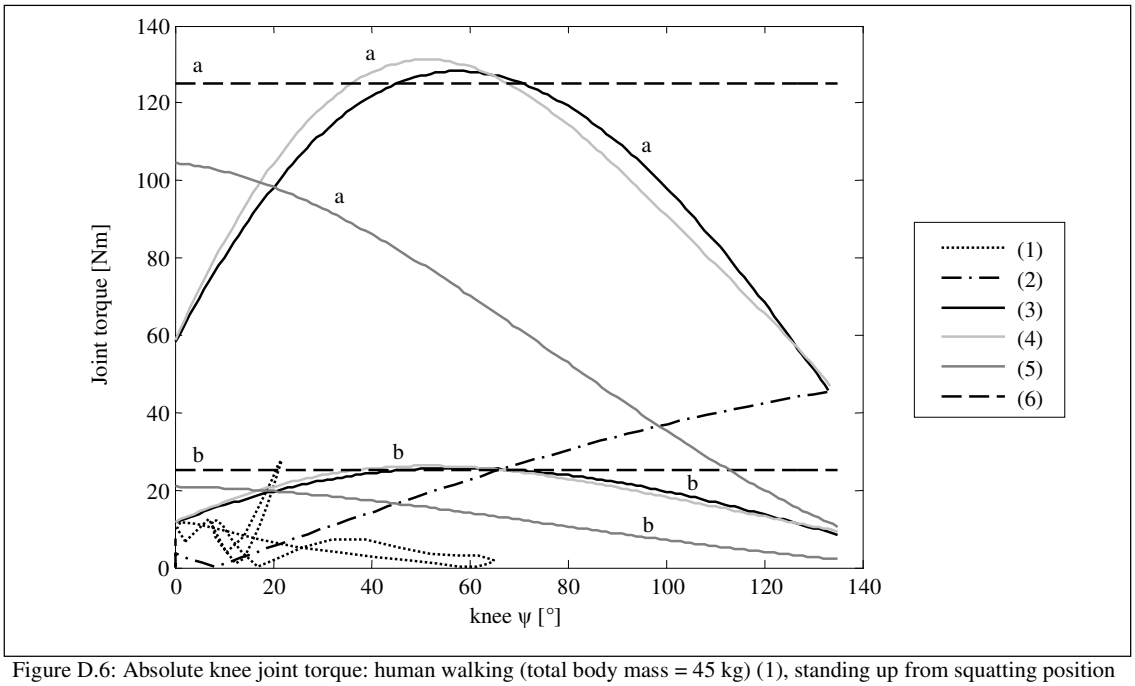

Figure D.6: Absolute knee joint torque: human walking (total body mass = 45 kg) (1), standing up from squatting position (total body mass = 45 kg) (2), Direct ball screw (3), Indirect ball screw with push pull rod (4), Indirect ball screw with excavator bar linkage (5) and Harmonic Drive (6). Note that for (3, 4, 5 and 6): a = stall torque and b = nominal torque.

All concepts can provide enough torque for walking, moreover; almost the whole stride is done with nominal torque. However, the movement; standing up from a squatting position, shows that the indirect ball screw actuation with an 'excavator' bar linkage as a secondary transmission can not provide enough torque, even when the motor is close to stall torque. This is due to the dropping transmission ratio which ensures a small ball screw stroke (about 21 mm).

The direct ball screw actuation, the indirect ball screw actuation with a push pull rod as a secondary transmission and the Harmonic Drive actuation are sufficient because they can provide ample torque. The first two concepts have a knee ψ dependent ratio. In the ψ range close to the stretching of the knee, the ratio increases (1/i decreases, see Figure D.5,) which implies that the provided torque drops and the joint velocity increases. This has a major advantage: if the knee is stretched, the particular leg can be either the stand leg or 'in the air'. In both cases, the requested knee torque is relatively low because if the leg is the stand leg, the COM is above the foot, which implies a short moment arm, and if the leg is in the air, the only torque subjected on the knee, is the torque as a consequence of the mass of the lower leg and foot which is relatively low.
So, in the case that the knee is almost stretched, the torque is low, but it can be actuated faster due to the increased ratio.

Actuation Stiffness
For this comparison, the three actuations which incorporate ball screws have 2 axial needle roller bearings (INA FAG AXK1528), in parallel, to fix the ball screw to the motor. The stiffness of these bearings is estimated on $2 \cdot 10^8$ N/m. The ball screw spindles have a nominal diameter of Ø 10 mm and the Young's modulus is 210 GPa. The computation takes the effective length of the spindle into account. Furthermore, the contact stiffness of the nut (via the balls) on the spindle is estimated to be $10 \cdot 10^7$ N/m and the axial stiffness of the push pull rod is estimated on $1 \cdot 10^8$ N/m.
Together with the effective radius of the actuation, the rotational stiffness of the knee is computed and depicted in Figure D.7. Finally, the stiffness of the Harmonic Drive actuation is taken from the catalogue (HarmonicDrive, 2010) and also depicted.

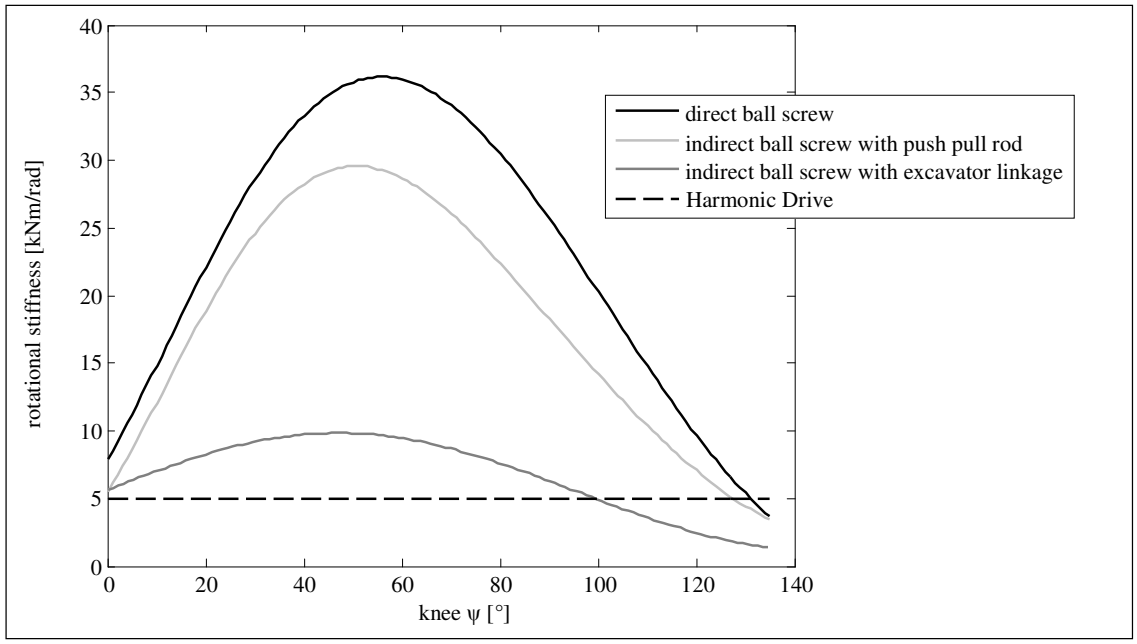

Figure D.7: Rotational stiffness estimation of four knee ψ actuation concepts.

The direct ball screw comprises the highest stiffness, due to the fact that it has less components (each with their own stiffness) in series than the two concept which have a indirect ball screw. The Harmonic Drive has a relatively low stiffness due to the 'flexible spline' (see section 2.4).

Efficiency and hysteresis
The efficiencies of the ball screw actuations, direct as well as indirect, are estimated on 90 %, because the energy loss due to friction in bearings is considered to be negligible. The efficiency of the Harmonic Drive is around 78 % (HarmonicDrive, 2010).

Compactness, complexity of the construction and compatibility with other DOF actuations
The Harmonic Drive needs very little space to transmit the torque, but it has to be concentric with the knee axle to avoid a secondary transmission which will decrease stiffness even more. Because it is concentric with the knee axle, the COM of the actuation is also close to the knee axis; this is unfavorable with respect to the total COM of the robot. The construction, to statically constrain the actuation, can be very simple with a Harmonic Drive.

Indirect ball screw actuations contain many components to statically constrain the actuation, simply because there is a secondary transmission. For example; the indirect ball screw with a push pull rod as a secondary transmission must incorporate a linear guide for the nut, which becomes a rather complex construction in order to avoid unnecessary additional moments and forces to the ball screw.

The direct ball screw is simple to construct, which implies few components and thus; high stiffness and high accuracies can be reached while hysteresis and backlash can be prevented easier.

Costs
As mentioned in section 2.4, the Harmonic Drive costs around € 1500,-, whereas ball screw actuations cost approximately a few hundred Euros. Ball screw actuations need more other components to statically constrain the actuation, but these components are expected to be cheap contrary to the Harmonic Drive. The direct ball screw incorporates fewer components than the other two ball screw concepts, so the concept of a direct ball screw is expected to be the most cost effective.

Final choice
The *anterior direct ball screw actuation* concept is chosen;
- it provides ample torque,
- it is the stiffest actuation,
- it is an efficient transmission,
- the construction concept is one of the least complex,
- and (of the four concepts) it is the most cost-effective.

To compromise between the buckling-resistance and the rolling movement (due to the effective length between the pivots), the chosen concept of the direct ball screw from Figure D.2 is b or c. Because a motor cup (containing the motor) which is fixed to the spindle has a higher torsion stiffness (proportional to D^3t) and bending stiffness (proportional to D^4) than a sleeve which contains the nut, the concept with a motor cup has been chosen, so: Figure D.2 c.

After this comparison, the design is further detailed and dimensioned, see section 3.2. The above displayed ratios, torques and stiffness of the chosen design were subjected to changes to improve the design, this is why the final design has slightly different (better) specs.

Appendix E
Ground contact dynamics for SimMechanics™

To test generated trajectories in simulation environment, truthful contact dynamics are of great importance. When walking, the ground is the fixed world and the only source of disturbances to the robot (assuming wind still, no stick-slip and no play).
Each point that is in contact with the ground experiences a force F that can be decomposed in three (Cartesian) forces: the normal force F_N, and two frictional forces F_{fx} and F_{fy}, depicted in Figure E.1 (left).

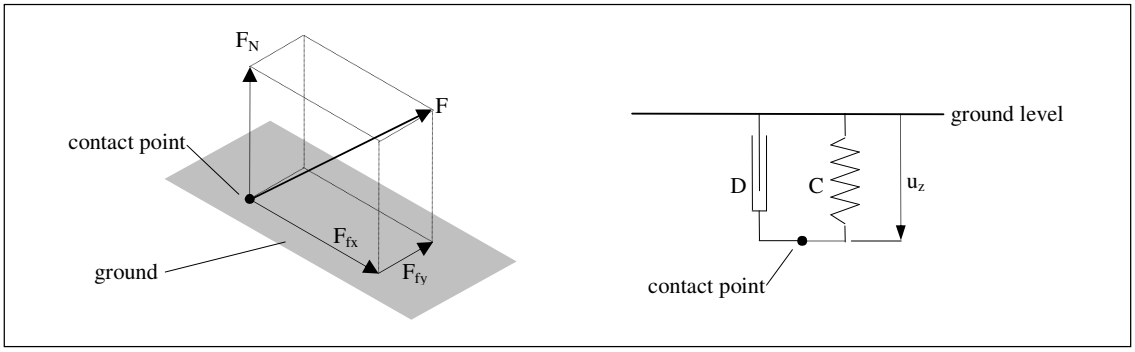

Figure E.1: Ground reaction forces on a contact point (left) and a spring-damper unit connected to a contact point (right).

Assume that on each contact point, a spring-damper unit is connected, see Figure E.1 right. The spring-damper unit has a nominal length of zero, and if the contact point moves below the ground level the distance from ground level to the contact point is denoted with u_z. This distance is zero when the contact point is above ground level.
The vertical component F_N, can be computed if the contact stiffness c and damping D is known:

$$F_N = \left| cu_z + D\dot{u}_z \right| \tag{E.1}$$

c is the stiffness of the sole, assuming the ground is infinitely stiff and D the damping factor of the sole. Note that the impact force equation (eq. 3.7), does not have to be incorporated in this model because u_z is a result of the impact speed and mass (moreover: $\dot{u}_z = v_{impact}$).

The measured can only be positive because the floor can not be penetrated.
Now, with the known vertical force F_N, the magnitude of the friction forces F_{fx} and F_{fy} can be derived if the friction constants μ_x and μ_y (frequently similar) are known:

$$F_{fx} = \mu_x \cdot F_N \tag{E.2}$$

and

$$F_{fy} = \mu_y \cdot F_N \tag{E.3}$$

However, the direction of these forces is (still) unknown. The contact point could be anywhere on the floor, so the position (u_x, u_y) of the contact point can not be used: the friction forces act in the negative horizontal velocity direction. The friction forces are not proportional to the speed, so only the sign of the velocity must be incorporated:

$$F_{fx} = -\text{sign}(\dot{u}_x) \cdot \mu_x \cdot F_N \tag{E.4}$$

and

$$F_{fy} = -\text{sign}(\dot{u}_y) \cdot \mu_y \cdot F_N \tag{E.5}$$

Sign functions are discontinuous and consequently, slow down ODE (Ordinary Differential Equation) solvers in Matlab®. A so called *Sigmoidal function*[F] can be used for a continuous function that imitates a sign function, see Figure E.2.

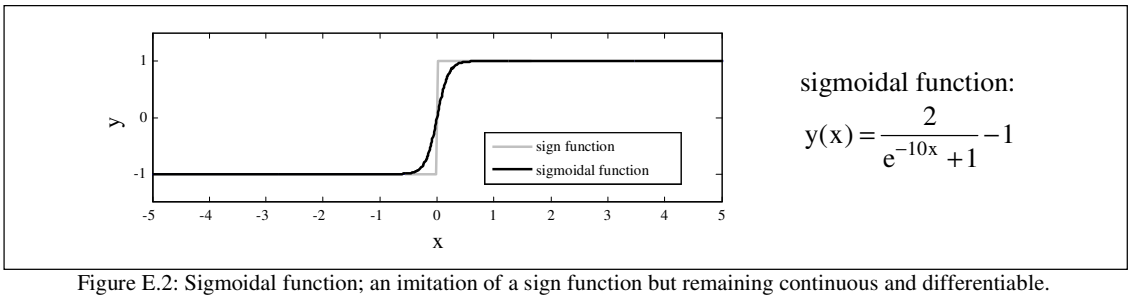

Figure E.2: Sigmoidal function; an imitation of a sign function but remaining continuous and differentiable.

Implemented in a Matlab Simulink the forces can be derived as depicted in Figure E.3. The inputs can be obtained from the Matlab SimMechanics model, the outputs can be used as inputs for the SimMechanics model.

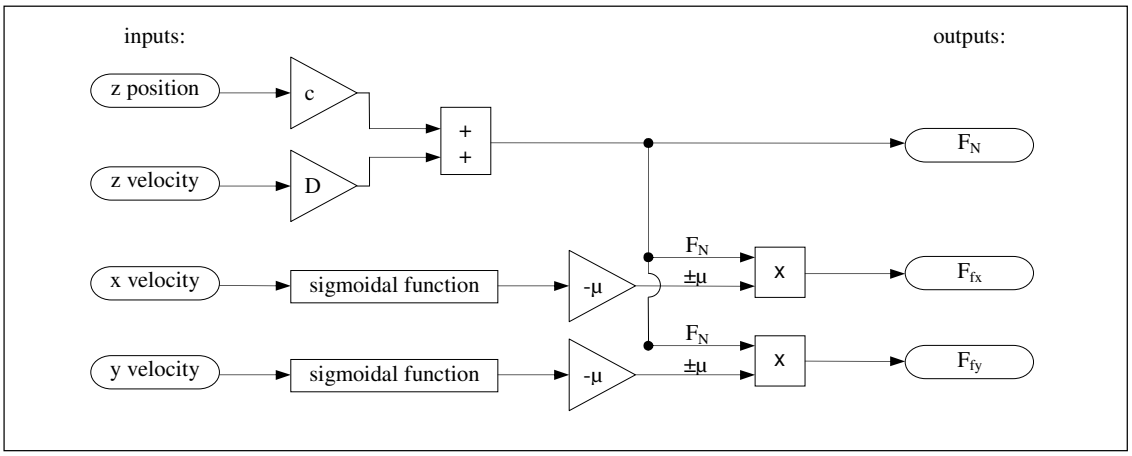

Figure E.3: Computation of contact forces in a Matlab Simulink model. Note that another function determines if the contact point is on (or 'below') the ground.

[F] A sigmoid curve is produced by a mathematical function having an 'S' shape. Basically, the equation looks like: $y(x) = a/(e^{bx}+1)$. It is continuous, differentiable and has a pair of horizontal asymptotes (0 and a). The parameter b is a measure for the saturation speed.

Appendix F
Hip ψ joint actuation concepts

In this Appendix, five concepts for the hip ψ joint actuation are mentioned after which arguments for the chosen concept are given. Note that the figures in this Appendix are schematic, just to give an idea of the concept, rather than proper scaled kinematic figures.

F.1 Planetary gearbox with secondary transmission

The concepts in Figure F.1 comprise a DC motor that is screwed on a planetary transmission (done by supplier). The planetary gearbox is, subsequently, fixed to the waist.
In Figure F.1 can be seen that the secondary transmission can be either a gear set (pinion and ring gear segment with external teeth) or a steel wire rope (or steel belt or toothed belt) on pulleys.

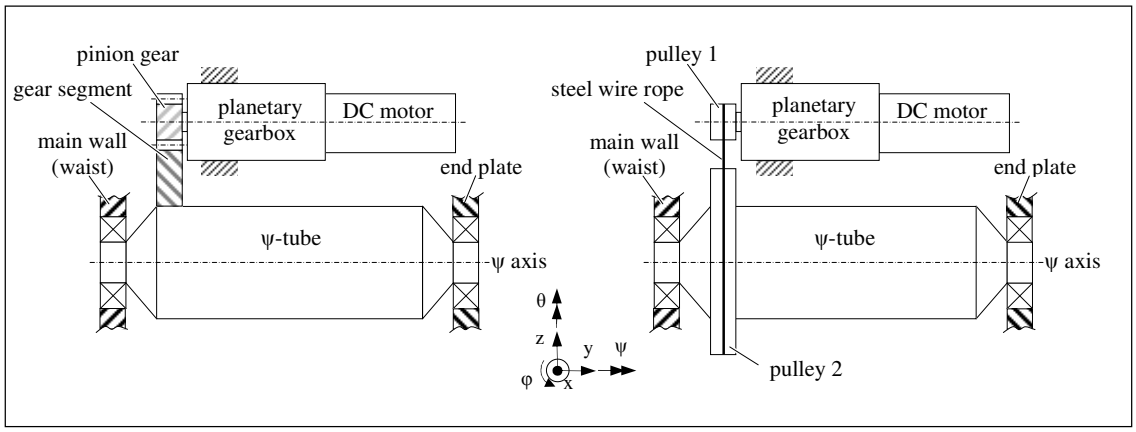

Figure F.1: Actuation of hip ψ, with a DC motor and planetary gearbox. As secondary transmission a gear set (left) or e.g. steel wire rope (right) can be used.

Both concepts have a secondary transmission for the following arguments: a final reduction implies a planetary gearbox with fewer stages, which is beneficial for the efficiency, and a final reduction reduces the backlash that is present in the planetary gearbox.
An additional advantage is that the motor and gearbox can be placed eccentrically to the ψ axis. In this case, the ψ-tube can be of maximum length (between the bearings) to provide space for hip φ actuation.

F.2 Indirect ball screw

This concept, depicted in Figure F.2, incorporates a DC motor with a ball screw spindle fixed to the waist. The ball screw nut is linearly guided and prevented from rotating in such way that it can translate over the ball screw axis. Onto the ball screw nut, a steel wire rope is fixed and this steel wire rope is redirected, by means of pulleys, to the disc that is fixed to the ψ-tube. Therefore, the linear motion of the ball screw nut is transformed by the steel wire rope into a rotating motion of the disc, and consequently, of the ψ-tube.
In Figure F.2 (left), the position of the motor is schematically; it can be placed elsewhere, as long as it actuates the spindle. The steel wire rope is fourfold applied, to prevent the nut from additional moment loads (the forces apply to the center of the ball screw nut, see Figure F.2 right).

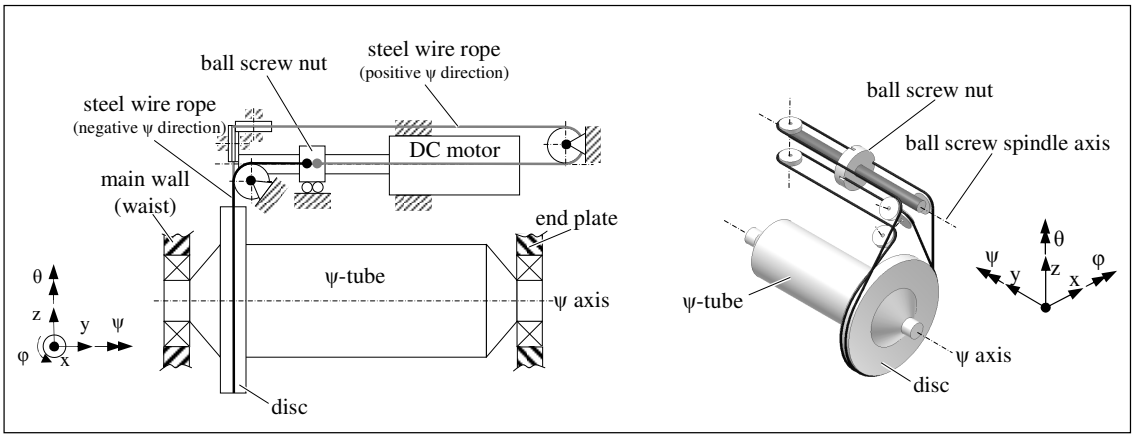

Figure F.2: Actuation of hip ψ, with a DC motor and a ball screw spindle. On the ball screw nut, steel wire ropes ar connected to transform the linear motion of the ball screw nut to a rotation of the ψ -tube, via the disc.

F.3 Direct ball screw

In this concept, the ball screw nut is directly connected to the ψ-tube, through two discs on both sides of the nut (double shear principle for the axles).
Because this is a direct ball screw actuation, the motor has to pivot and the ball screw has to elongate or shorten, in order to allow the ψ-tube to rotate. For this, the same arguments as mentioned in section D.1, hold.

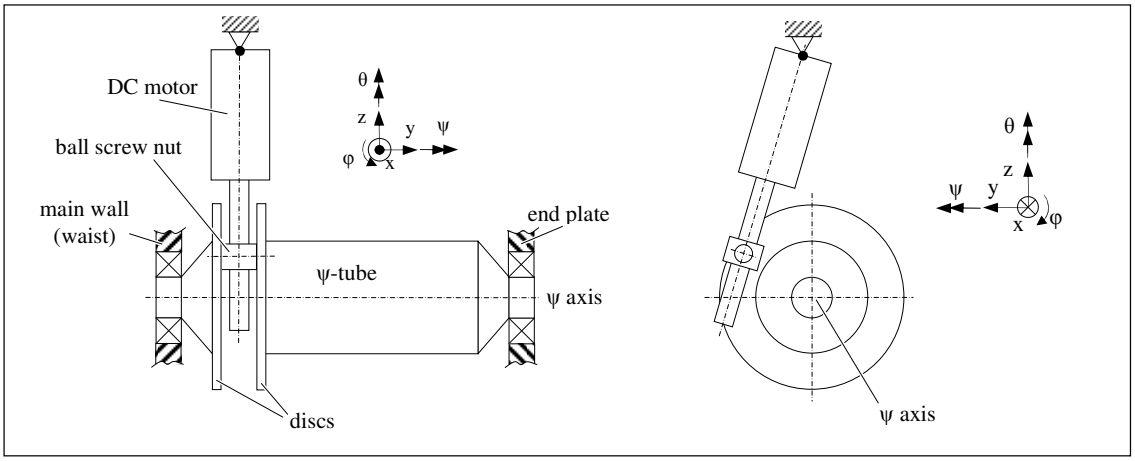

Figure F.3: A direct ball screw actuation of hip ψ. The ball screw nut is connected through two disc to the ψ-tube: the translation of the ball screw nut is transformed to a rotary motion of the ψ-tube.

To statically constrain this actuation, the ball screw nut should be between two universal joints.

F.4 Harmonic Drive

A motor, fixed to the waist, actuates the wave generator of the HD via a steel wire rope or a belt drive. The circular spline of the HD is also fixed to the waist and the flexible spline is fixed to the ψ-tube.

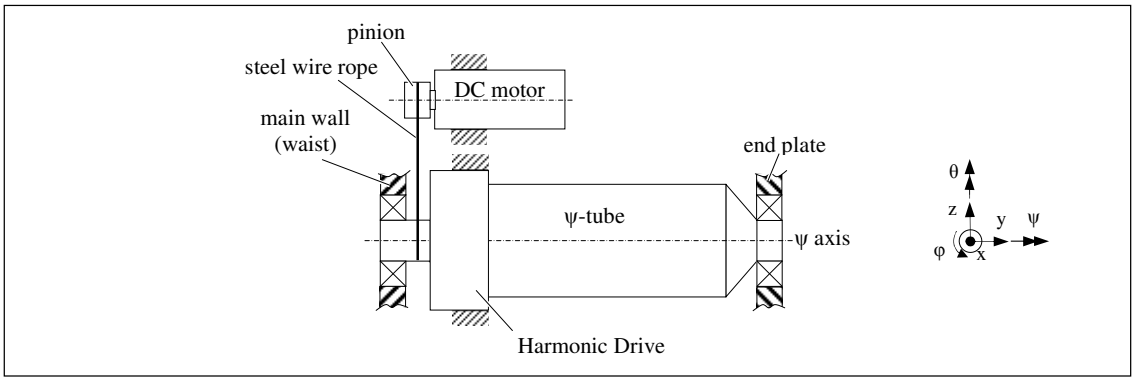

Figure F.4:

F.5 Final choice

All concepts have a reduction that actuates the ψ-tubes as close as possible to the main wall of the waist. In this way, the hip φ joint and its actuation are not obstructed.

Comparison on transmission stiffness, efficiency and backlash.
The concepts are compared to each other to provide equal joint torque; 50 Nm. After the choice of the concept, it was decided that more torque is needed and the design, shown in section 4.1, is upgraded. The justification of the choice of concept is not affected by this. In Table F.1, the transmission stiffness, the efficiency and the backlash of the concept is displayed.

Table F.1: Hip ψ concept comparison on stiffness, efficiency and backlash.

	Concepts:				
Aspects:	Planetary gearbox + belt or cable	Planetary gearbox + (large) gear	Ball screw + steel wire rope	Direct ball screw	Ratio 1:1 + Harmonic Drive (1:50)
Stiffness [kNm/rad]	8	high	4*	15*	5
Efficiency [-]	0.79	0.87	0.90	0.91	0.78
Backlash/Play [°]	0.02	0.02	0	0	0.02

*These concepts have a stiffness that is dependent on the position of the joint; an indication is given.

From this, it can be seen that the concept with a planetary gearbox and a gear set has the highest stiffness and the direct ball screw comprises no play while being stiffer and more efficient than the other three concepts.

Compactness, complexity of the construction and compatibility with other DOF actuations
The concepts with a planetary reduction followed by a final reduction have the advantage that the motor is placed eccentric to the ψ-tube and a pulley ring or a gear ring can be mounted on the outside of this ψ-tube. Therefore, space is provided in, and around, the ψ-tube to design a joint actuation of the hip φ, with more freedom. This is a major advantage with respect to the concept of the direct ball screw and the concept with a Harmonic Drive.

The ball screw combined with a steel wire rope has this same advantage. However this concept is more complex and incorporates more components in order to load the ball screw in center of the ball screw nut. As a consequence of this complexity, also the compactness above the ψ-tube is affected. Therefore, it is less compatible with the torso DOFs; it most likely will obstruct the ROM of the torso φ.
The concepts with a planetary reduction followed by a final reduction have the advantage that they do not obstruct the torso DOF while construction remains simple; planetary gearboxes have lead-in edges that can ensure alignment and threaded holes that can ensure fixation.

Costs
Ball screws and planetary gearboxes are costing approximately a few hundred Euros, whereas a Harmonic Drive costs at least a factor 10 more. The concept of planetary gearbox and a final reduction incorporate the least components and therefore, it is expected that these concepts are the most cost-effective.

Final choice
The concept with a planetary gearbox and a gear set as a final reduction has been chosen. To summarize; compared to the other concepts it has the following advantages:
- stiff and efficient actuation,
- compact and simple,
- compatible with torso DOFs and hip φ,
- inexpensive.

Appendix G
Motor and gearbox specifications

G.1 Motors

All motors used in the design are brushed DC motors of Maxon motor company (Maxon, 2010). They are all from the RE series and have a nominal voltage of 24 V. Individual properties are in Table G.1.

Table G.1: Motors specifications.

	RE	order no.	power [W]	mass [kg]	η [%]	stall torque [mNm]	max. velocity [rpm]
toe ψ	25	339152	20	0.115	83	316	14000
ankle φ, ankle ψ, torso φ and torso θ	30	310007	60	0.238	87	1020	12000
hip φ and leg θ	35	323890	90	0.340	84	1160	12000
knee ψ and hip ψ	40	148867	150	0.480	91	2280	12000

G.2 Planetary gearboxes

The planetary gearboxes used in the design are of Maxon motor company (Maxon, 2010). They are all from the GP series mounted on the motor in the factory. Accordingly, the motor and gearboxes come in sets. The properties of the gearboxes are in

Table G.2: Planetary gearboxes specifications.

	GP	ratio [-]	η [%]	stages	mass [kg]	nominal torque [Nm]	stall torque [Nm]	on motor
torso φ and torso θ	32 A	1/14	75	2	0.162	2.25	3.4	RE 30
leg θ	32 HP	1/51	70	3	0.213	8	12	RE 35
hip ψ	42 C	1/43	71	3	0.460	15	22.5	RE 40